Department of Chemical, Materials and Production Engineering

University of Naples Federico II

POLYSACCHARIDES BASED SYSTEMS TOWARDS REGENERATIVE MEDICINE AND DRUG DELIVERY APPLICATIONS

PhD candidate

Pooyan Makvandi

Supervisors

Assunta Borzacchiello

Ch.mo Prof. G. Mensitieri

Ph.D. Thesis in

Materials Science and Engineering

XXXII cycle

Abstract

Infection is a crucial and generally unsolved issue in tissue engineering applications such as in wound healing and bone regeneration. In this study, we have prepared different antibacterial platforms containing hyaluronic acid and silver nanoparticles. Silver nanoparticles (Ag NPs) were biosynthesized by a microwave-assisted green technique using corn silk extract in an organic solvent-free medium. The thermosensitive and injectable hydrogels were prepared and their potential use as wound care materials and bone regeneration were investigated. Rheological analysis demonstrated that the nanocomposites have good mechanical properties with gelation temperature close to the body temperature; hence, they can be easily administrated locally on wounded skins and bone defect. The samples exhibited antibacterial activity toward gram-positive and gram-negative bacteria. Cytotoxicity assay showed that the hydrogels have good biocompatibility. Interestingly, an *in-vitro* model of wound healing revealed that the nanocomposites allow faster wound closure and repair, compared to the control. Regarding the bone tissue engineering applications, mesenchymal stem cells seeded in the nanocomposite exhibited high bone differentiation which indicate that they could be a good candidate as a potential scaffold for bone tissue regeneration.

In another study, we exploited the advantages of local drug delivery by developing a platform with improved efficacy. Having this in mind, we prepared hyaluronic acid-based device containing diclofenac sodium-encapsulated (2-Hydroxypropyl)-β-cyclodextrin (CD) that possess high drug loading along with prolonged release. The platform showed high mechanical properties along with low friction indications high lubricity of the platform. L929 cell morphology and viability assay showed a over the 100 % (approximately 110%) for the injectable device.

Contents

Chapter 1

Introduction on thermosensitive hydrogels containing hyaluronic acid

1.1. Hydrogels

Hydrogels are extremely suitable for a variety of applications in the pharmaceutical and medical industry. Because they are capable of retaining large amounts of water and because of their soft and rubbery consistence, they closely resemble living tissues. Hydrogels offer many advantages as they are composed of hydrophilic polymer chains which can be synthetic or natural in origin [1]. A hydrogel is a three-dimensional structure that can absorb and contain a high amount of water or biological fluid. Its polymer network structure can be formed by chemical cross-linking, physical cross-linking or both simultaneously [2]. Hydrogels have attracted research attention as wound dressings since they are an excellent source for providing moisture to a dry lesion, monitoring fluid exchange from within the wound surface, and helping to cool down a wound [3]. The wound closure after physical injury or surgery is of significant clinical and research importance. Hydrogel dressing can protect the body from wound infection and promote efficient healing [4].

Smart hydrogels are hydrogels that change their network structures, mechanical strengths, permeability, and swelling behavior in response to environmental stimuli. Intelligent hydrogels are an interesting class of materials that could be programmed to react to specific stimuli such as pH,

temperature, light, electric, and magnetic field. Smart hydrogel materials will call for a comprehensive understanding of the materials, bioprinting systems, and bioprinting processes [5, 6].

1.2. Thermosensitive hydrogels

Hydrogels that show a sol-gel transition near body temperature have attracted interest for their potential biomedical application since no organic solvents or toxic crosslinkers are involved during gelation [7]. Among the different types of hydrogels, thermosensitive based hydrogels have attracted significant attention in pharmaceutical industries [8]. Thermosensitive hydrogels, such as those based on poly(*N*-isopropylacrylamide) (PNIPAM) and its copolymers as well as amphiphilic block copolymers, such as polyethylene oxide-polypropylene oxide copolymers (Pluronic, PPO-PEO-PPO), could be applied as drug/biomolecule carrier to protect them from a hostile environment and modulating delivery in response to temperature change. PNIPAM polymer or its derivatives demonstrate coil-to-globule transition behavior in aqueous media. In fact, under lower critical solution temperature (LCST), the polymer expands and swells in water while above the LCST, the polymer chains shrink and collapse repealing some water molecules [5, 9]. This transition behavior is caused by the change of the macromolecules from an expanded coil state to a collapsed globule state. PNIPAAm can connect with a hydrophilic acrylic acid (AAc) group or hydrophobic butyl methacrylate (BMA) group to generate negative or positive temperature-responding hydrogels, respectively. When the temperature is raised above the LCST, the shrinking behavior of the hydrogel indicates negative feedback, whereas swelling indicates a positive response. It has been found that when PNIPPAm, as the LCST monomer, was cross-linked with bis-vinyl-terminated polydimethylsiloxane (VTPDMS), as the more hydrophobic macromer, a heterogeneous thermal- sensitive hydrogel was formed [10].

In contrary, Pluronic concentrated aqueous solutions undergo a sol-to-gel phase transition at a critical temperature, namely, lower critical gelation temperature (LCGT). Below LCGT and in a suitable concentration range, aqueous solutions of Pluronics exist as low-viscosity liquids, while, above LCGT, their viscosity sharply increases for a slight increase in temperature and gelification occurs [11]. In fact, the aqueous solution of this triblock copolymer exhibited both sol-to-gel and gel to sol phase transitions when heated from a low to a high temperature. The gel-state region in the sol–gel transition diagram can be adjusted according to the concentration or composition of the polymer. When the consistency of the polymer in an aqueous solution is higher than a particular critical value, aggregation and bridges of micelles can induce the gelation of the whole solution [2].

In these PEO-PPO-PEO triblock copolymers, the amphiphilic characteristics are critically dependent on the molecular architecture, such as total molecular weight, relative block size and block sequence as well as thermodynamic parameters, such as temperature and pressure. Pluronic triblock copolymer crosslinkers self-assemble into a wide variety of structures including spherical rods, pancake-shaped micelles, as well as complex-structured fluids like bicontinuous microemulsions. The self-assembling process occurs through a micellization characterized by two key parameters; the critical micellization concentration (CMC) and critical micellization temperature (CMT). These parameters depend on the PEO-PPO-PEO chemical–physical parameters such as block composition (PEO/PPO ratio) and molecular weight as well as the respective PEO and PPO block length. Therefore, CMC and CMT can be tailored to obtain materials with final properties suitable for a wide range of applications [12].

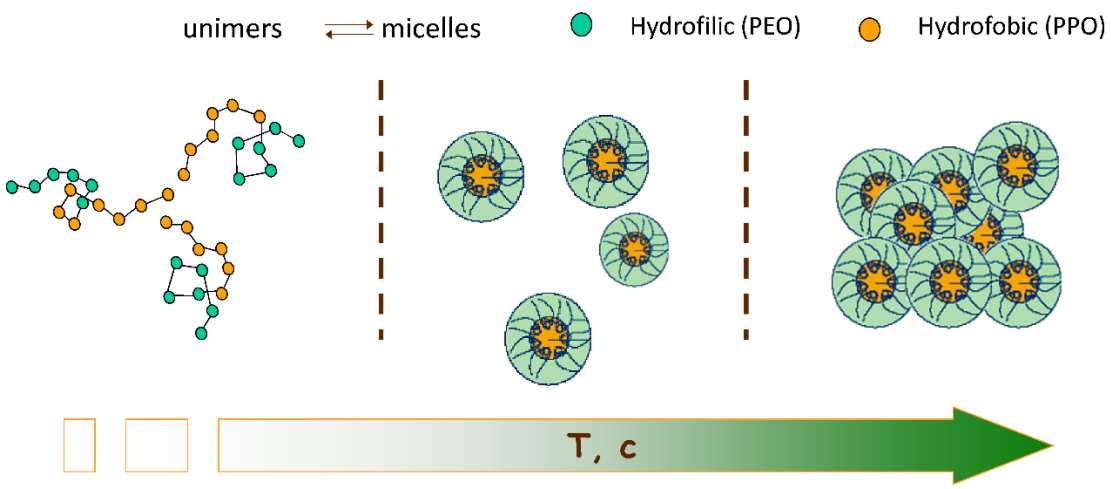

Fig. X1 Schematic mechanism of gelation driven by shifting of hydrophobic interaction under the change of temperature.

The pluronic consist of more than 30 different non-ionic surface-active agents. These polymers are ABA-type triblock copolymers composed of PEO (A) and PPO units (B). The pluronic series covers a range of liquids, pastes, and solids, with molecular weights and ethylene oxide-propylene oxide weight ratios varying from 1100 to 14,000 kDa and 1:9 to 8:2, respectively. Concentrated aqueous solutions of pluronic form thermoreversible gels [9].

The gelation mechanism of pluronic solutions has been investigated extensively. Micelle formation occurs at the critical micellization temperature as a result of PPO block dehydration. With increasing temperature, micellization becomes more important, and at a definite point, micelles come into contact and no longer move. In addition, the formation of highly ordered structures, such as cubic crystalline phase, has been proposed as the driving force for gel formation, but this hypothesis has been questioned recently. Thus, packing of micelles and micelle entanglements may be possible mechanisms of poloxamer solution gelation with increased of temperature [13, 14].

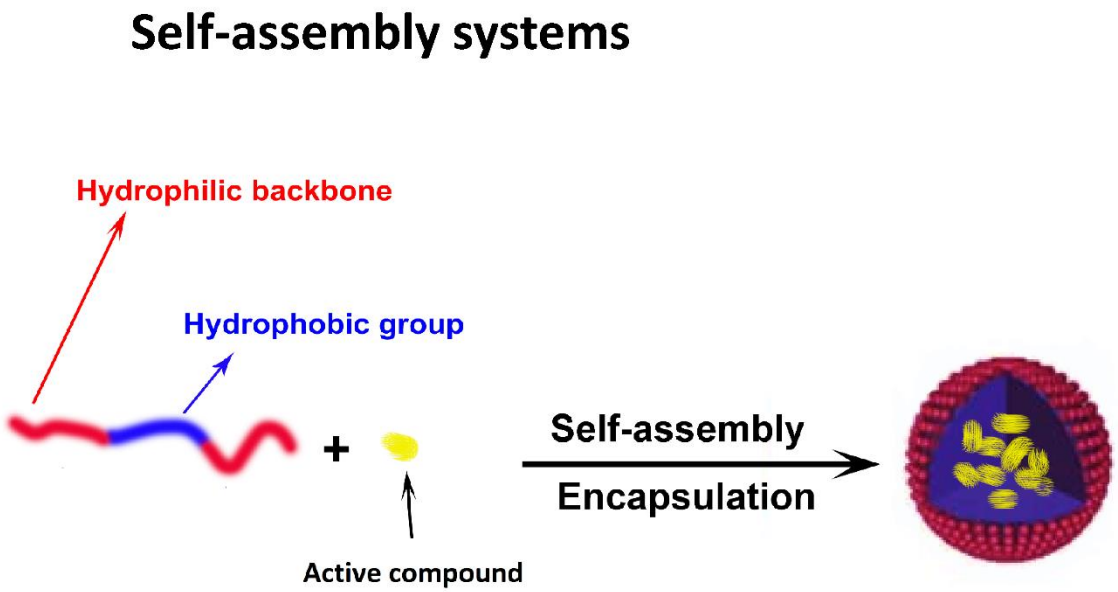

Fig. X2 Self-assembly of pluronic in presence of a biomolecules.

The thermosensitive hydrogels could be applied as drug/biomolecule carrier to protect them from a hostile environment and modulating delivery in response to temperature change. This enhances the bioavailability of drugs. Amphiphilic Pluronic molecules self-assemble in aqueous media in presence of a drug. Then, gradually they release their contents (**Fig. X2**) [12, 15, 16]. Due to their properties, Pluronic based hydrogels have been used in wound healing applications because as pomade or injectable fluid they can be easily applied, fill the cavities of wounds and become gel in situ at body temperature (T_b) [17, 18].

1.3. Hyaluronic acid

Thermosensitive hydrogels containing hyaluronic acid (HA) have been exploited in biomedicine for sustained drug delivery and tissue engineering. HA (**Fig. X3**) is naturally occurring

glycosaminoglycan and a main macromolecular component of the intercellular matrix of most connective tissues e.g. cartilage, vitreous of the human eye, and synovial fluid [19].

Hyaluronan, an extracellular matrix component, is a high molecular weight glycosaminoglycan composed of disaccharide repeats of *N*-acetylglucosamine and glucuronic acid. Specifically, HA consists of repeating polyanionic disaccharide units of glucuronic acids and N-acetyl-glucosamine connected by alternating b 1–3 and b 1–4 bonds. This relatively simple structure is conserved throughout all mammals, suggesting that HA is a biomolecule of considerable importance. In the body, HA occurs in the salt form, hyaluronate, and is found in high concentrations in several soft connective tissues, including skin, umbilical cord, synovial fluid, and vitreous humor. Significant amounts of HA are also found in lung, kidney, brain, and muscle tissues. Solutions of hyaluronan manifest very unusual rheological properties and are exceedingly lubricious and very hydrophilic [20].

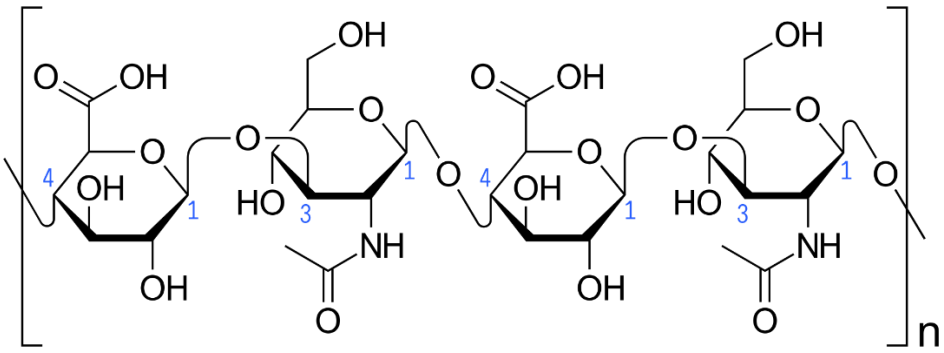

Fig. X3 Chemical structure of hyaluronic acid.

In contrast to collagen, HA is extremely hydrated and thus fundamental for biology and a functional determinant in cellular water homeostasis. Since highly hydrated matrices facilitate cell

migration and proliferation, HA is also an acknowledged major compound controlling and regulating cell behavior and cell-cell interaction, especially in the course of tissue healing [21].

HA offers many advantages as a tissue scaffold which include [1, 22]:

a) Biodegradability, biocompatibility and bioresorbability;

b) HA is a major intracellular component of connective tissues where it plays an important role in lubrication, cell differentiation and cell growth. These functions can be transferred to the scaffold;

c) HA contains functional groups (carboxylic acids and alcohols) along its backbone that can be used to introduce functional domains or to form a hydrogel by crosslinking;

d) Since HA is part of every step in the wound healing process exogenous HA has the potential to provide faster healing;

e) Due to its ability to maintain a hydrated environment conducive for cell infiltration, HA based hydrogels are ideal as wound grafts to treat chronic wounds or wounds in patients with impaired healing such as diabetic patients;

f) HA can be part of a new kind of tissue engineering scaffold that is bioactive both in its full length and in the degraded form. It exhibits low non-specific adsorption of proteins and specific interactions between the scaffold and growing cells can be tailored using cell receptors (CD44, RHAMM, ICAM-1) to enhance tissue growth and repair.

The presence of HA in thermoresponsive hydrogels leads to the improvement of gels viscoelastic and mucoadhesive properties that allow an increased adhesion to injured tissues and it leads to an enhancement of the biological activity [11, 13]. Hyaluronic acid or hyaluronan (HA) represents one biopolymer that can be modified and processed to form hydrogels for biomedical applications.

Owing to their biocompatibility, tunable properties, and native biofunctionality, hydrogels built from HA are increasingly versatile for a myriad of applications. HA has inherent biological importance HA hydrogels are now evolving in their design to be responsive to a range of cues, to present dynamic environments, and to possess multiple functionalities such as sophisticated structures and biochemical signals [23, 24]. HA promotes dermal regeneration and, hence, it is widely utilized in various therapeutic field such as dermal fillers, wound dressings, and substrates for dermal engineering applications [25].

Currently there are two production processes employed to obtain HA polymer in commercial quantities: extraction from animal tissues, typically rooster combs, or more recently though the application of bacterial expression systems in Streptococcus. Both approaches have faced considerable concerns over the safety of using biomedical products derived either from animal products or *Streptococcus*, a known pathogen that produces several endotoxins [26].

References

[1] M.N. Collins, C. Birkinshaw, Hyaluronic acid based scaffolds for tissue engineering—A review, Carbohydrate polymers 92(2) (2013) 1262-1279.

[2] Q.V. Nguyen, J.H. Park, D.S. Lee, Injectable polymeric hydrogels for the delivery of therapeutic agents: A review, Eur. Polym. J. 72 (2015) 602-619.
[3] T.M.D. Le, H.T.T. Duong, T. Thambi, V.H. Giang Phan, J.H. Jeong, D.S. Lee, Bioinspired pH-and Temperature-Responsive Injectable Adhesive Hydrogels with Polyplexes Promotes Skin Wound Healing, Biomacromolecules 19(8) (2018) 3536-3548.
[4] A. GhavamiNejad, C.H. Park, C.S. Kim, In situ synthesis of antimicrobial silver nanoparticles within antifouling zwitterionic hydrogels by catecholic redox chemistry for wound healing application, Biomacromolecules 17(3) (2016) 1213-1223.
[5] P. Wang, W. Chu, X. Zhuo, Y. Zhang, J. Gou, T. Ren, H. He, T. Yin, X. Tang, Modified PLGA–PEG–PLGA thermosensitive hydrogels with suitable thermosensitivity and properties for use in a drug delivery system, Journal of Materials Chemistry B 5(8) (2017) 1551-1565.
[6] M.K. Nguyen, D.S. Lee, Injectable biodegradable hydrogels, Macromolecular bioscience 10(6) (2010) 563-579.
[7] H. Tan, K.G. Marra, Injectable, biodegradable hydrogels for tissue engineering applications, Materials 3(3) (2010) 1746-1767.
[8] M. Prabhakar, P. Sudhakara, M. Subha, K.C. Rao, J.I. Song, Novel thermoresponsive biodegradable nanocomposite hydrogels for dual function in biomedical applications, Polymer-Plastics Technology and Engineering 54(16) (2015) 1704-1714.
[9] X. Tu, C. Meng, Z. Liu, L. Sun, X. Zhang, M. Zhang, M. Sun, L. Ma, M. Liu, H. Wei, Synthesis and phase transition of poly (N-isopropylacrylamide)-based thermo-sensitive cyclic brush polymer, Polymers 9(7) (2017) 301.
[10] Y. Qiu, K. Park, Environment-sensitive hydrogels for drug delivery, Adv. Drug Del. Rev. 53(3) (2001) 321-339.
[11] L. Mayol, M. Biondi, F. Quaglia, S. Fusco, A. Borzacchiello, L. Ambrosio, M.I. La Rotonda, Injectable thermally responsive mucoadhesive gel for sustained protein delivery, Biomacromolecules 12(1) (2010) 28-33.
[12] S. Fusco, A. Borzacchiello, P. Netti, Perspectives on: PEO-PPO-PEO triblock copolymers and their biomedical applications, J. Bioact. Compat. Polym. 21(2) (2006) 149-164.
[13] L. Mayol, F. Quaglia, A. Borzacchiello, L. Ambrosio, M.I. La Rotonda, A novel poloxamers/hyaluronic acid in situ forming hydrogel for drug delivery: rheological, mucoadhesive and in vitro release properties, Eur. J. Pharm. Biopharm. 70(1) (2008) 199-206.
[14] C. Liu, C. Gong, Y. Pan, Y. Zhang, J. Wang, M. Huang, Y. Wang, K. Wang, M. Gou, M. Tu, Synthesis and characterization of a thermosensitive hydrogel based on biodegradable amphiphilic PCL-Pluronic (L35)-PCL block copolymers, Colloids Surf. Physicochem. Eng. Aspects 302(1-3) (2007) 430-438.
[15] H. Deng, A. Dong, J. Song, X. Chen, Injectable thermosensitive hydrogel systems based on functional PEG/PCL block polymer for local drug delivery, J. Control. Release 297 (2019) 60-70.
[16] M. Sharma, L. Jingjunjiao, A. Seyfoddin, Thermosensitive Hydrogels for Drug Delivery and Tissue Engineering, Hydrogels, CRC Press2018, pp. 184-207.
[17] V. Kant, A. Gopal, D. Kumar, A. Gopalkrishnan, N.N. Pathak, N.P. Kurade, S.K. Tandan, D. Kumar, Topical pluronic F-127 gel application enhances cutaneous wound healing in rats, Acta histochemica 116(1) (2014) 5-13.
[18] E.A. Khalil, F.U. Afifi, M. Al-Hussaini, Evaluation of the wound healing effect of some Jordanian traditional medicinal plants formulated in Pluronic F127 using mice (Mus musculus), Journal of ethnopharmacology 109(1) (2007) 104-112.

[19] R. Barbucci, S. Lamponi, A. Borzacchiello, L. Ambrosio, M. Fini, P. Torricelli, R. Giardino, Hyaluronic acid hydrogel in the treatment of osteoarthritis, Biomaterials 23(23) (2002) 4503-4513.
[20] J. Necas, L. Bartosikova, P. Brauner, J. Kolar, Hyaluronic acid (hyaluronan): a review, Vet. Med. (Praha) 53(8) (2008) 397-411.
[21] S. Reitinger, G. Lepperdinger, Hyaluronan, a ready choice to fuel regeneration: a mini-review, Gerontology 59(1) (2013) 71-76.
[22] J. Baier Leach, K.A. Bivens, C.W. Patrick Jr, C.E. Schmidt, Photocrosslinked hyaluronic acid hydrogels: natural, biodegradable tissue engineering scaffolds, Biotechnol. Bioeng. 82(5) (2003) 578-589.
[23] C.B. Highley, G.D. Prestwich, J.A. Burdick, Recent advances in hyaluronic acid hydrogels for biomedical applications, Current opinion in biotechnology 40 (2016) 35-40.
[24] J.A. Burdick, G.D. Prestwich, Hyaluronic acid hydrogels for biomedical applications, Adv. Mater. 23(12) (2011) H41-H56.
[25] J. Kablik, G.D. Monheit, L. Yu, G. Chang, J. Gershkovich, Comparative physical properties of hyaluronic acid dermal fillers, Dermatologic Surgery 35(s1) (2009) 302-312.
[26] Z. Kang, L. Liu, S. Liu, Microbial Production of Hyaluronic Acid: Current State, Challenges, and Perspectives, Functional Carbohydrates, CRC Press2017, pp. 21-42.

Chapter 2

Antibacterial injectable hydrogels based on hyaluronic acid/Ag Nanoparticles for wound healing applications

Abstract

The wounds closure after physical injury or surgery is of significant clinical and research importance. In this study, thermosensitive and injectable hydrogels based on hyaluronic acid (HA), corn silk extract (CSE) and nanosilver were prepared and their potential use as a wound care material was investigated. Silver nanoparticles (Ag NPs) were biosynthesized by a microwave-assisted green technique using corn silk extract in an organic solvent-free medium. Rheological analysis demonstrated that the nanocomposites have good mechanical properties with gelation temperature close to the body temperature; hence, they can be easily administrated locally on wounded skins. The samples exhibited antibacterial activity toward gram-positive and gram-negative bacteria. Cytotoxicity assay showed that the hydrogels have good biocompatibility. Interestingly, an *in-vitro* model of wound healing revealed that the nanocomposites allow faster wound closure and repair, compared to the control. The obtained results highlight the potential application of these novel injectable hydrogels as wound dressing.

Keywords: Hyaluronic acid, antibacterial properties, corn silk extract, thermosensitive hydrogels, wound healing, green synthesis

2.1. Introduction

2.1.1 Wounds

Once a proper dermal bed has been well developed, wound closure is facilitated spontaneously or by applying a skin graft. Nevertheless, immediate coverage with autologous skin is not always available or possible. In these cases, alternative solutions may be taken into considerations to favor an adequate repair and effective functional recovery of the burned area [1].

Dermal wound repair is a very dynamic process, consisting of four overlying stages (**Fig. 1**). The first immediate response to the injury is hemostasis, the process in which the blood loss held at the wound site. The second stage occurs right after the injury and includes inflammation that takes from 24 h to 4-6 days. This stage is called the inflammatory phase and starts with the emitting of proteolytic enzymes and pro-inflammatory cytokines over invaded immune cells to the wound zone. These inflammatory cells generate reactive oxygen species (ROS). The quantity of ROS correlated with the kind of wound, but it is usually higher in burns and chronic wounds. Indeed, ROS preserve the organism from bacteria and infection [2]. In spite of having a positive impact on wound healing in low concentrations, ROS in high concentrations could be destructive for wound healing through its contribution to the chronic pathogenesis, and chronic wounds, which increases oxidative stress, lipid peroxidation, and severe cell damage [3].

Skin wounds that destroy the epidermis and part of the dermis have functional impacts as well, such as the impairment of skin oxygenation and effects on the tissue healing ability. Consequences can be very severe in terms of fluid management with the possibility of leading to dehydration and shock. Protein loss can also be serious, as well as the risk of contracting infections. To avoid all these dramatic consequences, prompt wound covering is an essential measure to be taken [4].

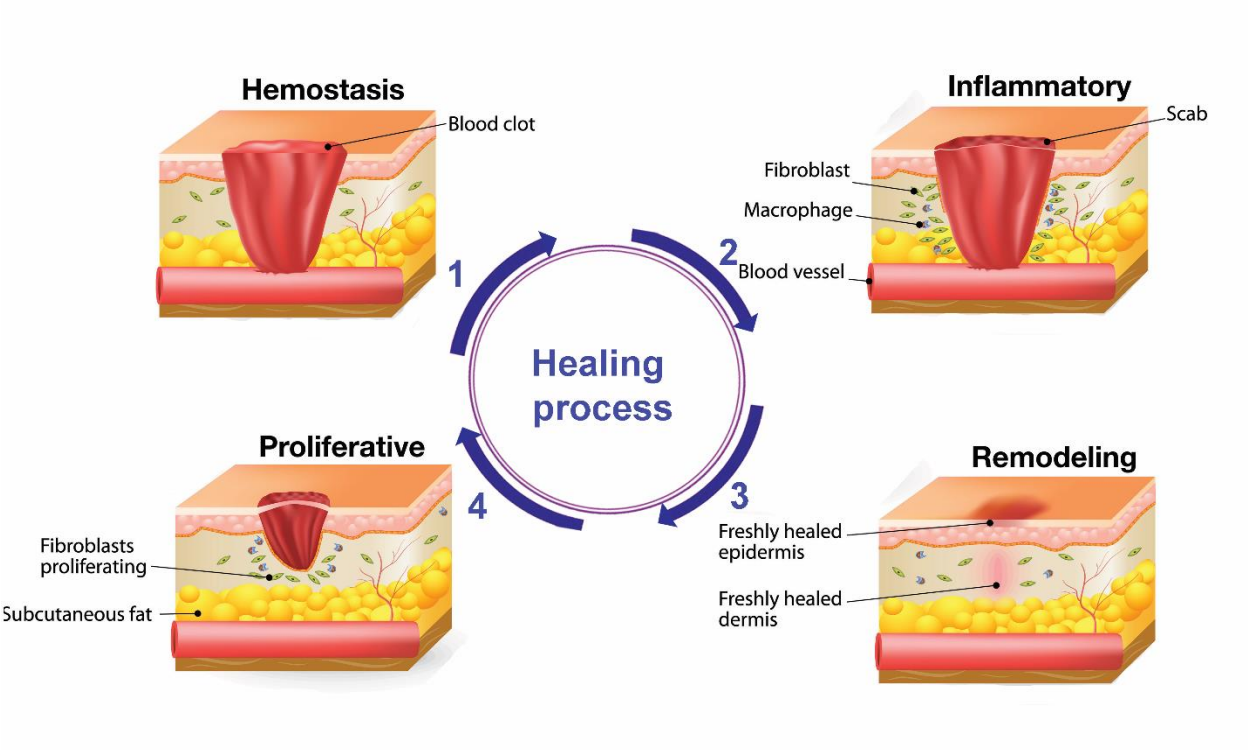

Fig. 1 Wound healing process.

Standard clinical procedure comprises early escharotomy, followed by immediate tissue reconstruction with a skin graft [5]. This protocol represents the optimal solution for decreasing the risks related to wound infection, scar formation and excessive fluid loss and also allows the reduction of patient hospitalization time. In this light, the gold standard is represented by the use of autologous skin to cover the injury; nevertheless an immediate coverage with autologous skin in deep and extensive burns is not always possible. In these cases, alternative solutions have to be taken into considerations. For example, the grafting of cryopreserved, whole cadaver skin is a possible option to consider when autograft is not feasible, but problems related to availability and risk of viral transmission represent limitations for this technique [1].

Therefore, synthetic alternatives like dermal substitutes and advanced wound dressings have been designed and proposed for specific clinical use. Dermal substitutes are generally preferred in full-thickness lesions (such as traumas, surgical wounds, chronic ulcers, etc.) and have been shown to minimize hypertrophic scarring, contractures and increase scar elasticity in wounds [6, 7].

A variety of biomaterials for medical applications has been designed and developed in recent years and large efforts have been dedicated to the development of new biocompatible and biodegradable polymers which should release safe degradation products that enter into the normal metabolic pathway. Many advanced wound dressings consist of biomaterials made from various components of the extracellular matrix (ECM) and are theorized to favor healing by providing a structural scaffold and the signals important to complex cellular interactions during the healing phases. Among a series of possible materials, HA chemistry represents an interesting and valuable option for the development of medical devices for epidermal and dermal wound treatment [1, 8].

2.1.2.Hyaluronic acid-based wound dresses

The scientific rationale for the development of biomaterials based on HA relies on the characteristics of the material, which is a structural component of the ECM architecture and has an important role in water homeostasis that could favor tissue hydration, which is conducive to wound healing [1].

Depending on the different molecular weights of the HA molecule, HA has been observed to play different roles in the body. Considering exogenous HA, the high molecular weight properties are related to angiogenesis inhibition and to a mostly physical role, while low molecular weight HA has been associated with a modulating effect on the inflammatory process due to its action on free radicals [9, 10].

2.1.3. Infection

It has to be highlighted that infection is a crucial and generally unsolved issue in wound healing. The most common type of wound infection is Skin and Soft Tissue Infections (SSTIs) and up to the kind of microbial invasion can be even life-threatening [11]. Indeed, gram-positive bacteria such as *Staphylococcus aureus* (*S. aureus*) and *Streptococcus pyogenes* (*S. pyogenes*) play the principal role in the first stage of the infection, and gram-negative bacteria such as *Escherichia coli* (*E.coli*) and *Pseudomonas aeruginosa* (*P. aeruginosa*) can be found when the wound is already developed [12]. In addition, fibroblasts and myofibroblasts are stimulated by the release of cytokines and enzymes, this phase, all foreign particles and tissue debris are removed from the wound bed by neutrophils and macrophages, thus preventing infections. In and the moisture essential for the healing is guaranteed by wound exudate [13, 14].

Therefore, materials containing antimicrobial compounds, such as quaternary ammonium salts [15-17], TiO_2 [18], and, Ag nanoparticles [19] have been utilized. Among these compounds, Ag NPs have shown the capability to inhibit or decline infections [20]. Various techniques, including chemical and physical approaches, have been developed to synthesise Ag NPs [19]. Unfortunately, in the aforementioned approaches, organic passivators, toxic both for the environment and human body, are used [21].

Biosynthesis of NPs, by using microorganisms and plants, has received considerable attention due to the growing need to develop environmentally and non-toxic technologies. Biosynthesis of NPs by using renewable materials to avoid utilization of toxic chemicals and non-environmentally benign solvents make them more suitable for the biomedical applications [22].

Corn silk extract (CSE), a waste material of the crop, has been used for the biosynthesis of Ag NPs as both a bioreducing and biostabilizing/capping agent, thus eliminating the use of any other toxic organic solvents and chemicals as reducing and stabilizing agents [23]. In addition, CSE possesses excellent antioxidant capacity [24], antiproliferative effects on human cancer cell lines [25] and antidiabetic activity [26]. In this frame, we formulated thermosensitive nanocomposites hydrogels based on Pluronics and HA and containing CSE and Ag NPs to be potentially used as a wound care material. To this aim, we produced Ag NPs using CSE via a microwave-assisted green approach in an organic solvent-free medium that is completely biocompatible and nontoxic. Subsequently, the Ag NPs were included in Pluronic/HA/CSE hydrogels to formulate the antibacterial thermosensitive nanocomposites that were further characterized.

2.2. Experimental section

2.2.1. Chemicals

Hyaluronic acid (HA), with average molecular weight (Mw) of 112 kDa, was kindly provided by Altergon Italia. Pluronics F127 [$(PPO)_{100}(PEO)_{65}(PPO)_{100}$, Mw= 12500 g/mol] and F68 [$(PPO)_{76}(PEO)_{29}(PPO)_{76}$, Mw= 8350 g/mol], silver nitrate ($AgNO_3$), and NaOH were purchased from Sigma-Aldrich.

2.2.2. Plant materials and preparation of corn silk extract

Corn silk was purchased from a local farm in Egypt. Corn silks were collected, washed several times and dried in an oven at 40 ˚C before use. The dried corn silk fibers were grinded into a fine powder (mesh size 60 μm). Then, pulverized in a knife mill and sieved into a particle size of 0.4 μm, and kept refrigerated in glass containers before further processing.

CSE was obtained as reported in the literature [23]. Briefly, 5 g of the dried powder of corn silk was added to 50 ml of deionized water. The mixture was heated at 80 °C for three hours. Then, the corn silk mixture was filtered through Whatman No. 42 filter paper to remove the fibers and get CSE. Finally, CSE was stored at 4 ˚C until it was used for the experiments.

2.2.3. Biosynthesis of Ag NPs

The synthesis of Ag NPs was conducted by a microwave-assisted green chemistry approach as follows. 10 g of CSE was mixed with 1 ml of $AgNO_3$ aqueous solution (3.4 µg/ml) in Erlenmeyer flask and then were treated by microwave (700 w) for 180 s. A pulsed mode of on 5 s, off 5 s was applied to prevent intense boiling and aggregation of Ag NPs. The biosynthesized NPs in CSE were stored at 4 °C for further characterization.

2.2.4. Preparation of thermosensitive hydrogels

The hydrogels were prepared by dissolving different amounts of Pluronics F127 and F68 in CSE with and without Ag NPs (1.7 4 µg/ml) by mixing under continuous stirring at 4 ˚C. Subsequently, HA-containing formulations were prepared by adding HA to Pluronics blends, at room temperature to obtain concentration 1% w/w. The composition of the hydrogels was optimized by rheological analysis to obtain a gelation temperature (T_{gel}) around body temperature. The compositions and the acronyms of the optimized formulations containing CSE, HA and Pluronics are summarized in table 1. The nanocomposite hydrogels prepared in CSE containing Ag NPs, with and without HA were named AgSPHA and AgSP, respectively.

Table 1 Formulations of the thermosensitive hydrogels containing CSE, HA and Pluronics. Elastic (G') and viscous moduli (G") values at 1 Hz and 40 °C. Bound and free water in percentage for the formulations as calculated by DSC analysis.

Acronyms	CSE	F68	F127	HA
	(wt.%)			
SP	70	15	15	-
AgSP	70*	15	15	-
SPHA	69	15	15	1
AgSPHA	69*	15	15	1

*CSE containing Ag NPs

2.3. Measurements

2.3.1. Characterization of Ag NPs

To assess the formation of Ag NPs, Surface Plasmon band measurements were performed and UV–Vis spectrophotometer (JASCO, V-530), from 350 to 800 nm at a resolution of 64 nm, was used. The size distributions of the silver NPs were evaluated by DLS using a Nano-ZS Zetasizer apparatus (Malvern Instruments, United Kingdom). The morphologies and sizes of the Ag NPs were investigated by HR-TEM. JEM 2010 (Michigan, USA) instrument was used at an accelerating voltage of 200 kV equipped with selected area electron diffraction facility (SAED). The samples were prepared by placing a drop of NPs solutions onto a carbon film supported on a copper grid and by following evaporation of water in air at room temperature. Ag NPs, in the aqueous medium, were also visualized by hyperspectral microscopy using an enhanced resolution dark–field microscope system (BX51, Olympus, USA) equipped with CytoViva Hyperspectral Imaging System (HSI, Auburn, AL) [27]. 20 μL of each sample was deposited on a clean glass

slide and covered with a coverslip for imaging. Hyperspectral images were acquired using 100% light source intensity and 0.6 s acquisition time per line. Each pixel of the hyperspectral image contains a light reflectance spectrum, ranging from 400 to 1000 nm with a spectral step of 1.5 nm. Each pixel thus has a spectral signature modulated by the nature of the material it contains.

2.3.2. Characterization of hydrogels

DLS was used to assess the micelles formation of hydrogels and their size distribution [28]. For the DLS analysis, all solutions were prepared in deionized water (mean, n=3) with the concentration of 5 mg/ml at 40 ˚C. In order to perform qualitative elemental analysis, scanning electron microscopy (Quanta 200 FEG, FEI Company, Hillsboro, OR, USA) coupled with energy dispersive X-ray spectrometry (EDX; Inca Energy System 250, Oxford, UK) was used.

The thermal behavior of the hydrogel samples was determined using a differential scanning calorimeter (DSC). DSC measurements were performed using a TA Instruments (Discovery series, New Castle, DE, USA) under N_2 flow of 20 ml min^{-1} and a heating rate of 2.5 ˚C min^{-1} from -30 to 20 ˚C.

Small amplitude oscillatory shear tests were performed to evaluate the time-dependent response of the thermosensitive hydrogels and their linear viscoelastic properties i.e. G’ and G’. The frequency was in the range from 0.01 to 10 Hz. The measurements were carried out through a rotational rheometer (Mars III, HAAKE Rheometer, Waltham, MA, USA), using a parallel plate geometry. The tests were performed at the controlled temperatures of 20 and 40 °C using a thermostatic bath. In order to identify the linear viscoelastic response range of the materials, preliminary strain sweep tests were performed on the samples, at the oscillation frequency of 1 Hz. The tests were repeated at least three times on each sample. The gelation temperature of the

formulation was evaluated by monitoring the viscoelastic parameters (G' and G") as a function of the temperature ranging from 25 to 40 °C at a fixed oscillation frequency of 0.01 Hz. During all the tests, the samples were placed into a chamber properly designed to avoid solvent evaporation. For the viscosity analysis, steady state shear test in terms of flow curves was performed to evaluate the dependence of viscosity upon the shear rate.

The injectability of the thermosensitive hydrogels was evaluated by their ability to be injected through a 26-gauge (26-G) needle. This was based on the consideration for future in vivo injection, where needles as small as 26-G are used. To this aim 1 ml syringe (Basik, Denmark) fitted with a 26-G needle (0.4 × 13 mm) was used. The inner syringe diameter and the inner tip diameter were 15.4 ± 0.2 and 1.75 ± 0.1 mm, respectively. The samples were filled into the syringe equipped with the needle and they were manually injected (Himmelein, Lewe, Stuart, & Ravoo, 2014).

2.4. Antibacterial activity

Bacterial cell suspensions were prepared, for each tested Gram-positive and Gram-negative bacteria *(Bacillus Subtilis, Staphylococcus Aureus, Pseudomonas Aeruginosa, Escherichia Coli*), using sterile normal saline solution (0.9 % w/v NaOH) to obtain a final concentrations of 10^7 CFU/ml by comparison with a 0.5 Mc Farland turbidity standard. Equal weights of each Ag NPs solution were individually inserted in test tubes, each containing 10 ml of sterile Mueller–Hinton (MH) broth (composed of g/l: beef extract, 2.0; casein hydrolysate, 17.5 and starch 1.5; pH 7.3 ± 0.2). The medium was sterilized by autoclaving for 20 min at 120 °C and 1.5 atmospheric pressure. After sterilization, each test tube was inoculated with 100 µl of one of the previously prepared bacterial suspensions and 100 µl of Ag at different concentrations (3.4, 1.7, 0.85 µg/ml) and then incubated under moderate shaking of 100 rpm at 35 °C for 24 h (treated microorganisms).

Controlled test tubes, containing the same volume of MH medium without Ag, were inoculated by using the same inoculum size of the tested strains (untreated microorganisms). The cell growth of the tested bacteria was determined at the end of the incubation period, based on the optical density measurements at a wavelength of 620 nm. Results were expressed in terms of their cell dry weight (CDW) using the relation between the optical density of the cell and their cell CDW [29].

2.5. Cell cultures

In order to test the biological response to our biomaterials, L929 cells originating from Mouse C34/An connective tissue were obtained from the European Collection of cell cultures (Sigma-Aldrich, USA) and primary human dermal fibroblasts (HDF, provided by Lonza) were used. L929 cells were grown in T-75 cell culture flask (Falcon, Italy), in cell culture medium Dulbecco's Modified Eagle's Medium (DMEM, Hyclone, USA) supplemented with 10% fetal bovine serum (FBS) and antibiotics (penicillin G sodium 100 U/mL, streptomycin 100 μg/mL) at 37°C and 5% CO_2. HDF cells were cultured, at passage 5-6, with a complete medium, composed of Eagle's minimal essential medium (EMEM) supplemented with 20% FBS, 100 U/ml penicillin, 100 U/ml streptomycin and 2X non-essential amino-acids. HDF cells were maintained in 100 mm diameter cell culture dishes in a humidified and controlled atmosphere at 37°C and 5% CO_2. The medium was changed every 3-4 days.

2.5. Cell viability and morphology assay

In order to understand the cells viability, L929 cells were seeded at a density of 6×10^2 cells/ml on 96-wells (World Precision Instruments, Inc). The thermosensitive hydrogels were sterilized by steam autoclaving at 121 °C for 20 min. The cells were incubated with 5µl of the formulations SP, AgSP, SPHA, AgSPHA for each well in triplicate up to 72 h and then Alamar blue assay (AB)

was performed by adding AB reagent to the samples (at 10% v/v with respect to the medium) and incubated at 37°C for 4 hours. The absorbance of the samples was measured using a spectrophotometer plate reader (Multilabel Counter, 1420 Victor, Perkin Elmer) at 570 nm and 600 nm. AB is an indicator dye that incorporates an oxidation-reduction indicator that changes color in response to the chemical reduction in the growth medium, resulting from cell viability. L929 seeded wells were used as control. Data are expressed as the percentage difference between treated and control to evaluate the percentage of reduction (Reduction %), which was calculated with the following formula:

$$Reduction\ (\%) = \frac{(O_2 \times A_1) - (O_1 \times A_2)}{(O_2 \times P_1) - (O_1 \times P_2)} \times 100 \qquad (1)$$

where O_1 is the molar extinction coefficient (E) of oxidized AB at 570 nm; O_2 is the E of oxidized AB at 600 nm; A_1 is the absorbance of test wells at 570 nm; A_2 is the absorbance of test wells at 600 nm; P_1 is the absorbance of control well at 570 nm; P_2 is the absorbance of control well at 600 nm. The percentage of reduction for each sample was normalized to the percentage of reduction for the control to obtain the cell viability percentage. [30]

For cell morphology assay, cells were seeded at a density of 1×10^4 cells/ml on fluorodish-35 mm (World Precision Instruments, Inc) and 5µl of the formulations SP, AgSP, SPHA, AgSPHA were incubated for 24 h. Then, samples were washed two times with PBS and fixed with 10% formaldehyde for 1 hour at 4° C. The fixed cells were permeabilized with Triton X-100 0.1% in Phosphate-buffered saline (PBS) for 3-5 min. The actin filaments were stained with TRITC phalloidin (Cayman Chemical Company) in PBS for 30 minutes at room temperature. Finally, after two washes with PBS to remove unbound phalloidin conjugate, cell nuclei were stained with 4',6-diamidino-2-phenylindole, DAPI, (SIGMA-ALDRICH). The samples were observed by confocal

microscope system (Leica TCS SP8) with a 63X oil immersion objective. Images were acquired with a resolution of 1024×1024 pixel.

2.6. Wound Healing Assay

The wound healing potential of the realized formulations was assessed by wound healing assay [31, 32]. To this aim HDF cells were seeded at a density of 5×10^4 cells/ml on 48-wells (World Precision Instruments, Inc) to obtain a monolayer of cells. Wound healing assay was performed by scraping the cell monolayer in a straight line to create a ‘‘scratch’’ with a p200 pipet tip. The debris were removed by washing the cells once with 1 ml of the growth medium and then replaced with 500 µl of culture medium, which is specific for this in vitro assay. This assay medium is composed by a lower percentage of FBS (2%) than that used in the growth media, to minimize cell proliferation but just sufficient to prevent apoptosis and/or cell detachment. After the scraping, 10 µl of the thermosensitive hydrogels prepared in the assay medium were incubated in each well and placed at 37 °C for 24 and 48 h, and at each time point wells where the thermosensitive hydrogels were not incubated, were used as control. To study the HDF cells migration, crucial to obtain the wound closure, images were acquired at time zero, immediately after the scratch, and after 24 and 48 h for each sample in triplicate, using bright-field microscopy. At the different times, wound area was calculated using the Image J public domain software. The percentage of wound area reduction or wound closure, expression of the cell migration rate, can be expressed as:

$$Wound\ Closure\ \% = \frac{(A_{t=0} - A_t)}{A_{t=0}} \times 100 \qquad (2)$$

Where $A_{t=0}$ is the area of the wound measured immediately after scratching and A_t is the area of the wound measured h after the scratch is performed. The closure percentage increases as cells migrate into the scratch over time.

2.7. Results and discussion

2.7.1. Synthesis and characterization of Ag NPs

The UV absorption spectra of the CSE before and after microwave treatment are presented in **Fig. 1A**. The monotonic decrease of the UV–Vis spectrum of CSE before microwave treatment clearly indicates the absence of Ag NPs while, after microwave treatment, the peak of the Plasmon absorption at 440 nm reflects the presence of the colloidal dispersion of $Ag^{(0)}$ NPs. The peak appearance of the Plasmon absorption represents that Ag^{+} ions were reduced to $Ag^{(0)}$ NPs. The absorption band is caused by 4d→5s, p interband transitions as reported in other studies [19, 33].

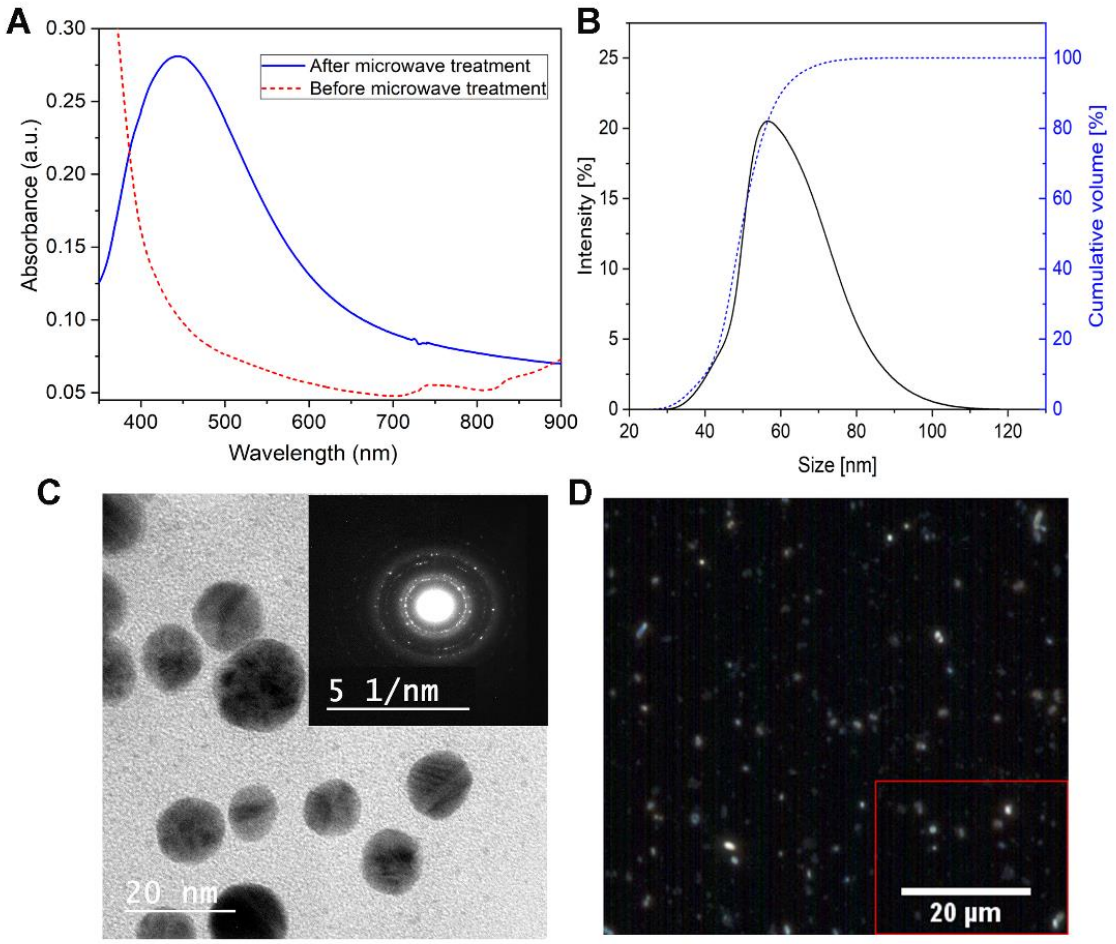

Fig. 1 (A) UV absorbance of CSE before and after microwave treatment. Size distribution measurements by DLS (B) and TEM image (C) of Ag NPs in CSE solution after microwave treatment. The bar for TEM image represents 20 nm. (D) Visualization of nanoparticles in CSE medium. Hyperspectral images of Ag NPs by using Dark-field microscopy in visible and near-infrared wavelengths. Hyperspectral images were acquired using 100% light source intensity and 0.6 s acquisition time per line. Each pixel of the hyperspectral image contains a light reflectance spectrum, ranging from 400 to 1000 nm with a spectral step of 1.5 nm.

The particle size of NPs was analyzed with DLS (**Fig. 1B**), the particles have a narrow size distribution with a volume mean diameter (VDM) of 49±2 nm. TEM image (**Fig. 1C**) shows well-dispersed silver NPs which are spherical in shape with an average size of 13±1 nm, recorded by measuring about 100 NPs. The selected area electron diffraction (SAED) patterns obtained for a representative silver NPs have face-centered cubic (fcc) crystallographic structure. In agreement with other literature studies [34, 35], there is a difference between DLS and TEM sizes measurements which is normally attributed to the fundamental difference between intensity and number-weighted particle size distributions and the differences between the dry and hydrodynamic radius of particles. Even, if Ag NPs are synthesized by green-methods, the particles size is comparable with the results of Tamiyakul et al.[36] that used toxic chemicals such as sodium borohydride ($NaBH_4$) as a reducing agent. The presence of Ag NPs in CSE medium was also visualised by means of dark field hyperspectral spectroscopy as shown in **Fig. 1D**. One major advantage of dark field hyperspectral imaging is to localize Ag NPs at relatively low magnification (400-1000×) and it is compatible with simpler sample preparations than electron microscopy.

2.7.2. Synthesis and characterization of hydrogels

More than 80% of the world's population still depends upon traditional medicines for various skin diseases [37]. Therefore, the aim of this study was to formulate thermosensitive platforms based

on a plant extract (CSE), Pluronic blends (F68 and F127) and HA with suitable viscoelastic properties that also possess antibacterial activity with potential application in wound healing.

Here, we report about the preparation of antibacterial thermosensitive HA-based nanocomposite hydrogels, which offers the advantages of green synthesis of silver NPs in aqueous medium. We used Pluronic blends, which gel close to body temperature as well as HA to enhance the biocompatibility of the formulations. Pluronic based hydrogels have attracted the attention for their potential biomedical application since no organic solvents or toxic crosslinking agents are involved during gelation. A possible mechanism of Pluronic gelation is driven by the self-assembling process occuring through a micellization in solution due to polymer-polymer interactions, which trigger the formation of a semi-solid phase [38].

Micelle formation and size distribution were examined using dynamic light scattering in very diluted samples and the measurements are presented in **Fig. 2A.** This analysis evidenced the presence of a population of micelles and that the presence of Ag NPs leads to a size increase (right panel vs left panel). Moreover, the presence of HA does not significantly alter the micelle size of samples. The elemental analysis by EDX of AgSPHA is reported in **Fig. 2B**. As expected, the presence of C and O as well as the presence of N, which comes from HA, are highlighted. The chemical map of carbon (C, red color) presents the appropriate distribution of carbon in the nanocomposite platform. Therefore, since the carbon comes mostly from HA, the EDX images confirmed that HA was uniformly dispersed in the hydrogel matrix.

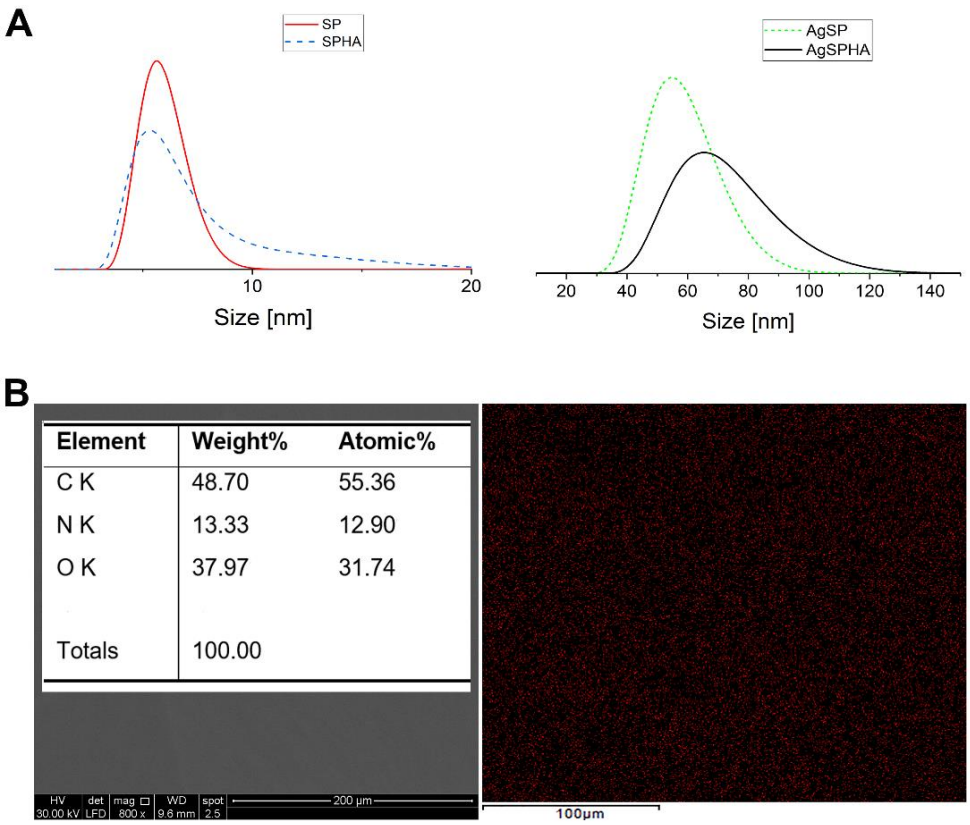

Fig. 2 (A) Dynamic light scattering (DLS) measurements of the final hydrogels. All solutions were prepared in deionized water (mean, n=3) with the concentration of 5 mg/ml at 40 ˚C. (B) Energy dispersive X-ray (EDX) image to assess the elemental analysis of the AgSPHA thermosensitive nanocomposite hydrogel. The presence of carbon, oxygen, and nitrogen are depicted (left panel). Carbon map is also presented (right panel) which confirms appropriate carbon distribution in the nanocomposite system.

The DSC thermogram of the samples are shown in **Fig. 3.** As it can be seen, two distinct endothermic peaks (around -10 and 0 °C) were observed for the thermosensitive hydrogels which are related to the fusion of H_2O in the samples. The first peak is associated with the fraction of water interacting with the Pluronic and HA network, e.g. bound H_2O, while the second one (around 0 °C) is related to the free water fraction. By integrating each peak, the total heat evolved during the fusion of H_2O as ΔH_{tot} was calculated, whereas the amount of bound and free water was

calculated as the ratio between the enthalpies associated to the first (ΔH_1) and the second peak (ΔH_2), and ΔH_{tot} as presented in table 1 (Mayol et al., 2011).

Table 2 Bound and free water in percentage for the formulations as calculated by DSC analysis.

Acronyms	**Bound water**	**Free water**
	(%)	(%)
SP	35	65
AgSP	40	60
SPHA	34	66
AgSPHA	15	85

For the platforms without Ag NPs, the ratio associated to bound water (in percentage) slightly reduced upon the addition of HA while the ratio related to free water slightly increased. When Ag NPs are included in the platforms, the respective reduction and increase of bonded and free water are higher. These results suggest that the addition of HA into Pluronics platforms hinders the interactions between water and Pluronics molecules thus favoring Pluronic-Pluronic interactions, in agreement with literature data (Mayol et al., 2011). Such polymeric interactions are further promoted by Ag NPs presence (Table 2).

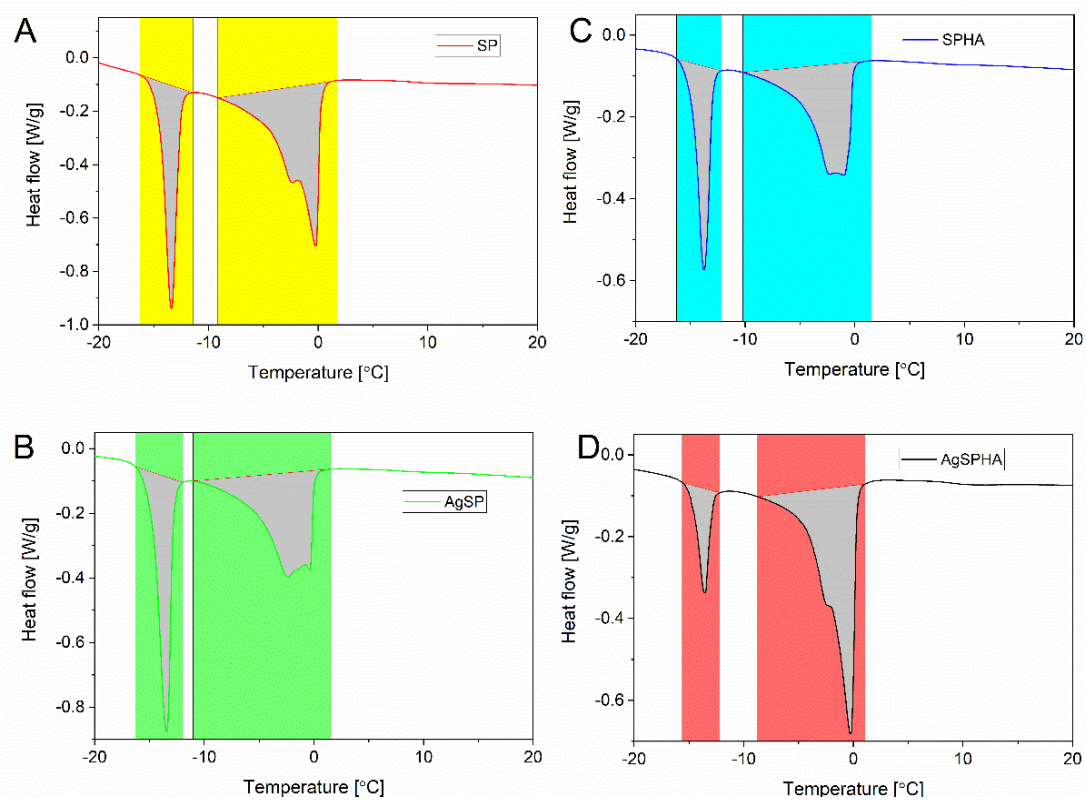

Fig. 3 DCS thermogram of the hydrogel samples at 2.5 ˚C/min: SP (A), AgSP (B), SPHA (C), AgSPHA (D).

Rheological measurements provide an excellent opportunity to monitor gelation of solutions. Gelation temperature (T_{gel}) was identified as the temperature at which the sample exhibited a switch from a prevalently viscous behavior (G”>G’) to a prevalently elastic one (G’>G”). The gelation process of the formulations was evaluated by monitoring the variation of the viscoelastic parameters upon temperature increase from 20 to 40 °C. The crossover point of elastic (G’) and viscous moduli (G”) was considered to be the gelation point [39]. The elastic and viscous moduli of samples, as a function of temperature, at a frequency value of 0.1 Hz are shown in **Fig. 4**. The T_{gel} were approximately 37, 34.5, 33, and 32.5 °C for SP, AgSP, SPHA, and AgSPHA, respectively. Separate Pluronic solutions, i.e. F127 or F68, do not show a T_{gel} close to the body

temperature in the concentration range from 10 to 30 wt.% either in water or in CSE. However, by formulating the blends of Pluronic F127/F68 at specific ratio and concentrations (table 1) it was possible to obtain platforms with a T_{gel} close to T_b. These systems are so able to become gel once in contact with the body and not when stored in shelf and hence they can be easily applied.

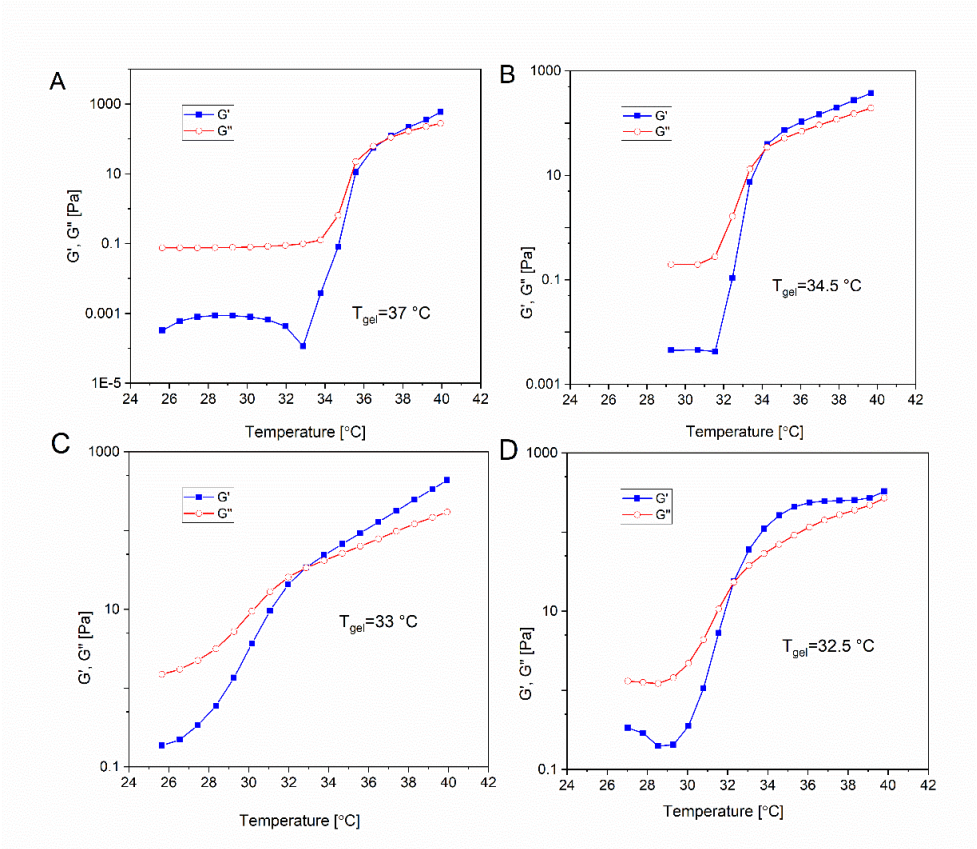

Fig. 4 The sol–gel phase transition by rheological experiments. The increase in G' over G" represents an increase in solid over liquid characteristics of the tested sample, which reflects a phase transition into a "gel" structure. A crossover between the elastic and loss moduli curves (G' vs G", respectively) indicates the gelation temperature. Elastic and viscous moduli as a function of the temperature of SP (A), AgSP (B), SPHA (C), AgSPHA (D) at a frequency value of 0.01 Hz. Results are the means of three measurements. SD was always lower than 10%. Error bars were omitted for clarity purpose.

Pluronic blends, thanks to their good tolerability and low irritancy/toxicity, have been utilized in the biomedical field such as for tissue engineering and drug delivery applications [40, 41]. The

mechanism of gelation for the Pluronic hydrogels is driven by the self-assembly of Pluronic chains in solution due to polymer-polymer interactions, which trigger the formation of a semisolid phase. In particular, with increasing temperature, PPO blocks undergo dehydration, and this in turn promotes unimer-to-micelle aggregation (Fusco et al., 2006). In addition, HA presence into Pluronic thermosensitive hydrogels hinders the interaction between water and Pluronic macromolecules and, hence, enhancing the interactions among macromolecular species resulting in a T_{gel} reduction (Mayol et al., 2011). Indeed, the T_{gel} decreased from 37 (SP) to 33 ˚C (SPHA) and from 34.5 (AgSP) to 32.5 ˚C (AgSPHA) for the systems without and with Ag NPs, respectively. However, very interestingly, the presence of HA improved significantly the viscoelastic properties of the final gel as determined through rheological measurements which will be discussed in the following paragraphs. Moreover, the presence of Ag NPs slightly altered the rheological properties of the hydrogels and their T_{gel} (from 37 (SP) to 34.5 ˚C (AgSP) and from 33 (SPHA) to 32.5 ˚C (AgSPHA) for the systems without and with HA, respectively). The results demonstrated that the hydrogels undergo gelation with a T_{gel} close to T_b. The use of CSE as medium to prepare thermosensitive hydrogels based on HA/Pluronic does not alter gelation temperature.

The mechanical properties of the formulations were studied through small amplitude shear tests at temperature both below (20 ˚C) and above T_{gel} (40 ˚C). The mechanical spectra, that is G' and G" as a function of frequency, as an example for SP and AgSPHA at 20 and 40 ˚C, are shown in **Fig. 5**. At 20 ˚C (**Fig. 5A** and **C**), G" is always higher than G' in all the frequency range analyzed which indicates that the rheological behavior of the formulations is typical of a viscous fluid. On the contrary, at 40 ˚C (**Fig. 5B** and **D**), the elastic modulus is higher than the viscous one and the

viscoelastic moduli are quite a frequency-independent showing a rheological behavior characteristic of a “gel-like material”.

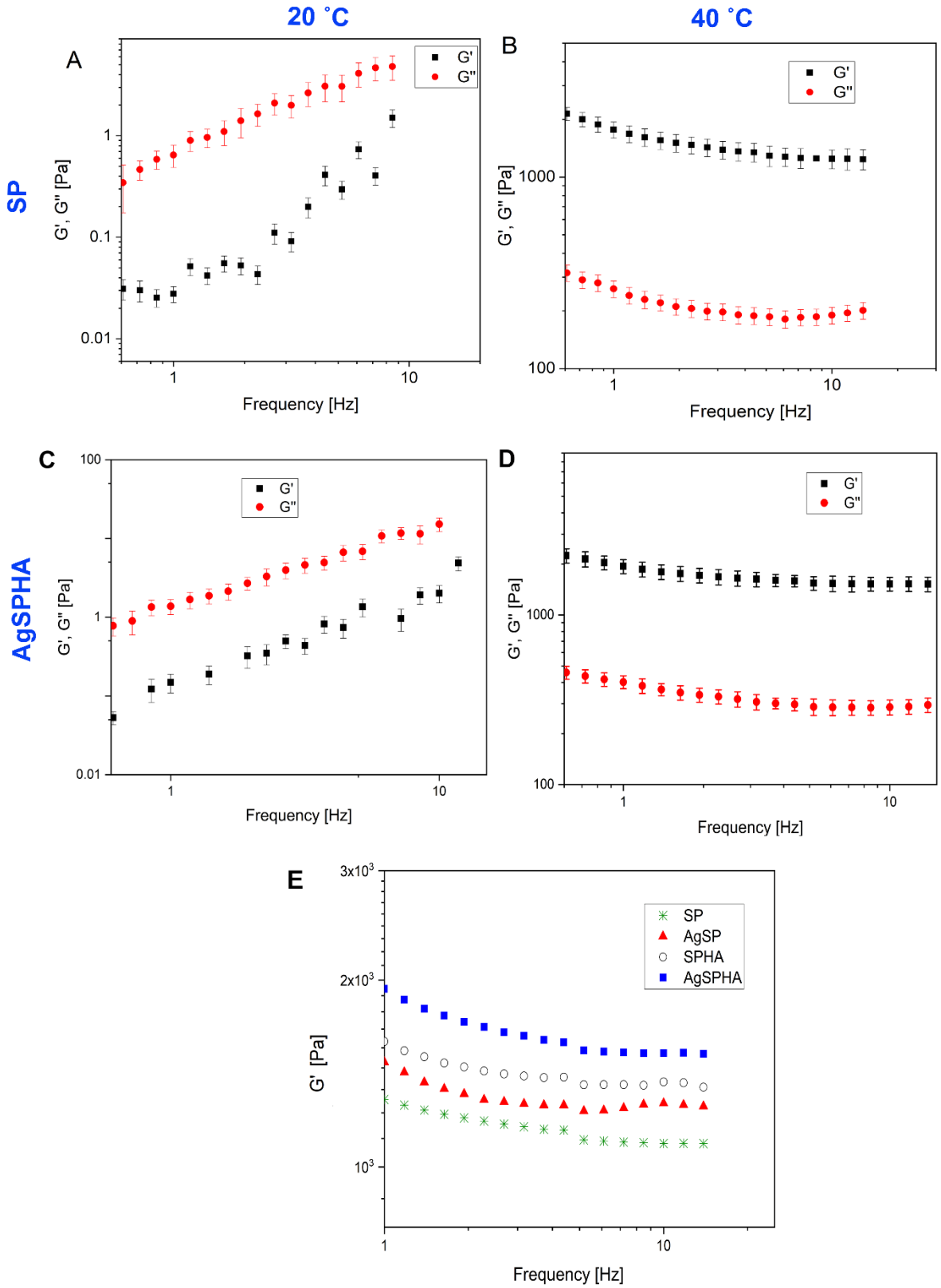
20 ˚C
40 ˚C
SP
AgSPHA
A
B
C
D
E
G'
G"
G', G" [Pa]
Frequency [Hz]
SP
AgSP
SPHA
AgSPHA
G' [Pa]

Fig. 5 Mechanical spectra of SP at 20 ˚C (A) and 40 ˚C (B). Mechanical spectra of AgSPHA at 20 ˚C (C) and 40 ˚C (D). (E) Comparison of elastic modulus as a function of frequency of all samples at 40 ˚C. Results are the means of three measurements.

Comparison of the elastic moduli of all samples as a function of frequency at 40 ˚C are presented in **Fig. 5C** whereas in table 1 the values of the elastic modulus at 1 Hz are reported. Interestingly, the addition of HA to the formulations resulted in an increase of G' from 1284 Pa (SP) to 1593 Pa (SPHA) and from 1475 Pa (AgSP) to 1900 Pa (AgSPHA). The presence of low molecular weight HA into CSE and Pluronics blends leads to an improvement of gel mechanical properties with an increase of elastic modulus in agreement with other literature studies [Mayol et al., 2008, Mayol et al., 2011]. This indicates that some interactions between Pluronics and HA could occur during Pluronic gelation process leading to microstructural changes of the sample due to HA presence [39]. Moreover, further enhancement of gel mechanical properties was achieved by the addition of Ag NPs. The addition of inorganic silver NPs to these Pluronics based materials lead a further reinforcement of systems [42]. The presence of HA leads to an improvement of the visocolaestic moduli and as reported in literature an increase of the mucoadhesive force thus resulting in an increase of formulations residence time and shearing resistance (Mayol et al., 2008). The hydrogel containing both HA and Ag (AgSPHA) has the highest mechanical properties associated with T_{gel} close to body temperature and, therefore, represents a good candidate for wound healing applications.

Fig. 6A shows the effect of storage time on the viscosity of AgSPHA hydrogel at 25˚C. The sample that was stored at 4°C for 7 days shows just a slighlty viscosity reduction compared to the samples at 0 day; but the samples, both before and after the storage, show the same *shear thinning* behavior. Indeed, the viscosity decreases upon shearing and reaches a peseudo-newtonian plateau at higher shear rates. This behaviour is typical of polymeric solutions and physical crosslinked gels and is

due to the breakage of physical bonds and topological interactions among the polymers chain upon the shearing. This leads to higher chain mobility and reduction of friction among polymer segments and the solvent within the hydrogel matrix. The reduction of viscosity at high shear rate and upon the storage is a preferred characteristic of materials that have to be injected through needles since it allows an easier injection (Gloria, Borzacchiello, Causa, & Ambrosio, 2012).

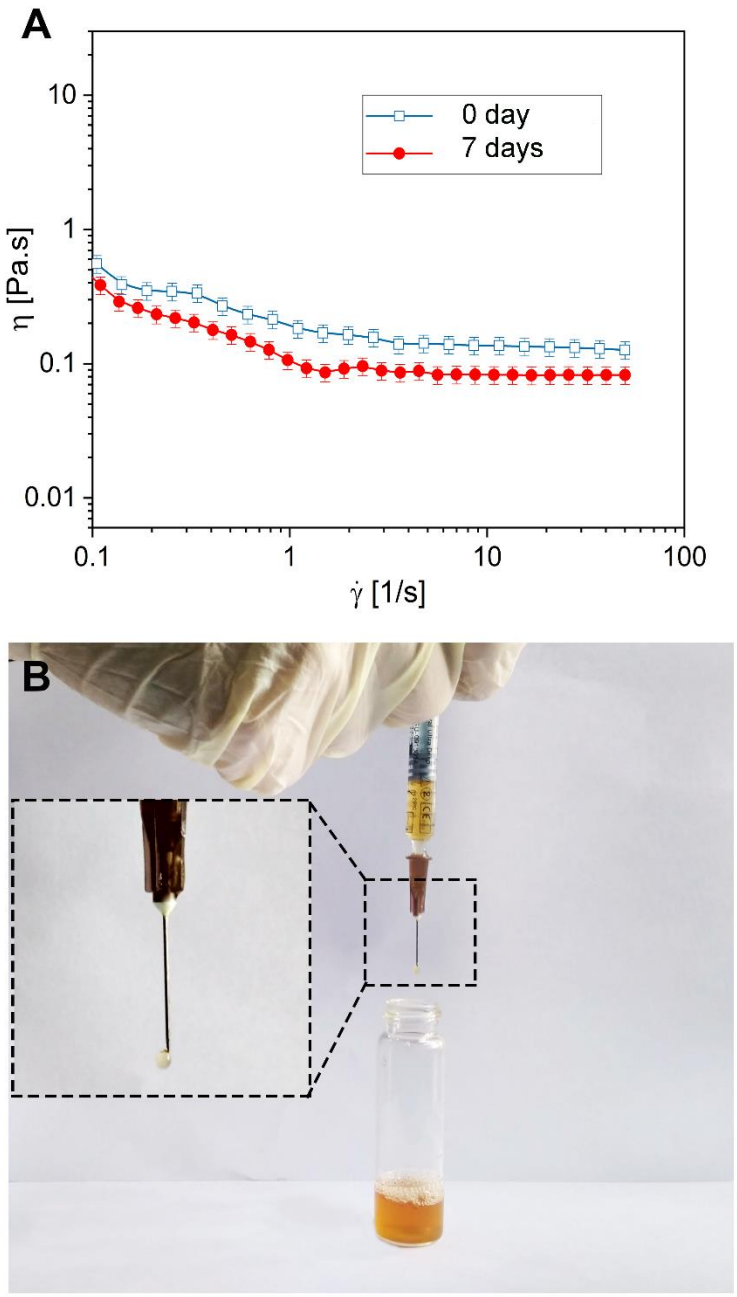

Fig. 6 (A) Shear rate-dependent viscosity changes of AgSPHA composites at 25 ˚C before and after 7 days of storage at 4°C. (B) Injectability test using 1 ml syringe fitted with a 26-G needle.

The formulations prepared with phase-sensitive polymers were tested to see if they were injectable through a 26-G needle (**Fig. 6B**). The hydrogels that can be injected through the needle were

considered as being injectable. This injectability criterion was based on the consideration that many clinical applications employ needles as small as 26-G (Himmelein, Lewe, Stuart, & Ravoo, 2014). The results showed that all thermosensitive hydrogels were injectable through a 26-G needle.

2.7.3. Antibacterial properties

Antibacterial activities of Ag NPs against several types of gram-positive and gram-negative bacteria are shown in **Fig. 7**. The antibacterial capability of the samples is expressed as bacterial reduction percentage in comparison with the control one. The control samples showed no growth inhibition. The results revealed that samples containing Ag NPs $\geq$ 1.7 µg/ml have an excellent growth inhibitory effect (approximately 100%) against all the tested microorganisms. However, at low concentration (0.85 µg/ml), the samples did not show antibacterial activity toward *E. coli* and *B. subtilis*. The antibacterial assay confirmed the capability of the samples in reducing bacterial growth in comparison with the control, and, as expected, improved antimicrobial properties were obtained upon increasing the Ag content.

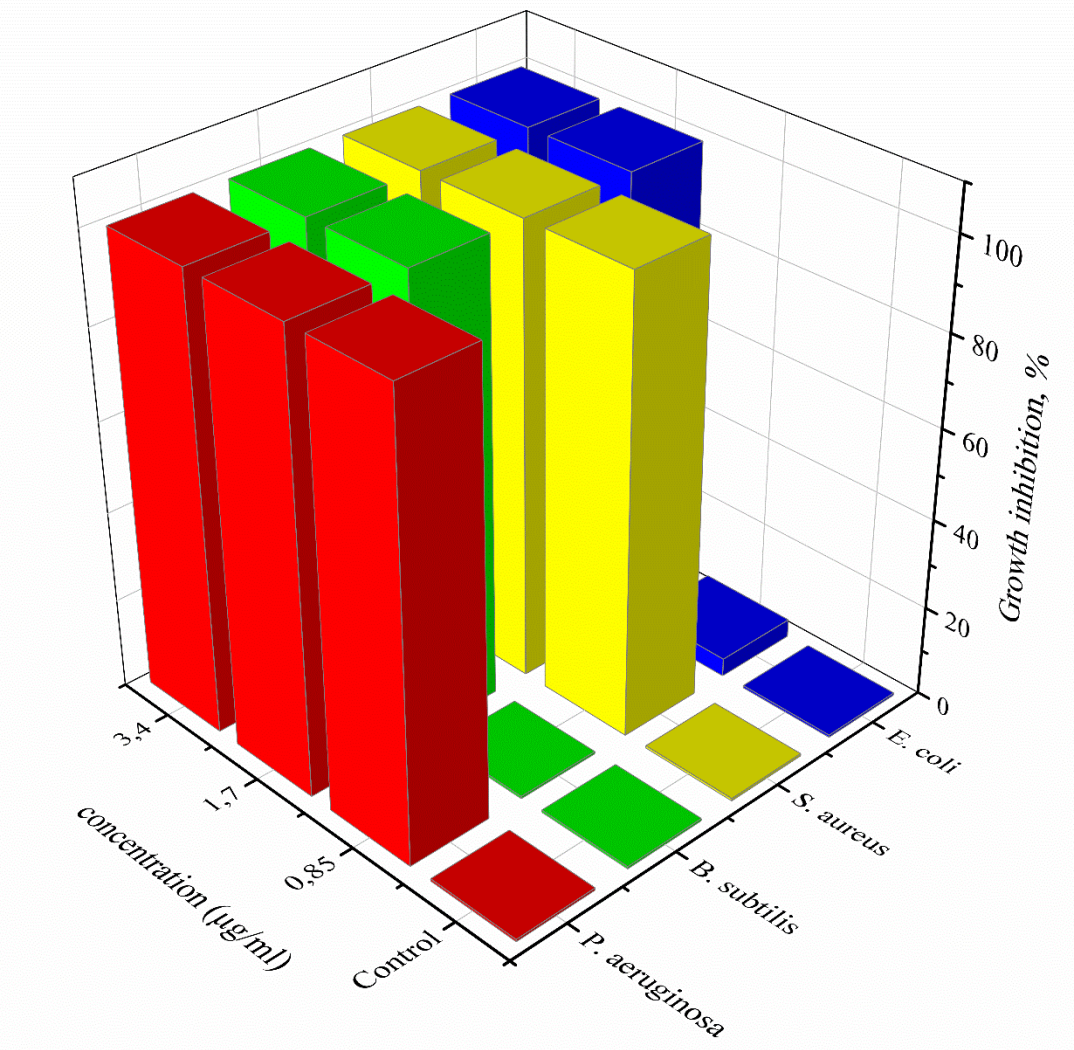

Fig. 7 Antibacterial activity of different concentration of Ag NPs against Gram-positive (*B. subtilis, S. aureus*) and Gram-negative (*P. aeruginosa, E. coli*) bacteria after 24 h The data are representative of 3 experiments in triplicate.

2.7.4. Cell viability and morphology

In order to investigate the biocompatibility of the thermosensitive hydrogels, L929 cells viability was evaluated by Alamar blue assay. It is clear from the results in **Fig. 8A** that the thermosensitive hydrogels samples (SP, Ag SP, SPHA, AgSPHA) showed good safety (cytocompatibility) against L929 cell lines after 24 and 72 h compared to the untreated control. After 24 h of incubation with

all formulations, L929 cells viability is around 100%, noting a cellular viability over 100% for the SP sample. At 72 h for SP sample, which does not contain HA and Ag NPs, the viability had a further increase. Conversely, for the other formulations, the viability decreased slightly at 72 h. In particular, the viability percentage decreases from 100 to 80 for AgSP, and from 101 to 85 for SPHA, as well as from 110 to 70 for AgSPHA. The collected results indicated that no prepared formulations are cytotoxic for the cells, proving good in vitro biocompatibility. According to previous studies in the literature, it has been demonstrated that HA/Pluronic hydrogels do also possess *in-vivo* biocompatibility. For instance, Lee *et al*. [43] developed dopamine-modified HA/Pluronic hydrogels and injected into 6-week-old mice. Inflammatory response and fibrosis were hardly visible after three weeks indicating that the hydrogels were biocompatible and non-immunogenic.

The biocompatibility of the realized thermosensitive hydrogels was also confirmed by cells morphology. Actin filaments, a constituent of the cytoskeleton, were stained with TRIC phalloidin after 24 h. of incubation with SP, Ag SP, SPHA, AgSPHA hydrogels. L929 cells, indeed, exhibited a no cytotoxicity and typical mouse fibroblast-like cellular morphology after incubation with the formulations (**Fig. 8B**). Their morphology was alike to the characteristic *in vitro* L929 cells morphology that is spread or spindle-shaped, often characterized by several extending processes, showing cells protrusion adhering at the flat surface.

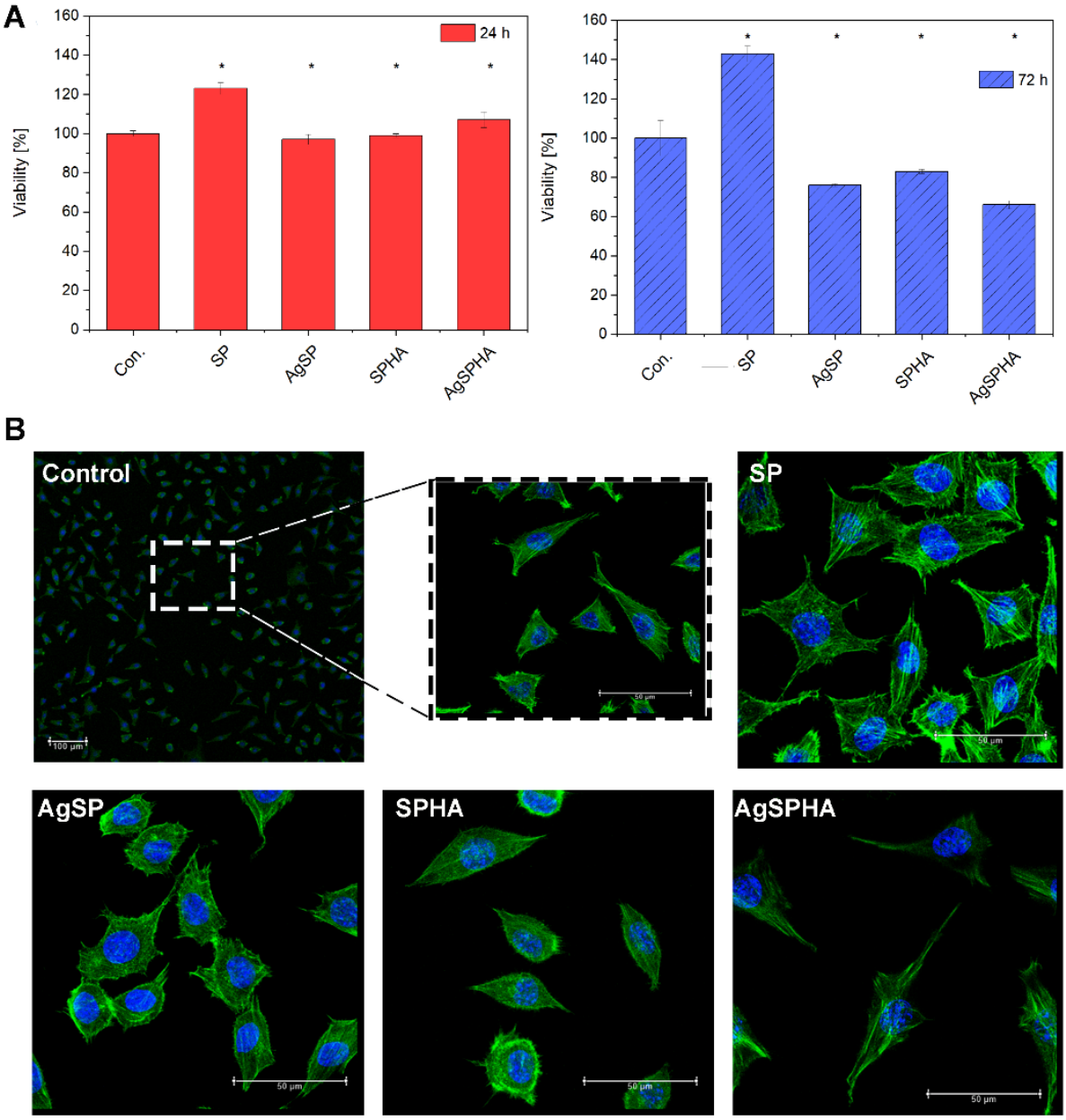

Fig.8 (A) Cytotoxicity of samples at 24 and 72 h. *p*-value < 0.05 for the same symbol as compared to SP. All results are presented as mean ± standard deviation. The data are representatives of three repeated. (B) Cell morphology for the control and thermosensitive hydrogels after 24 h. In Green Actin filaments stained by phalloidin-TRIC and in Blue DAPI stained nuclei cells. The typical cellular morphology of L929 cell lines was used. All bars represent 50 µm, except control which is 100 µm (up left).

2.7.5. Wound Healing Assay

Wound healing on the skin is an evolutionarily conserved, highly coordinated, spatiotemporally regulated process. It occurs over the sequential yet overlapping phases of hemostasis, inflammation, proliferation, and remodeling, and involving multiple cell types including keratinocytes, fibroblasts, and immune, endothelial, and progenitor cells. These steps involve multiple cellular and molecular events tightly controlled by numerous growth factors, chemokines, cytokines, and interleukins, are required to coordinate cell-cell and cell-extracellular matrix (ECM) interactions essential to fully heal a wound [44]. It has been reported in several works the potential of nanomaterials to improve the wound healing process, indeed, nanoscale particles provide for a high probability of interaction with the biological target and an enhanced penetration into the wound sites. Moreover, nanomaterials could exhibit intrinsic properties beneficial for wound treatment and are employed as delivery vehicles for therapeutic agents [45]. For this purpose, the *in vitro* wound healing assay of the realized thermosensitive corn silk extract-nanosilver hydrogels was performed on HDF cells. Representative bright-field images (**Fig. 9A**) show HDF cells, immediately after reproducing the scratch area (time 0) and after 24 and 48 h of incubation with CSE, SPHA, and AgSPHA formulations compared with the control without biomaterials. As it can be seen from **Fig. 9B**, the wound surface area decreases with the time increase (from 24 to 48 h) for all tested formulations and control but at 48 h for the formulations the wound area decreases from about 70 μm^2 to about 20 μm^2 while for the control the area decreases only to 40 μm^2. Interestingly we can observe that already at 24 h the wound area for the AgSPHA sample decreased at about 30 μm^2. Accordingly, the wound closure percentage (**Fig. 9C**) increases with the time increase after exposure to biomaterials and in particular at 48 h the wound closure of tested formulations (80%) increases up to twice compared to the control (40%). Similarly, to the wound area results, already at 24 h the wound closure is about 60% for AgSPHA. These results point out

the effect of the realized nanomaterials in speeding up the wound healing process. The individual biomaterials used in this assay could affect positively the wound healing process. The intrinsic antibacterial properties of silver nanoparticles may be able to mitigate inflammation through cytokine modulation and induce wound healing. Pluronics and more in particular HA, a physiological constituent of human tissues, mimicking the ECM properties, are able to improve cell migration speed, division, ECM production, and proliferation rate, highlighting the importance of the cell microenvironment to enhance wound healing process. However, the innovative component and the common denominator in these tested formulations is represented by CSE. The wound healing assay results show that CSE alone has a positive effect on wound repair. Taken all together the results highlight that CSE has dual function, it acts as medium for green synthesis of Ag nanoparticles along with improving the wound healing ability of the formulations.

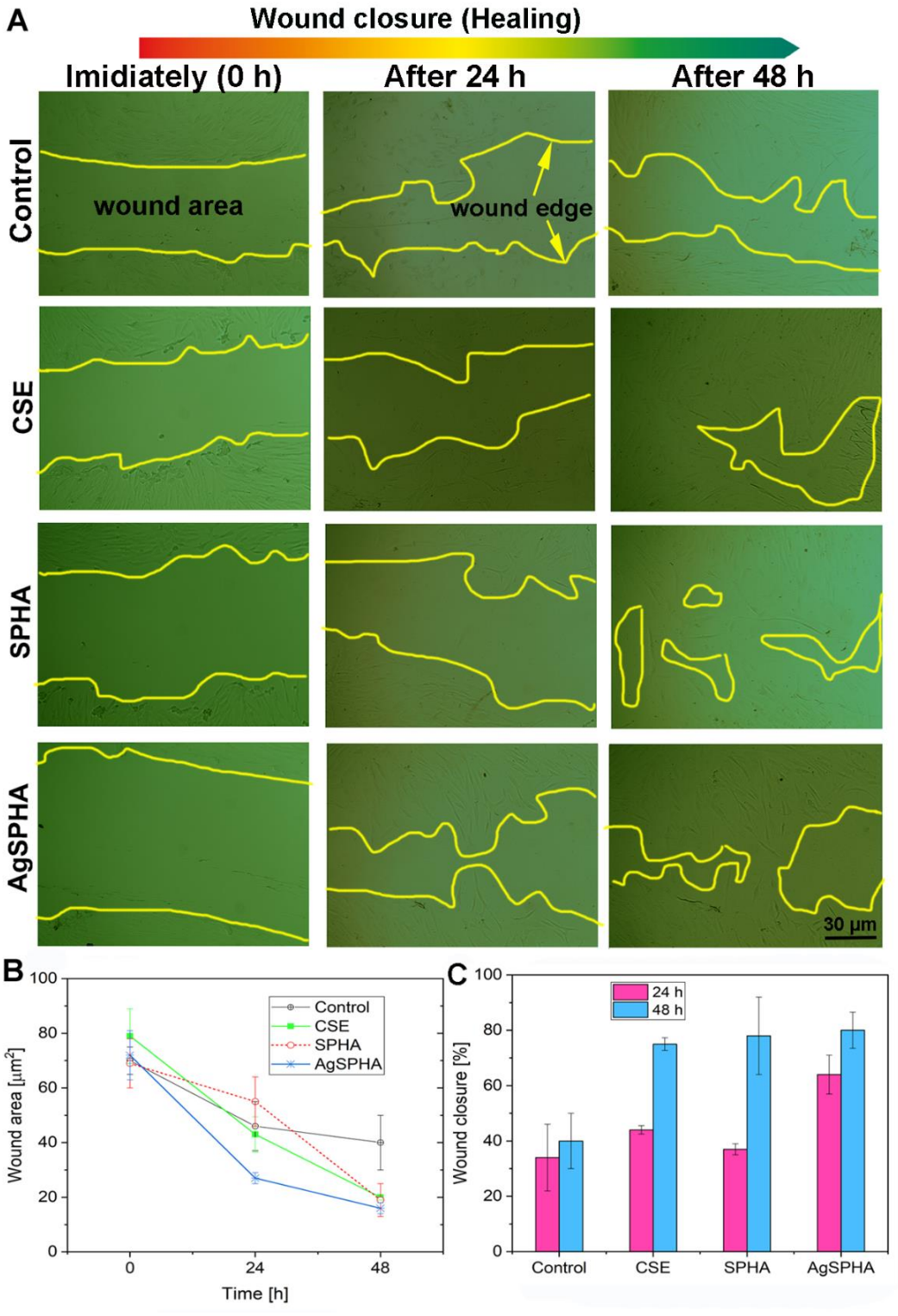

Fig. 9 A) Representative bright-field images show HDF cells migration after the scratch at time 0 and after 24 and 48 h of CSE, SPHA, AgSPHA incubation compared with controls. (B) Wound area expressed as the remaining area uncovered by the cells. The scratch area at time point 0 hours, and after 24 and 48 h of CSE,

SPHA, AgSPHA incubation. (C) Wound closure expressed as the percentage of the closure of the scratched gap after 24 and48 h of CSE, SPHA, AgSPHA incubation. Results are the means of three measurements.

References

[1] C. Longinotti, The use of hyaluronic acid based dressings to treat burns: A review, Burns & trauma 2(4) (2014) 162-168.
[2] N. Ojha, S. Roy, G. He, S. Biswas, M. Velayutham, S. Khanna, P. Kuppusamy, J.L. Zweier, C.K. Sen, Assessment of wound-site redox environment and the significance of Rac2 in cutaneous healing, Free Radic. Biol. Med. 44(4) (2008) 682-691.
[3] N. Bryan, H. Ahswin, N. Smart, Y. Bayon, S. Wohlert, J.A. Hunt, Reactive oxygen species (ROS)–a family of fate deciding molecules pivotal in constructive inflammation and wound healing, Eur Cell Mater 24(249) (2012) e65.
[4] R. Rutan, Physiologic response to cutaneous burn injury, Carrougher GJ. Burn care and therapy. St. Louis: Mosby (1998) 9-11.
[5] J. Kearney, Quality issues in skin banking: a review, Burns 24(4) (1998) 299-305.
[6] L.K. Branski, D.N. Herndon, C. Pereira, R.P. Mlcak, M.M. Celis, J.O. Lee, A.P. Sanford, W.B. Norbury, X.-J. Zhang, M.G. Jeschke, Longitudinal assessment of Integra in primary burn management: a randomized pediatric clinical trial, Crit. Care Med. 35(11) (2007) 2615-2623.
[7] W. Haslik, L.-P. Kamolz, G. Nathschläger, H. Andel, G. Meissl, M. Frey, First experiences with the collagen-elastin matrix Matriderm® as a dermal substitute in severe burn injuries of the hand, Burns 33(3) (2007) 364-368.
[8] S. Dhivya, V.V. Padma, E. Santhini, Wound dressings–a review, Biomedicine 5(4) (2015).
[9] B. Kvam, E. Fragonas, A. Degrassi, C. Kvam, M. Matulova, P. Pollesello, F. Zanetti, F. Vittur, Oxygen-derived free radical (ODFR) action on hyaluronan (HA), on two HA ester derivatives, and on the metabolism of articular chondrocytes, Exp. Cell Res. 218(1) (1995) 79-86.
[10] D. Presti, J.E. Scott, Hyaluronan-mediated protective effect against cell damage caused by enzymatically produced hydroxyl (OH·) radicals is dependent on hyaluronan molecular mass, Cell Biochemistry and Function: Cellular biochemistry and its modulation by active agents or disease 12(4) (1994) 281-288.
[11] V. Ki, C. Rotstein, Bacterial skin and soft tissue infections in adults: a review of their epidemiology, pathogenesis, diagnosis, treatment and site of care, Canadian Journal of Infectious Diseases and Medical Microbiology 19(2) (2008) 173-184.
[12] A.F. Cardona, S.E. Wilson, Skin and soft-tissue infections: a critical review and the role of telavancin in their treatment, Clin. Infect. Dis. 61(suppl_2) (2015) S69-S78.
[13] S. Das, A.B. Baker, Biomaterials and nanotherapeutics for enhancing skin wound healing, Frontiers in bioengineering and biotechnology 4 (2016) 82.
[14] G. Suarato, R. Bertorelli, A. Athanassiou, Borrowing from Nature: biopolymers and biocomposites as smart wound care materials, Frontiers in bioengineering and biotechnology 6 (2018).

[15] P. Makvandi, M. Ghaemy, M. Mohseni, Synthesis and characterization of photo-curable bis-quaternary ammonium dimethacrylate with antimicrobial activity for dental restoration materials, Eur. Polym. J. 74 (2016) 81-90.
[16] P. Makvandi, R. Jamaledin, M. Jabbari, N. Nikfarjam, A. Borzacchiello, Antibacterial quaternary ammonium compounds in dental materials: A systematic review, Dental Materials 34(6) (2018) 851-867.
[17] P. Makvandi, C. Esposito Corcione, F. Paladini, A.L. Gallo, F. Montagna, R. Jamaledin, M. Pollini, A. Maffezzoli, Antimicrobial modified hydroxyapatite composite dental bite by stereolithography, Polymers for Advanced Technologies (2017).
[18] V.K.H. Bui, D. Park, Y.-C. Lee, Chitosan combined with ZnO, TiO2 and Ag nanoparticles for antimicrobial wound healing applications: a mini review of the research trends, Polymers 9(1) (2017) 21.
[19] P. Makvandi, N. Nikfarjam, N. Sanjani, N. Qazvini, Effect of silver nanoparticle on the properties of poly(methyl methacrylate) nanocomposite network made by in situ photoiniferter-mediated photopolymerization, Bull Mater Sci 38(6) (2015) 1625-1631.
[20] R. Lalani, L. Liu, Electrospun zwitterionic poly (sulfobetaine methacrylate) for nonadherent, superabsorbent, and antimicrobial wound dressing applications, Biomacromolecules 13(6) (2012) 1853-1863.
[21] M. Pattabi, J. Uchil, Synthesis of cadmium sulphide nanoparticles, Solar energy materials and solar cells 63(4) (2000) 309-314.
[22] J.K. Patra, K.-H. Baek, Green nanobiotechnology: factors affecting synthesis and characterization techniques, Journal of Nanomaterials 2014 (2014) 219.
[23] J.K. Patra, K.-H. Baek, Antibacterial activity and synergistic antibacterial potential of biosynthesized silver nanoparticles against foodborne pathogenic bacteria along with its anticandidal and antioxidant effects, Frontiers in microbiology 8 (2017) 167-182.
[24] K. Hasanudin, P. Hashim, S. Mustafa, Corn silk (Stigma maydis) in healthcare: a phytochemical and pharmacological review, Molecules 17(8) (2012) 9697-9715.
[25] S. Habtemariam, Extract of corn silk (Stigma of Zea mays) inhibits tumour necrosis factor-α- and bacterial lipopolysaccharide-induced cell adhesion and ICAM-1 expression, Planta medica 64(04) (1998) 314-318.
[26] O. Rau, M. Wurglics, T. Dingermann, M. Abdel-Tawab, M. Schubert-Zsilavecz, Screening of herbal extracts for activation of the human peroxisome proliferator-activated receptor, Die Pharmazie 61(11) (2006) 952-956.
[27] H. Weinkauf, B.F. Brehm-Stecher, Enhanced dark field microscopy for rapid artifact-free detection of nanoparticle binding to Candida albicans cells and hyphae, Biotechnology Journal: Healthcare Nutrition Technology 4(6) (2009) 871-879.
[28] K. Al Khateb, E.K. Ozhmukhametova, M.N. Mussin, S.K. Seilkhanov, T.K. Rakhypbekov, W.M. Lau, V.V. Khutoryanskiy, In situ gelling systems based on Pluronic F127/Pluronic F68 formulations for ocular drug delivery, International journal of pharmaceutics 502(1-2) (2016) 70-79.
[29] W.I. Abdel-Fattah, N. Atwa, G.W. Ali, Influence of the protocol of fibroin extraction on the antibiotic activities of the constructed composites, Progress in biomaterials 4(2-4) (2015) 77-88.
[30] P. Kumar, V.-K. Lakshmanan, R. Biswas, S.V. Nair, R. Jayakumar, Synthesis and biological evaluation of chitin hydrogel/nano ZnO composite bandage as antibacterial wound dressing, Journal of biomedical nanotechnology 8(6) (2012) 891-900.

[31] C.-C. Liang, A.Y. Park, J.-L. Guan, In vitro scratch assay: a convenient and inexpensive method for analysis of cell migration in vitro, Nature protocols 2(2) (2007) 329.
[32] A. Grada, M. Otero-Vinas, F. Prieto-Castrillo, Z. Obagi, V. Falanga, Research techniques made simple: analysis of collective cell migration using the wound healing assay, J. Invest. Dermatol. 137(2) (2017) e11-e16.
[33] W.I. Abdel-Fattah, A.S.M. Sallam, N.A. Atwa, E. Salama, A.M. Maghraby, G.W. Ali, Functionality, antibacterial efficiency and biocompatibility of nanosilver/chitosan/silk/phosphate scaffolds 1. Synthesis and optimization of nanosilver/chitosan matrices through gamma rays irradiation and their antibacterial activity, Materials Research Express 1(3) (2014) 035024.
[34] T.G.F. Souza, V.S.T. Ciminelli, N.D.S. Mohallem, A comparison of TEM and DLS methods to characterize size distribution of ceramic nanoparticles, IOP Publishing, 2017, p. 012039.
[35] M. Kaasalainen, V. Aseyev, E. von Haartman, D.Ş. Karaman, E. Mäkilä, H. Tenhu, J. Rosenholm, J. Salonen, Size, stability, and porosity of mesoporous nanoparticles characterized with light scattering, Nanoscale research letters 12(1) (2017) 74-83.
[36] H. Tamiyakul, S.T. Dubas, W. Warisnoicharoen, Preparation and Characterization of Hydrocolloid Stabilized Silver Nanoparticles, Advanced Materials Research 1060 (2015) 115-118.
[37] R.A. Muzzarelli, Chitosan composites with inorganics, morphogenetic proteins and stem cells, for bone regeneration, Carbohydrate Polymers 83(4) (2011) 1433-1445.
[38] L. Mayol, M. Biondi, F. Quaglia, S. Fusco, A. Borzacchiello, L. Ambrosio, M.I. La Rotonda, Injectable thermally responsive mucoadhesive gel for sustained protein delivery, Biomacromolecules 12(1) (2010) 28-33.
[39] L. Mayol, F. Quaglia, A. Borzacchiello, L. Ambrosio, M.I. La Rotonda, A novel poloxamers/hyaluronic acid in situ forming hydrogel for drug delivery: rheological, mucoadhesive and in vitro release properties, European Journal of Pharmaceutics and Biopharmaceutics 70(1) (2008) 199-206.
[40] C. Ju, J. Sun, P. Zi, X. Jin, C. Zhang, Thermosensitive micelles–hydrogel hybrid system based on poloxamer 407 for localized delivery of paclitaxel, Journal of pharmaceutical sciences 102(8) (2013) 2707-2717.
[41] W.S. Shim, J.S. Yoo, Y.H. Bae, D.S. Lee, Novel injectable pH and temperature sensitive block copolymer hydrogel, Biomacromolecules 6(6) (2005) 2930-2934.
[42] A.K. Gaharwar, N.A. Peppas, A. Khademhosseini, Nanocomposite hydrogels for biomedical applications, Biotechnology and bioengineering 111(3) (2014) 441-453.
[43] Y. Lee, H.J. Chung, S. Yeo, C.-H. Ahn, H. Lee, P.B. Messersmith, T.G. Park, Thermo-sensitive, injectable, and tissue adhesive sol–gel transition hyaluronic acid/pluronic composite hydrogels prepared from bio-inspired catechol-thiol reaction, Soft Matter 6(5) (2010) 977-983.
[44] S. Hamdan, I. Pastar, S. Drakulich, E. Dikici, M. Tomic-Canic, S. Deo, S. Daunert, Nanotechnology-driven therapeutic interventions in wound healing: potential uses and applications, ACS central science 3(3) (2017) 163-175.
[45] I. Kalashnikova, S. Das, S. Seal, Nanomaterials for wound healing: scope and advancement, Nanomedicine 10(16) (2015) 2593-2612.

Chapter 3

Antibacterial injectable hydrogels based on hyaluronic acid/Ag Nanoparticles as biomimetic scaffold for bone regeneration

Abstract

Injectable hydrogels have revealed the great potential for use as scaffolds in cartilage and bone tissue engineering. Here, thermosensitive and injectable hydrogels containing β-tricalcium phosphate, hyaluronic acid, and corn silk extract-nanosilver (CSE-Ag NPs) were synthesized for their potential use in bone tissue regeneration applications. Spherical nanoparticles of silver were biosynthesized through microwave-assisted green approach using CSE in organic solvent-free medium. Rheological experiments demonstrated that the thermosensitive hydrogels have gelification temperature (T_{gel}) close to body temperature. The samples containing Ag NPs showed antibacterial activity toward gram-positive (*Bacillus Subtilis, Staphylococcus Aureus*) and gram-negative (*Pseudomonas Aeruginosa, Escherichia Coli*) bacteria along without cytotoxicity after 24 h. Mesenchymal stem cells seeded in the nanocomposite exhibited high bone differentiation which indicate that they could be a good candidate as a potential scaffold for bone tissue regeneration.

Keywords: Thermosensitive hydrogels, bone tissue engineering, green synthesis, antibacterial properties, corn silk extract

3.1. Introduction

3.1.1. Scaffolds

Evidences of clinical needs related to bone reconstruction date back to ancient Egypt and made their ways up-to-date. A more rigorous scientific method has been followed since 1889, when "modern" researchers began to focus their efforts on what can be defined as the early bone tissue regeneration [1]. Even if nowadays we are talking about several hundred millions of surgical intervention per year, worldwide, the current clinical gold standard for the treatment of critical sized and non-union bone defects still remains autograft bone. Being advantageous for immunocompatibility, autografts nevertheless carry a wide spectrum of risks such as general anaesthesia, complex surgical manoeuvres, secondary infections, secondary fractures, pain, site morbidity, *etc*.; since they lead to high percentage of failure (more the 10%) and that are also followed by important costs increases [2-4]. Furthermore, it is generally accepted that not all the defects can be addressed, particularly the bigger ones, as far as few healthy sites can be harvested without loss of function [4].

The need of adequate bone substitutes for the remodeling of native bone tissue is hence evident and sees a wide spectrum of proposed solutions, belonging to academia, clinics and industry [5].

In this framework, surgeons can choose from substitutes that can be divided into three main categories, a part from autografts:

1) allografts, *i.e.* bone segments taken from cadavers and duly sterilized;

2) xenografts, *i.e.* bone segments taken from animal bones (bovine, equine, porcine, *etc*.), duly acellularized and sterilized;

3) synthetic scaffolds.

Allografts derived from cadavers bone have been an accepted alternative, but concerns related to diseases transmission, toxicity associated with sterilization needed methods, immunologic rejection risks and very high sample variability are progressively leading to other alternatives, when these are available; the challenge still remains an open scientific and clinical topic but current focus remains on autografting versus xenografts and synthetic ones [1].

Cartilage and subchondral bone damage can be caused by a variety of conditions, such as trauma, arthritis, and sports-related injuries. Bone defects are one of the leading causes of morbidity and disability in elderly patients.18 Medical restoration of the damaged cartilage and bone tissue remains to be achieved. Therefore, developing a method to perfectly and permanently repair the damaged cartilage and bone tissue is of significant clinical interest for patients with cartilage lesions and bone defects. To fully reconstruct the damaged cartilage and bone tissue, it is important to synthesize biocompatible and biodegradable scaffolds that mimic the native features of the specific tissue, successfully transport cells and growth factors to the damaged tissue, and provide support to the newly formed tissue until it matures [6-10].

The scaffold, by definition, is a temporary supporting structure for growing cells and tissues. It is also called synthetic extracellular matrix (ECM) and plays a critical role in supporting cells. These cells then undergo proliferation, migration, and differentiation in three dimensions, which leads to the formation of a specific tissue with appropriate functions as would be found in the human body. To facilitate these measures, the scaffold should possess a few basic characteristics.

Synthetic bone graft materials available as alternatives to autogenous bone for repair, substitution or augmentation include: metals; resorbable and non-resorbable polymers; inert ceramics (e.g., alumina, zirconia); special glass ceramics described as bioactive glasses; calcium sulfates, calcium carbonates and calcium phosphates (CaP). These inorganic materials differ in composition and physical properties from each other and from bone. Since bone

mineral is made of non-stoichiometric and polysubstituted CaP apatite, CaP materials were rapidly preferred as they can be part of the bone remodeling process. Based on composition, synthetic calcium phosphates presently used as biomaterials are classified as calcium hydroxyapatite (HA), $Ca_{10}(PO_4)_6(OH)_2$; and alpha- or beta-tricalcium phosphate (a- or b-TCP), $Ca_3(PO_4)_2$ [11]. In fact, in bone tissue engineering, biomimetic scaffolds comprising calcium phosphate bioceramics, e.g. β-tricalcium phosphate (β-TCP) and hydroxyapatite, are aimed to serve as an artificial temporary extracellular matrix in order to support cell adhesion and guide new bone tissue formation [12-14].

The following section highlights the general characteristics of a scaffold that are desirable for most tissue engineering applications [15]. Biomedical scaffolds for tissue engineering should meet several design criteria [7, 16, 17]:

- The surface should permit cell adhesion, promote cell growth, and allow the retention of differentiated cell functions;
- The scaffolds should be biocompatible, neither the polymer nor its degradation by-products should provoke inflammation or toxicity *in vivo*;
- The scaffold should be biodegradable and eventually eliminated;
- The implanted scaffold must have sufficient mechanical integrity to function from the time of implantation to the completion of the remodeling process. A balance between mechanical properties and sufficient porous architecture to allow cell infiltration and vascularization is key to the success of any scaffold;
- The porosity should be high enough to provide sufficient space for cell adhesion, extracellular matrix (ECM) regeneration and minimal diffusional constraints during culture, and the pore structure should be interconnected to allow even spatial homogeneous tissue formation. Cells primarily interact with scaffolds via chemical

groups (ligands) on the material surface. Scaffolds synthesized from natural extracellular materials (e.g. collagen) naturally possess these ligands in the form of Arg-Gly-Asp (RGD) binding sequences, whereas scaffolds made from synthetic materials may require deliberate incorporation of these ligands through, for example, protein adsorption. The ligand density is influenced by the specific surface area of pores to which cells can adhere. Pores thus need to be large enough to allow cells to migrate into the structure, where they eventually become bound to the ligands within the scaffold, but small enough to establish a sufficiently high specific surface, leading to a minimal ligand density to allow efficient binding of a critical number of cells to the scaffold. Therefore, for any scaffold, a critical range of pore sizes exists which may vary depending on the cell type used and tissue being engineered;

- The material should be reproducible and processable into three-dimensional structures with properties or design variables tailored for the intended scaffold application and environment into which the scaffold will be placed.

For tissue scaffold applications the following key properties can be analyzed:

- Physical properties (compressive stress and modulus, storage and loss modulus, porosity, density and swelling ratios)
- Degradation properties (enzymatic degradation, swelling studies)
- Biological properties (in vitro and in vivo studies, cell culture, histology, immunology)

3.1.2. Injectable hydrogels

Recently, injectable hydrogel scaffolds have attracted the attention of biomaterials scientists for cartilage- and bone tissue-engineering applications, because they can replace implantation surgery with a minimally invasive injection method and can form any desired shape, to match

irregular defects [18-20]. The schematic describing injectable hydrogels for cartilage- and bone tissue-engineering applications is illustrated in **Fig. P1**. Excellent biomaterials and appropriate fabrication methods play crucial roles in developing ideal injectable hydrogels that can function as scaffolds for cartilage and bone tissue-engineering applications. A variety of biomaterials, both natural and synthetic, have been exploited to prepare injectable hydrogels; these biomaterials include chitosan [18], collagen or gelatin[20, 21], alginate [22], hyaluronic acid [23, 24], heparin [25], chondroitin sulfate [26], poly (ethylene glycol) (PEG) [27], and poly(vinyl alcohol) [28].

Smart injectable hydrogels that are sensitive to temperature changes have recently attracted substantial attention for applications in cartilage tissue engineering, because of their gelation ability at physiological temperature. These injectable hydrogels are present in aqueous form at room temperature, but they rapidly gel at physiological temperature before solidifying in the desired tissue [29, 30]. The threshold temperature at which hydrogels transform from a solution to a hydrogel state is defined as the lower critical solution temperature. The most useful characteristic of temperature-sensitive hydrogels is that they can undergo a phase transition without any chemical stimulus. To date, the most common explanation of the phase transition mechanism of temperature-sensitive injectable hydrogels is that when the temperature changes, there is a change in the hydration state favoring intra- and intermolecular hydrogen bonding, thus eventually changing the hydrogel solubility [31, 32].

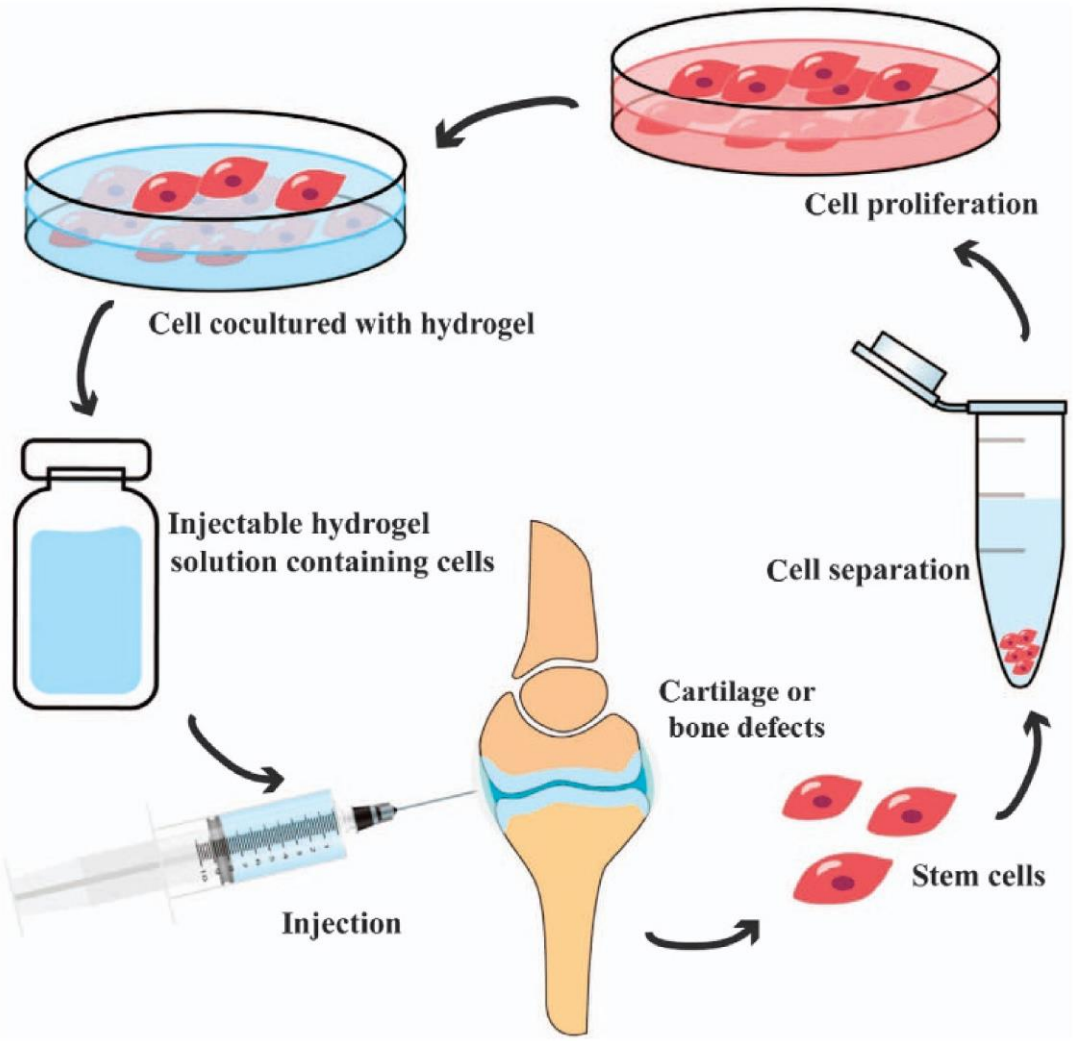

Fig P1. Schematic illustration of approaches to make injectable hydrogels for cartilage- and bone tissue-engineering applications [10].

Various biomaterials have been exploited for the fabrication of injectable hydrogel scaffolds for cartilage tissue engineering applications, including natural biomaterials and synthetic biomaterials. Natural biomaterial-based injectable hydrogels have been widely investigated because of their perfect biocompatibility, biodegradability, and similarity to the ECM [10].

Hyaluronic acid, which interacts with chondrocytes through surface receptors such as CD44 and RHAMM [33], is a linear polysaccharide in the adult cartilage ECM and is composed of disaccharide units of glucuronic acid and N-acetylglucosamine [34]. Hyaluronic acid plays very important roles in cartilage and limb bud formation, mesenchymal cell condensation,

chondrocyte matrix deposition, and chondrogenic differentiation [35]. Therefore, hyaluronic acid is regarded as an ideal biomaterial for cartilage tissue repair. Yu et al. [36] have fabricated an injectable hyaluronic acid/PEG hydrogel with excellent mechanical properties for cartilage tissue engineering. Cells encapsulated in the hydrogel in situ demonstrate high metabolic viability and proliferation. In addition, taking advantage of its biocompatibility, structural similarity to glycosaminoglycan, and ready formation of ionic complexes of chitosan, Park et al. [37] have successfully fabricated an injectable chitosan–hyaluronic acid hydrogel utilizing hyaluronic acid and methacrylated glycol chitosan. Chondrocytes encapsulated in the hydrogel show excellent proliferation and increased deposition of cartilaginous ECM; considering these results, this hydrogel has great potential for cartilage tissue repair. The physical and degradation properties of HA based scaffolds largely depend on the molecular weight of HA, whether HA is composited with another polymer, degree of grafting, crosslinker type and crosslink densities. Biological properties are largely influenced by interactions with cell surface receptors [8].

However, infections during or post scaffold transplantation are still challenging as they reduce the efficacy of bone healing [38]. After the transplantation, infections may also be distributed to the scaffold from other sources of inflammation through bloodstream [39]. In fact, the ideal tactic for bone regeneration is that tissue integration occurs prior to bacterial adhesion, thereby preventing material colonization for bacterial species. The growth of antibiotic-resistant bacterial strains has encouraged the researchers to develop novel antibacterial strategies [40]. Besides, the administration of antibiotic only possesses an initial burst followed by short antibiotic release and efficiency [41]. Hence, materials containing antimicrobial compounds, such as quaternary ammonium salts [42-44], TiO_2 [45], and silver nanoparticles (Ag NPs) [46] have been utilized to overcome infection. Between these compounds, Ag NPs have shown a

strong capability to inhibit or decline infections and have been also utilized for bone regeneration applications [47].

Methodologies of NPs synthesis

There are two approaches for synthesizing nanomaterials: top-down and bottom-up approaches (**Table M1**). “Top down” and “bottom up” are the two unique methodologies for the amalgamation of NPs. In top-to-bottom approach, suitable bulk material is broken down into smaller fine particles by size reduction using various techniques like grinding, milling, sputtering, thermal/laser ablation, etc. while in bottom-to-top approach, NPs are synthesized using chemical and biological methods by self-assembly of atoms to new nuclei, which grow into nanosize particles while the “bottom-up” methods include chemical reduction, electrochemical methods and sonodecomposition [1, 48, 49].

Physical approach

Physical approach for synthesizing NPs is mainly “top-down” approach in which the material is reduced in size by various physical approaches like ultra-sonication, microwave (MW) irradiation, electrochemical method etc. In this approach, a tube heater is utilized at barometrical weight for integrating NPs by evaporation condensation. Evaporation condensation and laser removal are the most essential physical methodologies. The source material inside a pontoon focused at the heater is vaporized into a bearer gas. Utilizing this dissipation build-up procedure different NPs of Ag, Au, PbS and Cd have been synthesized and reported already [48]. It should be noted that the materials employed for synthesis of nanostructures determine toxicity. For example, conversion of metal ions to metal nanoparticles using a plant extract with microwave-assisted approach is classified as a green method because the reducing- and stabilizing-agents are derived from non-toxic plant extracts.

Table M1. Techniques for synthesis of metal nanomaterials. The "assisted-methods" may be used for both green synthesis and chemical synthesis. The materials employed for synthesis of nanostructures determine toxicity.

Bottom-up approaches			**Top-down approaches**
Green methods	**Assisted-methods**	**Chemical methods**	**Physical methods**
Using microorganism Fungi Yeasts Bacteria Cell lines	Ultrasonic Photochemical Microwave Autoclaving	Chemical reduction Pyrolysis Electrochemical	Pulsed laser ablation Evaporation–condensation Arc discharge Spray pyrolysis Ball milling Vapor and gas phase Pulse wire discharge
Using Plant Plant and their extracts Plant biomasses Fruit juices Alga and diatoms			
Enzymes and other biomolecules			
Non-toxic methods		**Toxic methods**	

Chemical approach

In the chemical approach, the main components are the metallic precursors, stabilizing agents and reducing agents (inorganic and organic both). Reducing agents such as sodium citrate, ascorbate, sodium borohydride ($NaBH_4$), elemental hydrogen, polyol process, tollens reagent, *N*,*N*-dimethylformamide (DMF) and poly(ethylene glycol)- block copolymers are used [50]. Solvents and reducing operators utilized for the reduction of the NPs have great effect on morphology of incorporated particles like their size, physicochemical properties, shape and this morphology impacts on the utilization of NPs [51].

Green synthesis

Traditional methods are used from past many years but researches have proved that the green methods are more effective for the generation of NPs with the advantage of less chances of failure, low cost and ease of characterization. Physical and chemical approaches of synthesizing NPs have posed several stresses on environment due to their toxic metabolites. Plant-based synthesis of NPs is certainly not a troublesome procedure, a metal salt is synthesized with plant extract and the response is completed in minutes to couple of hours at typical room temperature. This strategy has attracted much more attention amid the most recent decade particularly for silver (Ag) and gold (Au) NPs, which are more secure as contrasted with other metallic NPs. Generation of NPs from green techniques can be scaled up effortlessly and they are fiscally smart too. In light of their exceptional properties the greenly orchestrated NPs are currently favored over the traditionally delivered NPs. Use of more chemicals, which are harmful and toxic for human health and environment, could increase the particle reactivity and toxicity and might cause unwanted adverse effects on health because of their lack of assurance and uncertainty of composition [50]. Green

methods of synthesis are significantly attractive because of their potential to reduce the toxicity of NPs. Accordingly, the use of vitamins, amino acids, plants extracts is being greatly popularized nowadays [51].

Green chemistry may be used for obtaining new metal nanoarchitectures with controlled shape and size. These nanomaterials are less toxic when compared to nanoarchitectures synthetized by conventional methods using sodium citrate, ascorbate, sodium borohydride, CTAB or Tollens reagent. Green chemistry is a low cost and efficient approach for synthesis of metal NPs. However, there are several concerns including acute and chronic toxicity, immunogenicity, biodegradability, bioaccumulation, disease-targeting ability, as well as scalable industrial production that are yet to be addressed before green synthesis can be scaled up for industrial applications [50, 52].

The use of green chemistry for synthesizing new metal nanoarchitectures has been a target of intense research over the last decade. Plant-based materials, e.g. plant extract, have been used in this capacity as stabilizing agents and for reduction of metal ions, such as conversion of Ag^{+} to Ag^{0} (Ag NPs) or from Au^{+} to Au^{0} (Au NPs)[45]. There are five routes for synthesizing metal nanostructures using Plant-based materials: a. ambient condition such as mixing at room temperature; b. temperature-assisted method such as hydrothermal and regular heating using thermal stirrer; c. microwave-assisted technique; d. sonochemistry by means of ultrasonics; e. photochemistry by means of UV-visible light irradiation. The methods for green synthesis of metallic and metal oxide nanostructures via the use of various gums are summarized in **Fig. 2**.

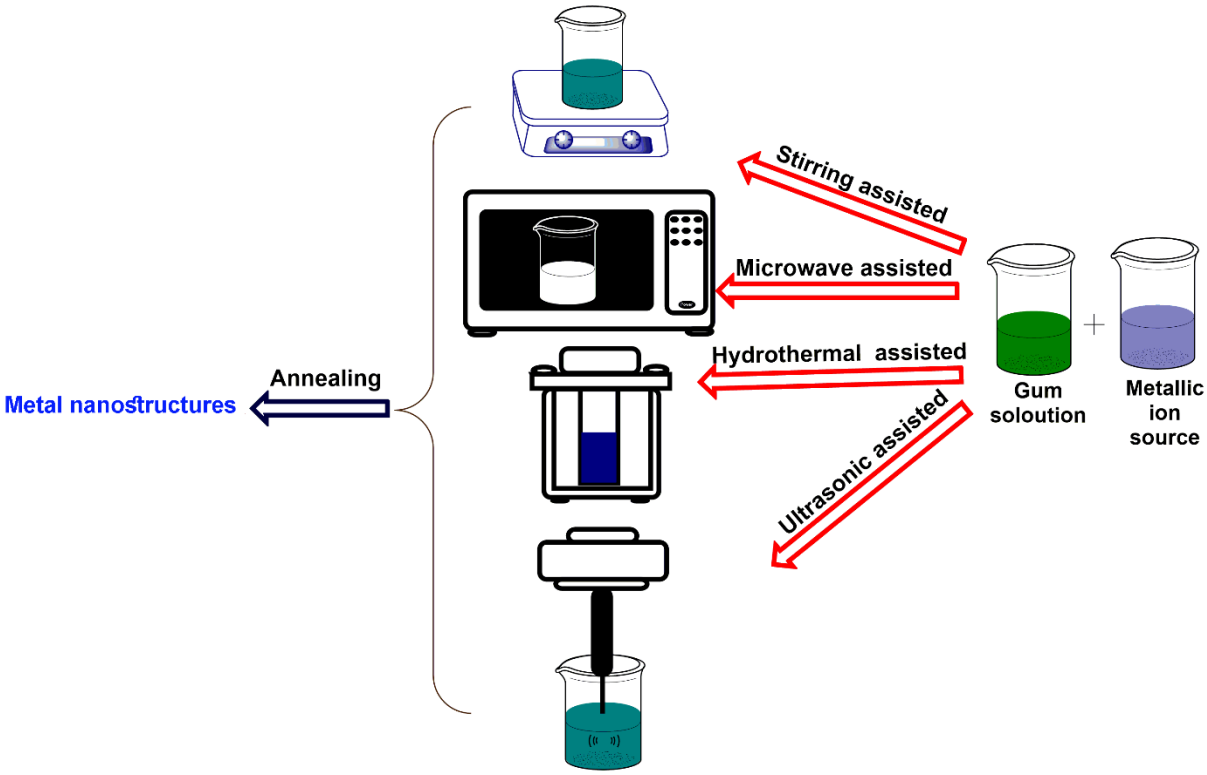

Fig. 2. Different methods for green synthesis of metallic and metal oxide nanostructures using various gums.

Corn silk extract (CSE), which is a waste material of the crop, has been used for the green synthesis of silver NPs as both bioreducing and capping agent, thus, allowing the elimination of any other toxic organic solvents and chemical agents [53]. In vivo study revealed that CSE is also effective to repair the histological profile of ovariectomized rat bone [54].Considering the properties of β-TCP, HA, and Ag NPs, our work aimed to fabricate thermosensitive biocomposite hydrogels for bone tissue repair to be easily injected which possess antimicrobial functions to prevent infection. Therefore, here, we produced silver nanoparticles by using CSE in an aqueous medium via microwave-assisted approach in an organic solvent-free process that is completely biocompatible and nontoxic. Subsequently, the Ag NPs were included in Pluronic/HA/β-TCP/CSE hydrogels to

formulate thermosensitive nanocomposites with sol/gel transition at body temperature for potential use in bone regeneration (**Figure M3**).

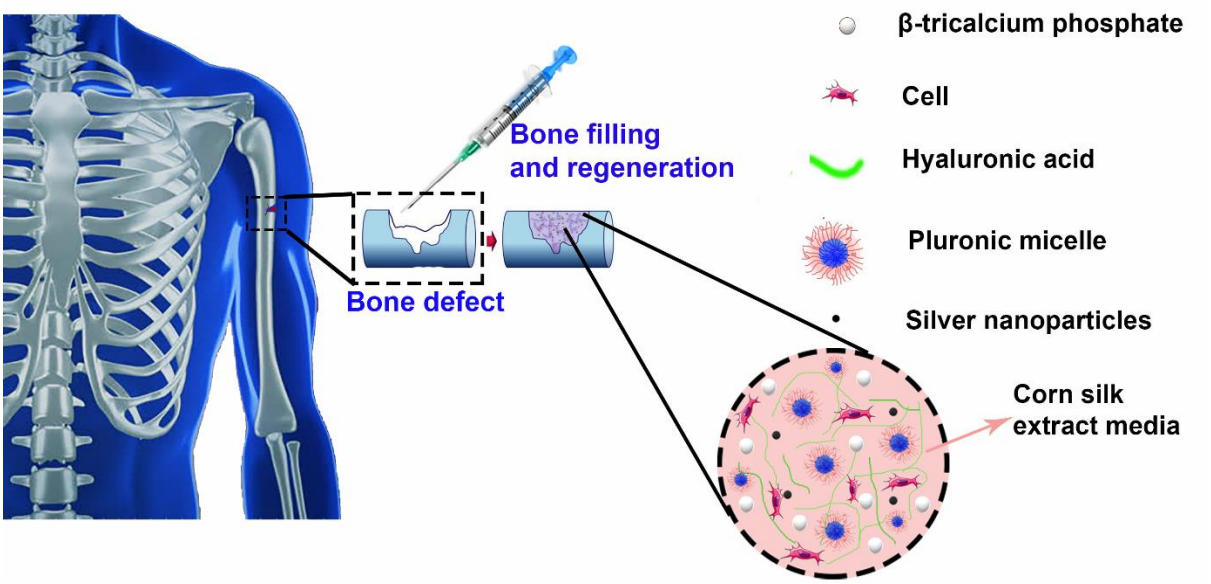

Figure M3 Schematic representation of injection of the thermosensitive nanocomposite containing β-tricalcium phosphate for bone tissue regeneration.

Materials and methods

Materials

Hyaluronic acid (HA) with a weight-average molecular weight (Mw) of 112 kDa was kindly provided by Altergon Italia. Pluronic F68 and F127, β-tricalcium phosphate (β -TCP) silver nitrate ($AgNO_3$), and NaOH were purchased from Sigma-Aldrich.

1.1.Plant materials and preparation of corn silk extract

High quality of corn silk was purchased from a local farm in Egypt. Corn silk was collected, washed several times and dried in an oven at 40 ˚C before use. The dried corn silk fibers were grinded into a fine powder (mesh size 60 μm). Afterward, pulverized in a knife mill and sieved into a particle size of 0.4 μm and, then, kept refrigerated in glass containers before further processing.

The corn silk powder was then processed to obtain CSE as reported in the literature [53]. Briefly, 5 g of the dried powder of corn silk was added to 50 ml of deionized water. The mixture was heated at 80 ℃ for three h. Then, the corn silk mixture was filtered through Whatman No. 42 filter paper to remove the fibers and get the corn silk extract (CSE). Finally, the CSE was stored at 4 ˚C until it was used for the experiments.

Biosynthesis of Ag NPs

The biosynthesis of silver NPs was conducted by microwave irradiation of silver nitrate employing green chemistry approach in an organic solvent-free medium (**Figure 2A**). Briefly, 10 g of CSE was mixed with 1 ml of silver nitrate aqueous solution (3.4 μg/ml) in Erlenmeyer flask and then were treated by microwave (700 w) for 180 s. A pulsed mode of on 5 s, off 5 s was applied to prevent intense boiling and aggregation of Ag NPs. The biosynthesized NPs in CSE were stored at 4 ℃ for further characterization.

Preparation of thermosensitive hydrogels

The hydrogels were prepared by adding of β-TCP (2% wt.), Pluronics F127 (15% wt.), and F68 (15% wt.) in silk extract with and without Ag NPs by mixing under continuous stirring at 4 ˚C.

Subsequently, HA was added to the previous mixture at room temperature to obtain the concentration of 1% wt. of HA. The hydrogels with and without Ag NPs are termed as HCPAg and HCP, respectively. The composition of the hydrogels was previously optimized by rheological analysis to obtain a gelification temperature (T_{gel}) around body temperature. To clarify the effect of corn silk extract (CSE) on gelation temperature, another sample without CSE and Ag was prepared and termed as "HWP" and its rheological characterizations were followed and presented in **Figure S1** and **S2**.

Measurements

Characterization of Ag NPs

To assess the formation of Ag NPs, surface Plasmon band measurements were performed using UV–Vis spectrophotometer (JASCO, V-530), from 350 to 800 nm at a resolution of 64 nm. The size distributions of the silver NPs were evaluated by dynamic light scattering (DLS) using a Nano-ZS Zetasizer apparatus (Malvern Instruments, United Kingdom). The morphologies and sizes of the Ag NPs were investigated by HR-TEM. JEM 2010 (Michigan, USA) instrument at an accelerating voltage of 200 kV. The samples were prepared by placing a drop of NPs solutions onto a carbon film supported on a copper grid and following evaporation of water in the air at room temperature.

Characterization of hydrogels

DLS was also used to determine the micelles formation of hydrogels and their size distribution. For the DLS analysis, all solutions were prepared in deionized water (mean, n=3) with a concentration of 5 mg/ml and were heated to 40 ˚C. In order to perform qualitative elemental analysis, scanning electron microscopy (Quanta 200 FEG, FEI Company, Hillsboro, OR, USA)

coupled with energy dispersive X-ray spectrometry (EDX; Inca Energy System 250, Oxford, UK) was used.

Thermal analysis

The thermal behavior of the samples was determined using a differential scanning calorimeter (DSC). DSC measurements were performed using a TA Instruments (Discovery series, New Castle, DE, USA) under N_2 flow of 20 ml min^{-1} and the heating rate of 2.5 $^{\circ}C$ min^{-1} from -30 to 20 $^{\circ}C$.

Thermal stability of the formulations was examined by thermogravimetric/differential thermogravimetric analysis (TGA/DTG) using TGA Q500 (TA instrument, New Castle, DE, USA). The weight change of each sample was evaluated by TGA as a function of the temperature from ambient temperature to 500 °C at 10 °C/min^{-1} in a nitrogen atmosphere (flow of 20 mL/min). In DTG, the onset, endset, peak temperature of each peak were recorded.

Rheological experiment

Small amplitude oscillatory shear tests were performed to evaluate the time-dependent response of the thermosensitive hydrogels and their linear viscoelastic properties i.e. elastic (G') and viscus (G'') modulus. The frequency was in the range from 0.01 to 10 Hz. The measurements were carried out through a rotational rheometer (Mars III, HAAKE Rheometer, Waltham, MA, USA), using a parallel plate geometry at 20 and 40 °C. In order to identify the linear viscoelastic response range of the materials, preliminary strain sweep tests were performed on the samples, at the oscillation frequency of 1 Hz. The tests were repeated at least three times on each sample. To evaluate the gelation temperatures and to optimize the composition preliminary, the viscoelastic parameters were monitored as a function of the temperature from 25 to 40 °C at a fixed oscillation frequency

of 0.01 Hz. During all the tests, the samples were placed into a chamber properly designed to avoid solvent evaporation. Steady-state shear test in term of flow curves was performed to evaluate the dependence of viscosity upon the shear rate.

Antibacterial assay

Bacterial cell suspensions were prepared, for each of the four tested gram-positive and gram-negative bacteria (*Bacillus Subtilis, Staphylococcus Aureus, Pseudomonas Aeruginosa, Escherichia Coli*), using sterile normal saline solution (NaCl 0.9% w/v) to obtain a final concentration of 10^7 CFU/ml by comparison with a 0.5 Mc Farland turbidity standard. Equal weights of each film were individually inserted in test tubes, each containing 10 ml of sterile Mueller–Hinton (MH) broth (composed of g/l: beef extract, 2.0; casein hydrolysate, 17.5 and starch 1.5; pH 7.3 ± 0.2). The medium was sterilized by autoclaving for 20 min at 120 °C and 1.5 atmospheric pressure. After sterilization, each test tube was inoculated with 100 µl of one of the previously prepared bacterial suspensions and 100 µl of samples containing different concentrations of Ag (3.4, 1.7, 0.85 µg/ml) and then incubated under moderate shaking of 100 rpm at 35 °C for 24 h (treated microorganisms). Controlled test tubes, containing the same volume of MH medium without Ag, were inoculated by using the same inoculum size of the tested strains (untreated microorganisms). The cell growth of the tested bacteria was determined at the end of the incubation period, based on the optical density measurements at a wavelength of 620 nm. Results were expressed in terms of their cell dry weight (CDW) using the relation between the optical density of the cell and their cell CDW [14, 55].

Cell cultures

In order to test the biological response to our injectable hydrogels, L929 cells originating from Mouse C34/An connective tissues were obtained from the European Collection of cell cultures (Sigma-Aldrich, USA) and Human Mesenchymal Stem Cells, extracted from umbilical tissue, and in particular from Wharthon Jelly (hUCMSCs) were used. L929 cells were grown in T-75 cell culture flask (Falcon, Italy), in cell culture medium Dulbecco's Modified Eagle's Medium (DMEM, Hyclone, USA) supplemented with 10% fetal bovine serum (FBS) and antibiotics (penicillin G sodium 100 U/mL, streptomycin 100 μg/mL) at 37°C and 5% CO2. hUCMSCs cells were cultured, at passage 1-6, with a complete medium, composed of DMEM supplemented with 10% FBS, 100 U/ml penicillin, 100 U/ml streptomycin and. hUCMSCs cells were maintained in 100 mm diameter cell culture dishes in a humidified and controlled atmosphere at 37°C and 5% CO2. The medium was changed every 3-4 days.

Cell viability and morphology assay

In order to understand the cells viability, L929 cells were seeded at a density of 6×10^3 cells/ml on 96-wells (World Precision Instruments, Inc). The thermosensitive hydrogels were sterilized by steam autoclaving at 121 °C for 20 min. The cells were incubated with 5μl of the formulations H, HCPAg for each well in triplicate up for 1, 3, 7 and 10 days of cells culture and then Alamar blue assay (AB) was performed by adding AB reagent to the samples (at 10% v/v with respect to the medium) and incubated at 37°C for 4 hours. The absorbance of the samples was measured using a spectrophotometer plate reader (Multilabel Counter, 1420 Victor, Perkin Elmer) at 570 nm and 600 nm. AB is an indicator dye that incorporates an oxidation-reduction indicator that changes color in response to the chemical reduction in the growth medium, resulting from cell viability. L929 seeded wells were used as a control. Data are expressed as the percentage difference between

treated and control to evaluate the percentage of reduction (Reduction %), which is calculated with the following formula:

$$Reduction\ (\%) = \frac{(O_2 \times A_1) - (O_1 \times A_2)}{(O_2 \times P_1) - (O_1 \times P_2)} \times 100 \qquad (1)$$

where O_1 is the molar extinction coefficient (E) of oxidized AB at 570 nm; O_2 is the E of oxidized AB at 600 nm; A_1 is the absorbance of test wells at 570 nm; A_2 is the absorbance of test wells at 600 nm; P_1 is the absorbance of control well at 570 nm; and P_2 is the absorbance of control well at 600 nm. The percentage of reduction for each sample was normalized to the percentage of reduction for the control to obtain the cell viability percentage [56].

For cell morphology assay, cells were seeded at a density of 1×10^4 cells/mL on fluorodish-35 mm (World Precision Instruments, Inc) and 5µl of the formulations HCP and HCPAg were incubated for 24 h Then, the samples were washed two times with PBS and fixed with 10% formaldehyde for 1 hour at 4 °C. The fixed cells were permeabilized with Triton X-100 0.1% in Phosphate-buffered saline (PBS) for 3-5 min. The actin filaments were stained with FITC phalloidin (Cayman Chemical Company) in PBS for 30 minutes at room temperature. Finally, after two washes with PBS in order to remove unbound phalloidin conjugate, cell nuclei were stained with 4',6-diamidino-2-phenylindole, DAPI, (SIGMA-ALDRICH). The samples were observed by confocal microscope system (Leica TCS SP8) with a 63X oil immersion objective. Images were acquired with a resolution of 1024×1024 pixel.

Bone tissue regeneration

DNA/alkaline phosphatase activity (ALP) measurement, Alzarin Red S (ARS) and human osteocalcin protein (Ocn/B.G.P.) expression analysis were used to evaluate the osteogenic

expression of hUCMSCs incubated with 5 µl of the injectable hyaluronic acid/corn silk extract-Ag based nanocomposite dissolved in Basal media, and Osteogenic media. Osteogenic media were obtained by addition of 10% FBS, 8mM L-glutamine, 100 U/ml penicillin, 100 mg/ml streptomycin, 20 mM β-glycerol phosphate, 50 mM ascorbic acid, 100 nM dexamethasone to the basal media, DMEM. hUCMSCs were incubated at a density of 50 000 cells/mL in a 24-wells and the osteogenic and basal medium was changed every 3 days. For the DNA/ALP test,

the samples were washed gently with ice-cold PBS, followed by washing with cold 1× assay buffer (BD Biosciences, Milano, Italy). The ALP activity was evaluated onto the cell lysates (50 µl) and, accordingly, the cultures were treated with 1× lysis buffer with 0.2% of Triton X-100. To correct the ALP values for the number of cells present on each scaffold, double-stranded DNA (dsDNA), as a marker for the cell number, was measured using a PicoGreen_dsDNA quantification kit (Invitrogen). To this aim, first, 100 µl of diluted Picogreen dsDNA quantification reagent was added to 100 µl of cell lysates in a flat-bottomed 96-well plate. After 10 min of incubation, the fluorescence of Picogreen was determined at a wavelength of 520 nm after excitation at 585 nm using a spectrophotometer (Victor X3, Perkin-Elmer, Italy). dsDNA was quantified according to a calibration curve of l-dsDNA standard in 10 mM Tris, 1 mM EDTA at pH 7.5 (buffer). Each experiment was performed three times in triplicate. The results of ALP activity were reported as nanograms (ng) of ALP normalized to the micrograms (µg) of total DNA content. Finally, the alkaline phosphatase activity of hMSC seeded with HPC and HPCAg was determined. Mineralized matrix synthesis was evaluated by osteogenesis ARS assay (Sigma-Aldrich). After 14 days of culture, the samples were fixed with 10% formaldehyde solution at 4°C for 1 h., rinsed three times with PBS and incubated with the dye at 1% for 30 min. The samples were then washed three times with dH_2O, incubated with 10% acetic acid for 30 min and sonicated. After heating at 85°C for 10

min, the acidic supernatant pH was neutralized with 10% ammonium hydroxide. The optical density of the solution was analyzed by a spectrophotometer working at 405 nm. All of the analyses were performed in triplicates.

To determine the expression of human Ocn/B.G.P. the supernatants for analysis were collected at days 21 and 28 of incubation, and then analyzed using Human Osteocalcin Instant ELISA kits (Elabscience) according to manufacturer protocol.

Statistical analysis

All statistical measurements were performed with SPSS 22 software package. The outcomes are presented as means ± standard error using Oneway ANOVA and Tukey test with importance reported when $p < \pm 0.05$.

Results and discussion

Synthesis and characterization of Ag NPs

Figure 2A shows the schematic illustration for the synthesis and stabilization of Ag NPs by CSE. The reduction of silver ions within CSE is mainly due to the antioxidant activity of flavonoid compounds in CSE and they also act as a biostabilizer to prevent agglomeration of Ag NPs [57, 58]. Flavonoids are plant phenolic compounds that are widely distributed in the CSE, which are effective antioxidants as well. The absorption spectra of samples before and after microwave treatment are presented in **Figure 2B**. After microwave irradiation, the appearance of the Plasmon absorption peak (~ 450 nm) in the UV–Vis spectrum of the CSE solution containing Ag NPs reflects the nano-sized character of the colloidal dispersion of $Ag^{(0)}$ particles [46].

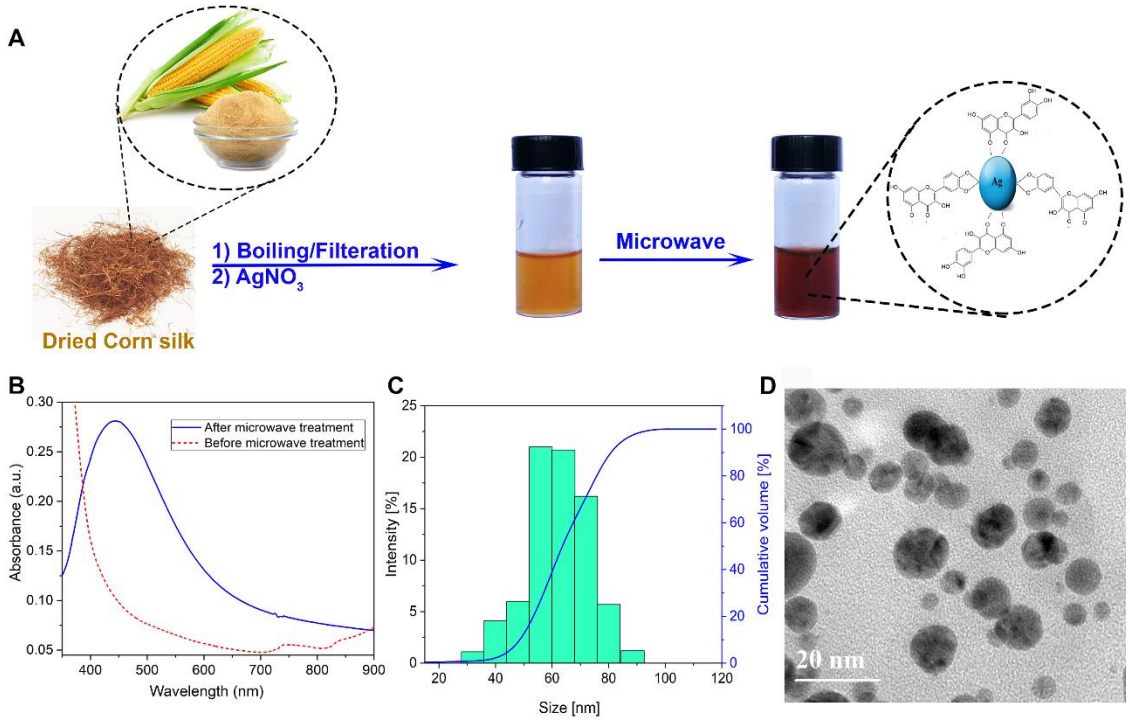

Figure 2 (A) Illustration of the synthesis of silver nanoparticles in corn silk extract via microwave-assisted green approach. The darker color of the solution indicates that Ag ions were converted to Ag NPs which are stabilized by flavonoid compounds of corn silk. (B) The UV absorbance of Ag NPs in corn silk extract before and after microwave treatment. Size distribution measurements by DLS (C) and TEM image (D) of Ag NPs in corn silk extract solution. The bar for TEM image represents 100 nm.

Figure 2C shows the results of DLS analysis of silver NPs and it can be seen that the prepared NPs have a narrow size distribution with a mean diameter of 49±2 nm. TEM image (**Figure 2D**) shows well-dispersed silver nanoparticles which are spherical in shape with an average size of 27±1 nm. In agreement with other literature studies [59, 60], there is a difference between DLS and TEM sizes measurements which are normally attributed to the fundamental difference between intensity and number-weighted particle size distributions and the differences between the dry and hydrodynamic radius of particles. Green synthesis of silver NPs has been reported by several studies using plant extract. For instance, Patra et al. biosynthesized Ag NPs by using corn silk extract; however, the bioreduction process was carried out up to 24 h where the particles size ranged from 100 to 450 nm [61]. In contrary, our synthesized silver NPs using a faster process of

5 min possess smaller size ranging from 30 to 90 nm by means of the microwave-assisted approach.

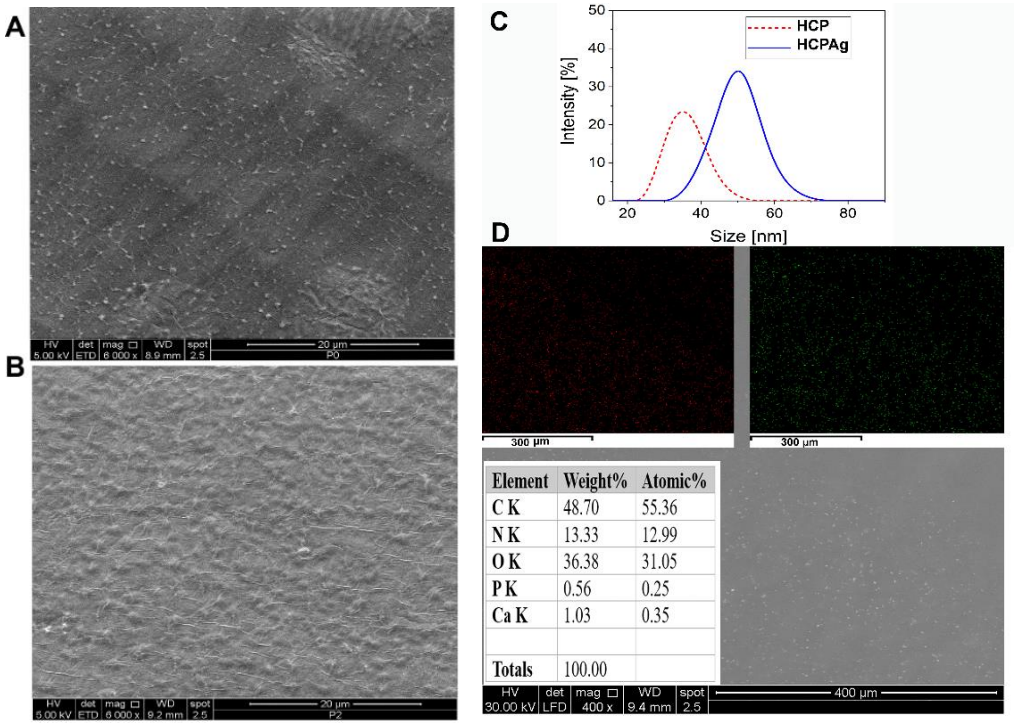

Element	Weight%	Atomic%
C K	48.70	55.36
N K	13.33	12.99
O K	36.38	31.05
P K	0.56	0.25
Ca K	1.03	0.35
Totals	100.00	

Figure 3 Scanning electron microscopy (SEM) images of HCP (A) and HCPAg (B) thermosensitive hydrogels at 40 °C. Bars represent 20 µm. (C) Dynamic light scattering (DLS) measurements of the diluted samples. All solutions were prepared in deionized water (mean, n=3) with concentration of 5 mg/ml at 40 ˚C. (D) SEM coupled with energy dispersive X-ray spectrometry (EDX) to assess the elemental analysis of the HCPAg thermosensitive nanocomposite hydrogel. Element distribution from EDX mapping of HCPAg nanocomposite hydrogels is shown on the top of the image. Chemical maps of P (red color, left side up) and Ca (green color, right side up) display the distribution of P and Ca in the nanocomposite, respectively. Maps bars represent 300 µm. The presence of carbon, oxygen, phosphorus, calcium, and nitrogen was depicted.

Preparation and characterization of the hydrogels

Figure 3A-B show the SEM images of the neat hydrogel without Ag NPs and the nanocomposite containing silver NPs at 40 °C. As can be seen, the nanocomposite containing Ag has more rough surface in comparison with the neat hydrogel which is essential for the cells adhesion and

spreading [62]. Nanomicellation was examined using DLS in very diluted samples as presented in **Figure 3C**. It can be seen the presence of Ag NPs slightly enlarged the nanomicelle size from 35 (for HCP sample) to 50 nm (for HCPAg).

The elemental analysis of HCPAg by EDX is demonstrated in **Figure 3D**. The chemical maps of phosphorus (P, red color) and calcium (Ca, green color) present the appropriate distribution of P and Ca in the nanocomposite platform, respectively. Therefore, the EDX images confirmed the uniform dispersion β-TCP within the hydrogel matrix. As expected, besides of P and Ca, the presence of C, O, and N, which come from HA, were detected.

The DSC thermograms of both samples are shown in **Figure 4A.** Two distinct endothermic peaks around -10 and 0 °C are detectable. The first one is associated with the fraction of water which interacts with the Pluronic and HA network as bound water; while the second one (around 0 °C) is related to the free water fraction. By integrating the peaks, the total heat involved during the fusion of H_2O as ΔH_{tot} can be obtained. Moreover, the amount of bound and free H_2O was calculated as the ratio between the enthalpies associated with the first (ΔH_1) and the second peak (ΔH_2), and ΔH_{tot} [31]. The results revealed that the presence of silver lead to decrease the first peak (from 70 to 52%) and increase the second one (from 30 to 48%), respectively which is directly related to the percentage of bonded and free water.

Figure 4B shows the TGA (left panel) and differential thermogravimetric analysis (DTG, right panel) curves of the thermosensitive hydrogels. The TGA curves of both samples show two weight loss stages. The first peak, which begins before 100 °C, is due to the water loss. The second peak, which is from 350 to 440 °C, may be due to the degradation of polymeric materials, e.g. Pluronic, HA, and other polysaccharides and compounds from CSE; the onset degradation temperature for

both formulations are equal. As can be seen from the DTG curve, the presences of Ag NPs slightly promoted the degradation rate of the 2nd-second peak.

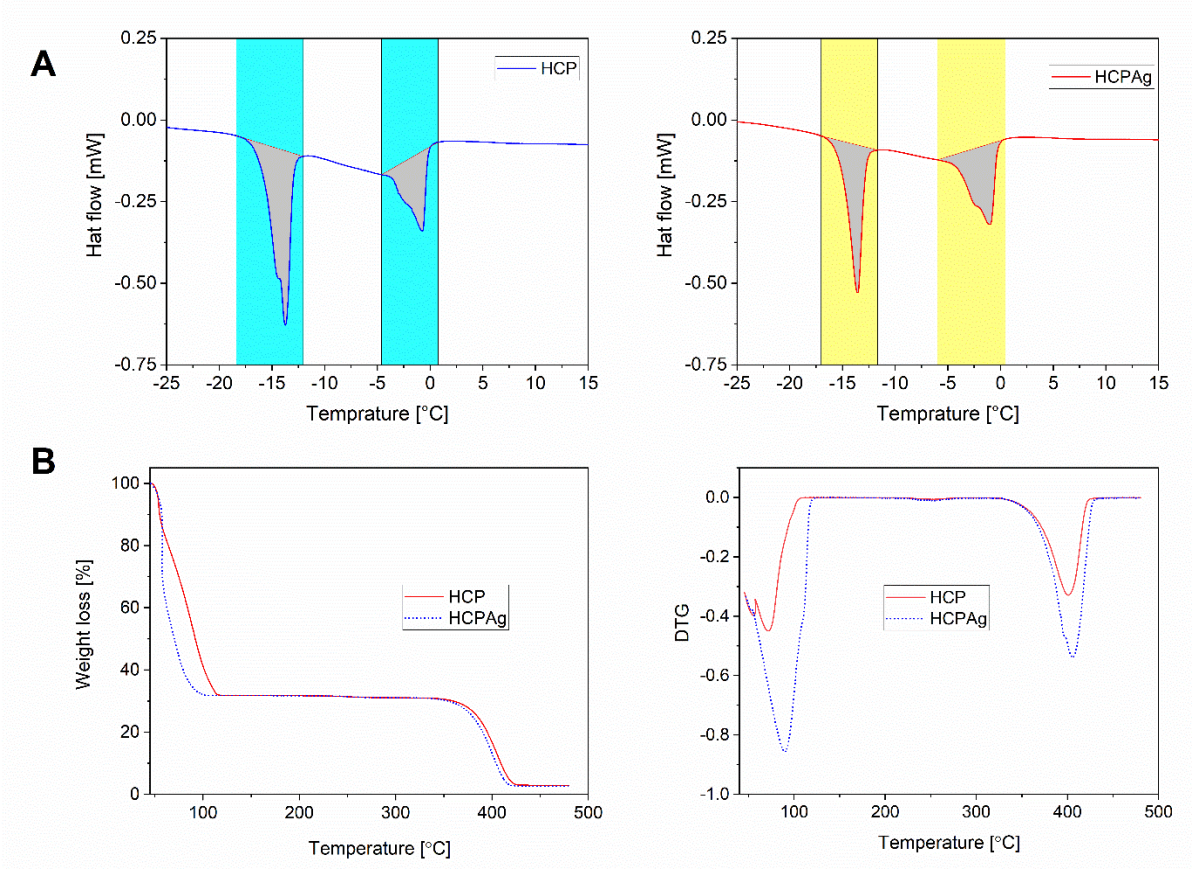

Figure 4 (A) DSC thermograms of HCP and HCPAg samples at 2.5 ◦C/min. (B) TGA (left panel) and DTG (right panel) curves of HCP and HCPAg hydrogels.

The elastic and viscous moduli of samples, as a function of temperature, at a frequency value of 0.1 Hz are presented in **Figure 5**. The transition from liquid-like behavior to elastic gel-like behavior occurs which was observed as T_{gel} [63]. Separate Pluronic F127 and F68 solutions did not display a T_{gel} close to the body one (data are not shown) in the concentration range from 10 to 30% w/w but by formulating Pluronic F127/F68 blends at specific concentrations, it was possible to obtain a medium with a T_{gel} close to T_b. For the formulated hydrogels, T_g were approximately 36 and 37 °C for HCP and HCPAg, respectively. Furthermore, the absence of CSE and Ag NPs in

the systems (hydrogels with distilled water) led to a platform to become gel at a lower temperature (**Figure S1**).

At room temperature, the systems are liquid and could be injectable whereas, at the body temperature, they become a gel. This fast sol-to-gel phase transition behavior is beneficial for cell entrapment to give a uniform distribution of cells within the gelled matrix [64]. Moreover, the presence of spherical nanoparticles of silver did not considerably affect the gelation temperature but introduce the antibacterial activity to the hydrogels as a disinfectant agent for using in bone repair applications.

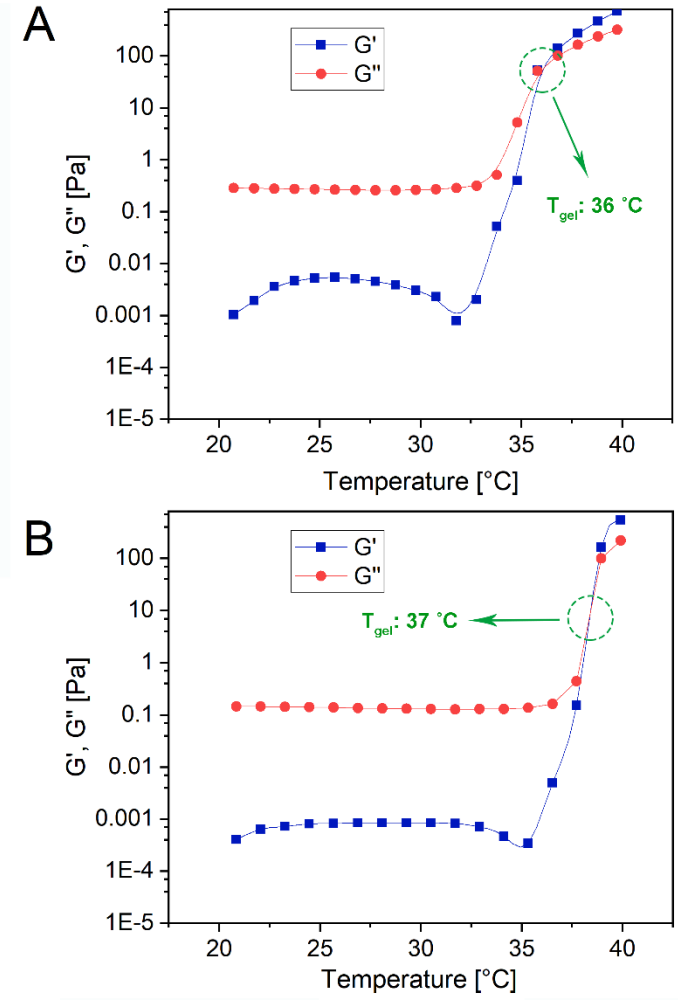

Figure 5 The sol–gel phase transition by rheological experiments. Elastic and viscous moduli as a function of the temperature of HCP (A) and HCPAg (B) at a frequency value of 0.01 Hz. The increase in G' over G" represents an increase in solid over liquid characteristics of the tested sample, which reflects a phase transition into a "gel" structure. A crossover of elastic with loss moduli (G' vs G", respectively) indicates the gelation temperature. Results are the means of three measurements. SD was always lower than 10%. Error bars were omitted for clarity purpose.

The mechanical properties of formulations were studied through small amplitude shear tests at temperature both below and above T_{gel} at 20 and 40 ˚C, respectively. The mechanical spectra, G' and G'' as a function of frequency, at 20 and 40 ˚C are shown in **Figure 6**. At 20 ˚C (upside panel), G'' is always higher than G' in all the frequency range analyzed which means the rheological behavior of the formulations is that typical of a viscous fluid. On the contrary, at 40 ˚C (downside panel), the elastic modulus is always higher than the viscous one and both the viscoelastic moduli are quite frequency-independent showing a rheological behavior characteristic of a gel-like material.

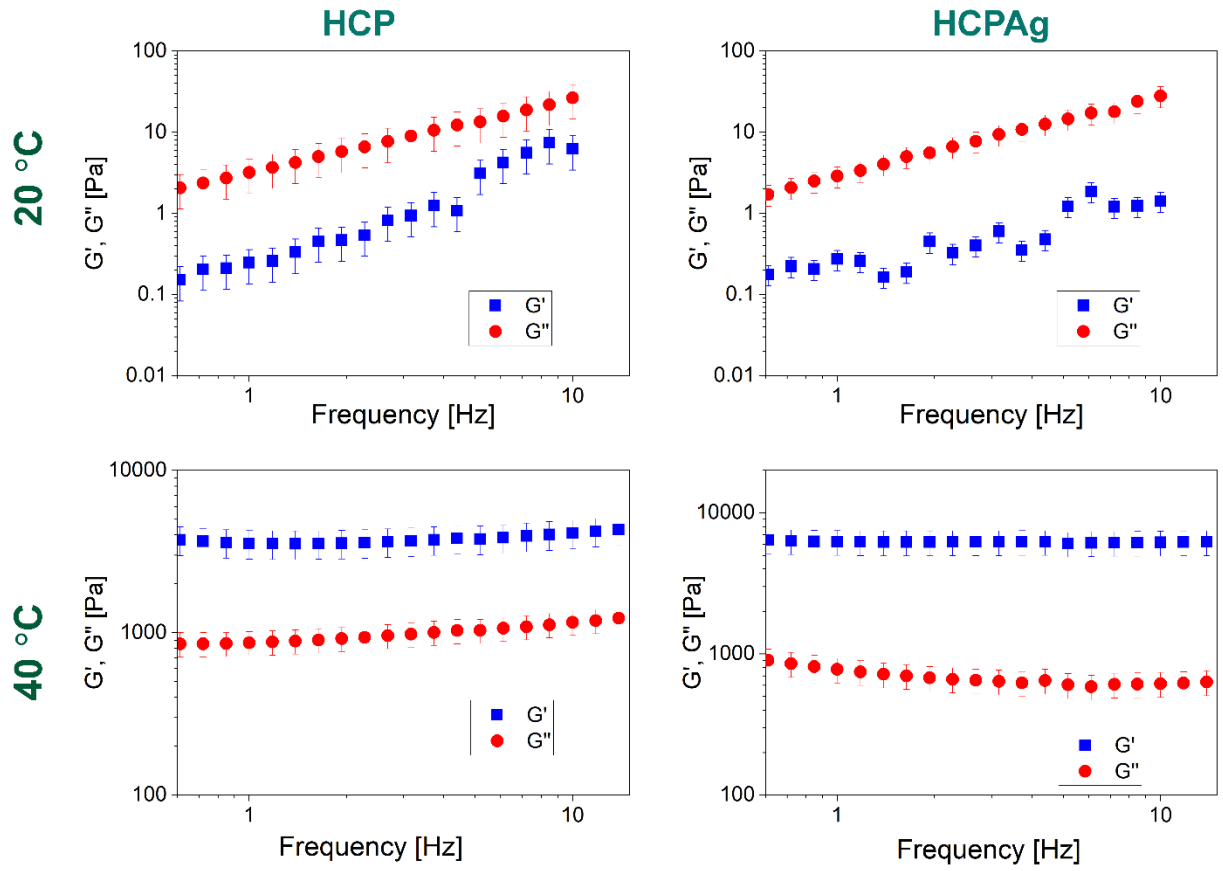

Figure 6 Mechanical spectra of the thermosensitive hydrogels at 20 ˚C and 40 ˚C. Results are the means of three measurements. Each error bar represents 1 standard deviation and serves as the estimate of standard uncertainty.

Figure 7 shows the viscosity of the injectable hydrogels at 20 and 37 ˚C. Due to the thermal gelation at body temperature, both formulations have more viscosity values at 37 ˚C compared to 25 ˚C. It is worth noting that, at 37 ˚C, the presence of silver particles significantly enhanced the viscosity from 0.8 to 3.5 Pas at shear rate of 10 s^{-1}. At low temperature (20 ˚C), the viscosity of both formulations is almost constant with shear rate showing pseudo-Newtonian behavior. The viscosity values are similar for both samples (0.1 Pas at shear rate of 10 s^{-1}). Below Tg, the formulations behave as viscous fluids as is in agreement with the oscillation frequency sweep test (**Figure 6**). While, at 37 ˚C, the samples show shear-thinning behavior and the viscosities decline

with the increase of shear rate. In fact, the viscosity endured a reduction upon the shearing reached a plateau at higher shear rates. This shearing thinning behavior is due to the breakage of physical crosslink and topological interaction among the macromolecules leading higher mobility of segments within the hydrogel matrix. Low viscosity upon the storage at room temperature along with reduction of viscosity at high shear rate is a preferred characteristic of materials that have to be injected through needles since it allows an easier injection [31].

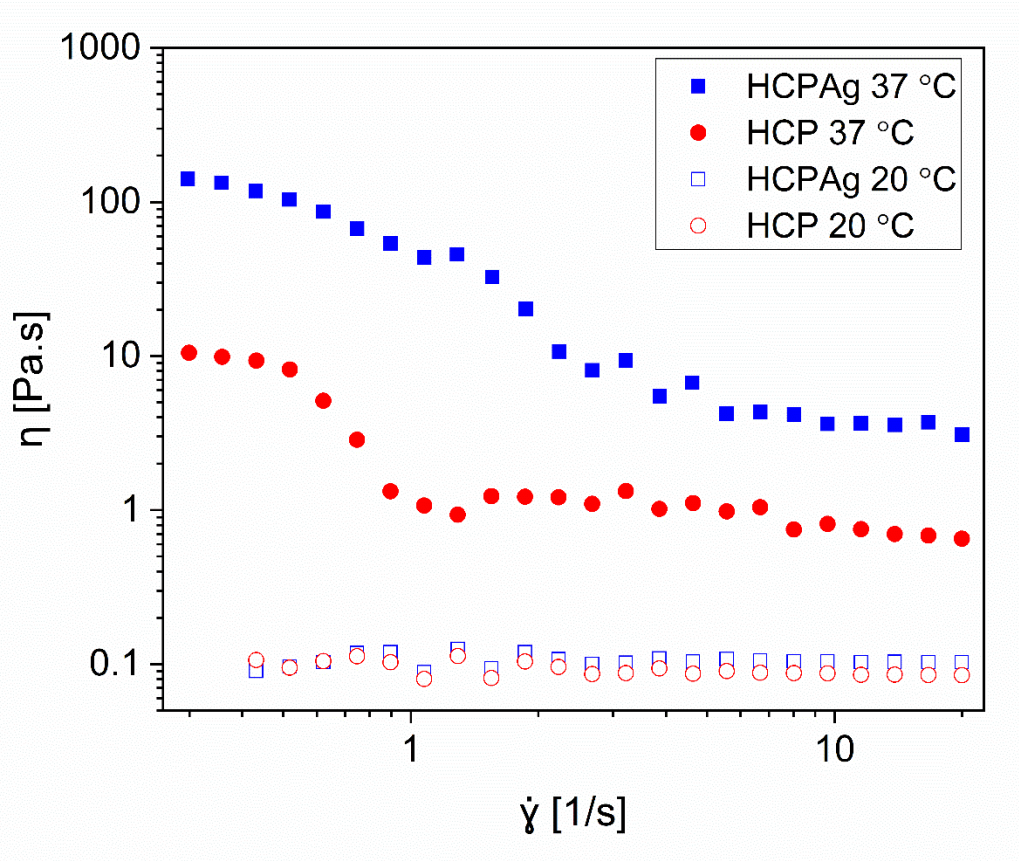

Figure 7 Shear rate-dependent viscosity changes of HCP and HCPAg samples at 20 and 37 ˚C. The standard deviation data were omitted for clarity.

Thermosensitive hydrogels, which possess good retention at the application site, have appealed a great deal in biomedical and clinical fields. These materials respond intelligently to temperature variations, remaining in liquid form at room temperature and become a solid gel at body

temperature [65]. Pluronics, as amphiphilic compounds, are able to become gel via micellization above their critical temperature or concentration [66]. The prepared formulations are injectable systems which can form a hydrogel at 37 ˚C in the body before solidifying within the targeted tissue. Researchers have developed scaffolds based on hyaluronic acid and Pluronic in the form of environmentally-sensitive hydrogels. HA offers many advantages as a tissue scaffold including biodegradability, biocompatibility, and bioresorbability as have been shown in many studies [67]. Hyaluronic acid could activate cell surface receptors, influencing intracellular signaling cascades for cell growth, migration, proliferation, and differentiation [68]. Moreover, β-TCP, a source of calcium which has a similar chemical structure with that of the bone mineral phase, facilitates bone regeneration capability of the injectable device [69].

Antibacterial properties

The antibacterial capability of the prepared samples against *E. coli, S. aureus, B. subtilis,* and *P. aeruginosa* is expressed as bacterial reduction percentage in comparison with the control sample (**Figure 8**). The control samples did not demonstrate growth inhibition against the gram-negative and -positive bacteria whereas all other samples containing Ag NPs exhibited significant effects on the growth inhibition. As can be seen, for the concentration of ≥1.17 μg/ml, the samples containing Ag NPs possess an excellent growth inhibitory effect against all the tested microorganisms.

One of the main reasons for scaffold failures is due to implant-associated bacterial infections. Hence, using antibacterial scaffolds could help to prevent infections that are detrimental for bone tissue formation which is of clinical importance [70]. In this study, we used spherical nanoparticles

of Ag to impart antibacterial activity to the thermosensitive hydrogels to avoid bacterial contamination.

Silver NPs can be converted to their ion form in the physiochemical environment. The antibacterial effect of Ag NPs-embedded samples is not only due to the released Ag^+ ions but also to the nanoparticle itself. Apparently, Ag ions interact with the peptidoglycan cell wall of bacteria, causing structural changes that increase membrane permeability and subsequently cell death. Antimicrobial agents are reported to disrupt the outer membrane of target cells, as shown in the case of silver ions This effect is observed at concentrations with a 10-fold higher magnitude than those used for silver nanoparticles. Taken together, silver ion is important in the antibacterial activity of silver nanoparticle. Silver nanoparticles physically interact with the cell surface of various microorganisms. In detail, they interact with the exposed sulfhydryl groups of bacterial proteins to prevent DNA replication. Ag NPs can attach to the bacterial cell membrane, and also penetrate inside the bacteria causing damage by interacting with phosphorous- and sulfur-containing compounds like DNA and, finally, leading to cell death [49, 71]. Radzig et al. studied the silver nanoparticles MIC values for isogenic E. coli wild type strains and mutant strains deficient in different repair systems and found that E. coli strains with mutations in genes responsible for the repair of oxidative lesions in the DNA were less resistant to the silver nanoparticles than the wild-type strains were. These genes may be involved in the repair of DNA damage caused by the silver nanoparticles. Similar results were found with silver ions, and the data suggested that the oxidative DNA damage plays an important role in the antibacterial effects of silver nanoparticle/silver ion [40].

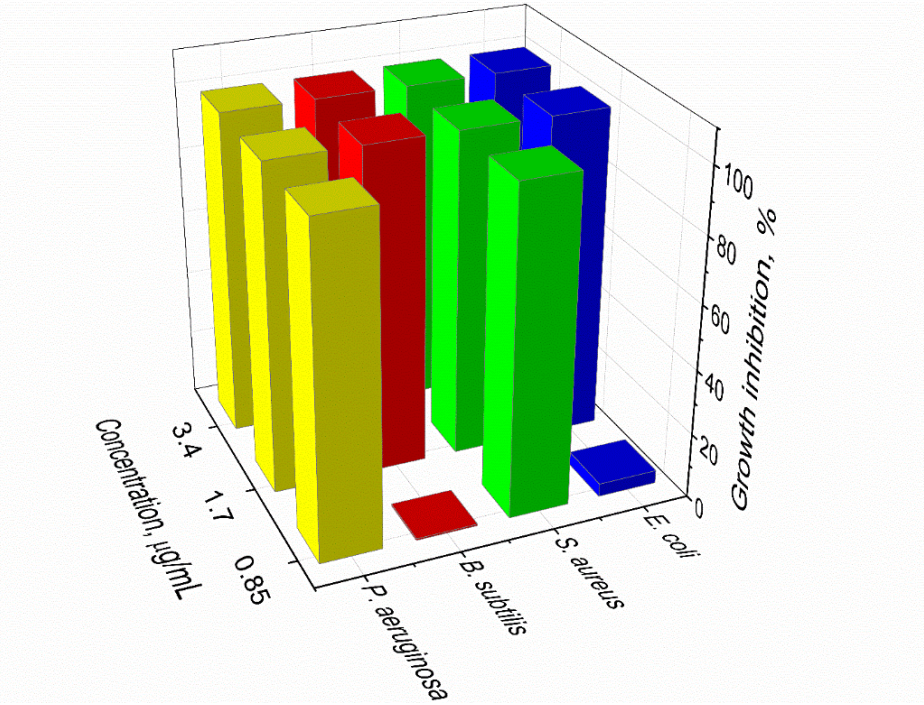

Figure 8 Antibacterial activity of samples containing different concentrations of Ag NPs against Gram-positive (*B. subtilis* and *S. aureus*) and Gram-negative (*P. aeruginosa* and *E. coli*) bacteria after 24 h. The data are representative of 3 repeated experiments.

Cell viability and morphology

In order to investigate the biocompatibility of the injectable nanocomposite, L929 cells viability was evaluated by Alamar Blue assay. It is clear from the results in **Figure 9A** that the thermosensitive hydrogels (HCP, HCPAg) showed good safety after 1, 3, 7 and 10 days of incubation with L929 cells, compared to the untreated controls. In particular, after one day of incubation with both formulations, L929 cells viability is around 100%, noting cellular viability over 100% for the HCPAg sample. On the third day, for HCPAg sample containing silver NPs, the viability had a 78% of viability percentage, conversely, for the HCP formulation, the viability decreased slightly around 70% viability percentage. After 7 days of incubation, the viability is around 73 and 78% for HCP and HCPAg, respectively; in addition, after 10 days, the viability for

both samples is around 75%. The results here collectively indicated that none of the prepared formulations are cytotoxic for the cells, exhibiting good *in vitro* biocompatibility. The biocompatibility of the realized hyaluronic acid/corn silk extract-Ag based nanocomposite was also confirmed by cells morphology. Actin filaments, a constituent of the cytoskeleton, were stained with TRIC phalloidin after 24 h of incubation with HCP and HCPAg hydrogels. L929 cells, indeed, exhibited a noncytotoxic and typical mouse fibroblast-like cellular morphology after the incubation with the formulations (**Fig 9B**). Their morphology was alike to the characteristic *in vitro* L929 cells morphology that is spread or spindle-shaped, often characterized by several extending processes, which consists of cells protrusion adhering at the flat surface. These results indicate that these materials have a good biocompatibility and the most important evidence is that the HAg, containing Ag NPs, maintain a good biocompatibility, which is comparable to the material without Ag, HCP, suggesting that biosynthesis, and combination with molecules, such as HA, Pluronics and silk extract, are able to enhance the compatibility of silver [72].

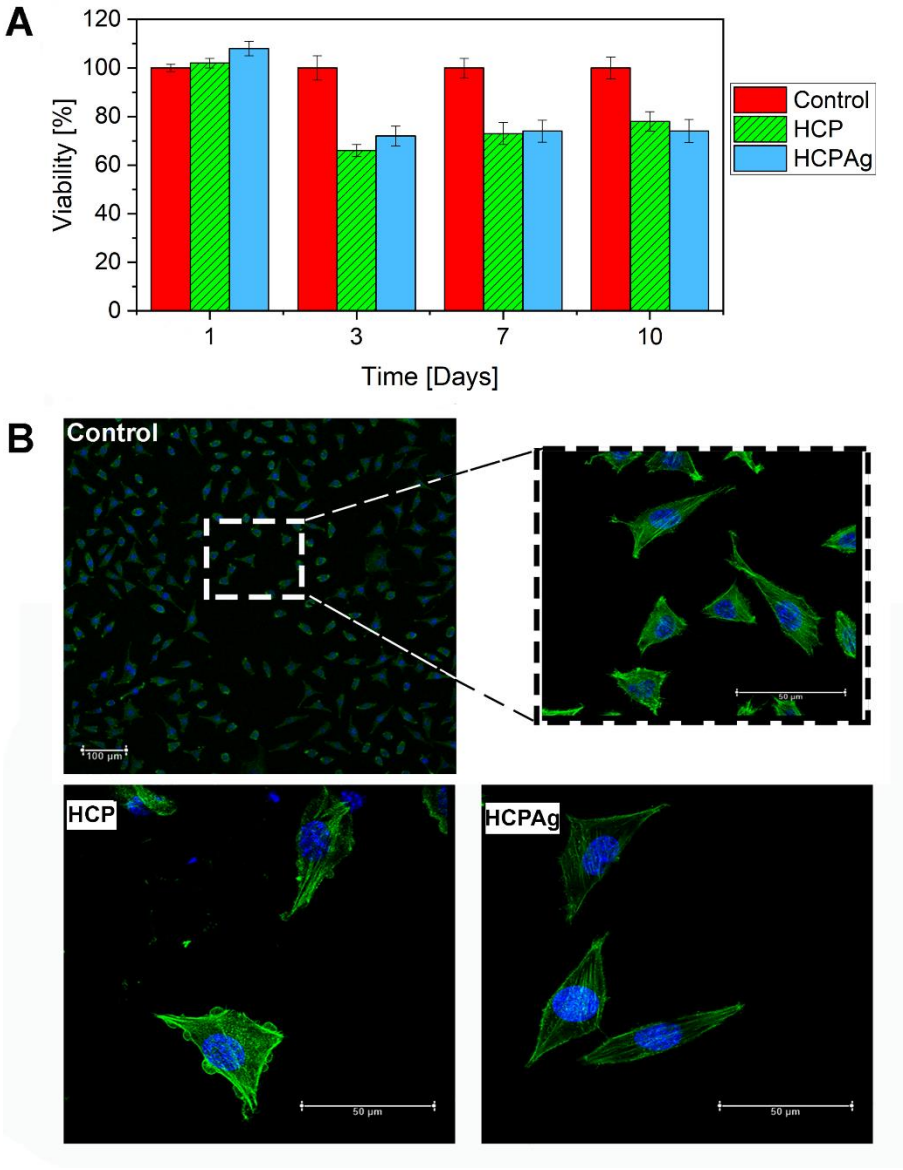

Figure 9 (A) Viability of the samples at 1, 3, 7, and 10 days. All results were presented as mean ± standard deviation. Each error bar represents 1 standard deviation and serves as the estimate of standard uncertainty. The data are representative of 3 repeated experiments in triplicate. (B) Cell morphology for the control and thermosensitive hydrogels after 24 h. The typical cellular morphology of L929 cell lines was used.

Bone tissue regeneration

ALP activity, ARS and Ocn/B.G.P assay were used as osteogenic markers to assess the bone regeneration potential of the injectable hyaluronic acid/corn silk extract-Ag based nanocomposite. The results of the ARS assay performed on the injectable scaffolds after 14 days of culture (**Figure**

10A) show differentiated osteoblasts after the incubation with HCP and HCPAg, in contrast to undifferentiated MSCs (CTR –OM), which accumulate extracellular calcium deposits (mineralization) in red. This process is associated with the formation of bone nodules and the osteoblast-mediated mineralization indicating the bone mass formation [73]. Moreover, **Figure 10B** shows a similar amount of calcium deposited expressed as OD^{450nm} by the cells cultured within the HCP and HCPAg injectable nanocomposite scaffolds compared with the control in the presence of Osteogenic Medium. As shown in **Figure 10C**, at day 7, the ALP activity of the osteogenically induced hUCMSC cells cultured within the HCP and HCPAg was equal to 3.7±0.8 and 4.1±1.0, respectively. After 14 days of incubation, the ALP activity was decreased to 1.7±0.1 and 1.6±0.4 for HCP and HCPAg, respectively. ALP is an early marker for the osteogenic differentiation of cells. The observed differences in ALP activity between the injectable nanocomposites and the control sample suggest that these hydrogels induce faster osteogenic differentiation of the hUCMSC cells after 7 days of incubation. While after 14 days, the ALP activity of hUCMSC cells decreased according to the expression of later-stage osteogenic markers and to the begin of calcium deposition.

Ocn/B.G.P, the most abundant non-collagenous bone matrix protein, is synthesized almost exclusively by highly differentiated osteoblasts and, hence, is a specific marker of bone formation [74]. Thus, also the levels of Ocn/B.G.P in the nanocomposite treated hUCMSC cells was evaluated using ELISA Kit assay (**Figure 10D**). Resulting data revealed that Ocn/B.G.P expression was lowest in the control group compared to treated groups at days 21and 28; this suggests the fundamental role of β-TCP to promote osteogenic differentiation, both for the samples incubated with -OM media and +OM media, highlighting an additive effect when the materials are dissolved in the OM media.

Comparative analysis of the expression levels of Ocn/B.G.P, between HCP and HCPAg formulations dissolved in OM media at 21 day, indicated that the levels of Ocn/B.G.P were similar for HCP and HCPAg dissolved in OM media (24,3 and 25,1 ng/mL respectively). While after 28 days of culture, an increase of the expression levels of Ocn/B.G.P from 24,7 ng/ml in HCP to 28,4 ng/ml in HCPAg. These findings suggest that Ocn/B.G.P is majorly expressed during late stages of differentiation and, thus, could promote the formation of mineralized nodules in hUCMSCs cells after the incubation with injectable hyaluronic acid/corn silk extract-Ag based nanocomposite. The presence of Ag nanoparticles showed a positive impact on the osteogenic differentiation of hUCMSCs, which has also been reported in other studies. Indeed, it has been demonstrated that Ag NPs could promote osteogenic differentiation of mammalian cells, aiding the proliferation and the osteogenic differentiation of MSCs *in vitro*, and improving bone fracture healing *in vivo* [75]. Additionally, it was found that Ag NPs also enhance the osteogenesis of human urine-derived stem cells by triggering the RhoA signaling pathway [76].

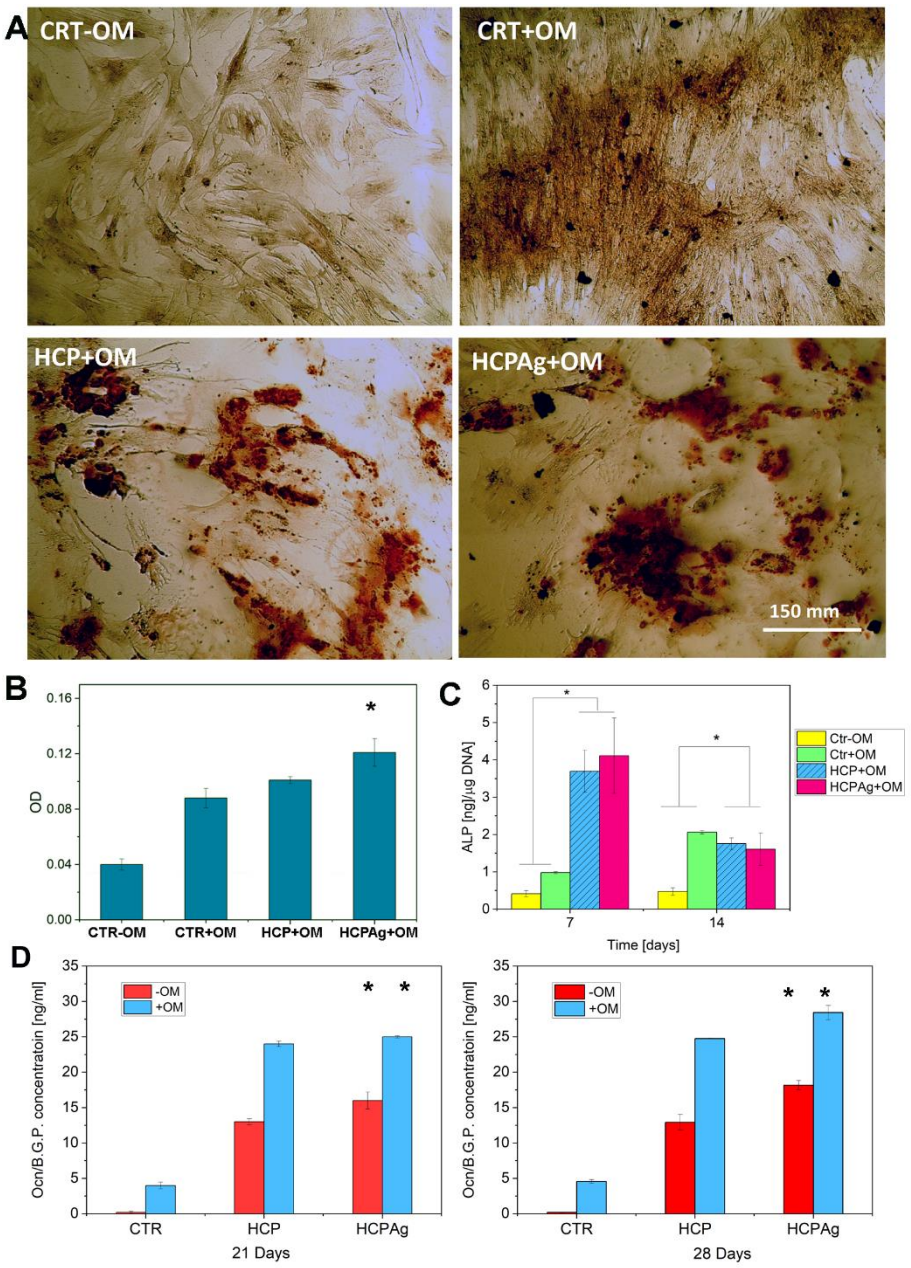

Figure 10: (A) Representative bright-field images show mineralized matrix synthesis (red) by hUCMSCs cells incubated with HCP and HCPAg hydrogel at 14 days of culture measured by ARS analysis. CTR cultures have been performed under standard (-OM) and osteogenic medium (+OM) for comparison. (B) Amount of calcium deposited expressed as OD^{450nm} by the cells cultured within the HCP and HCPAg injectable bionanocomposite scaffolds. (C) ALP/DNA assay at day 7 and 14 of culture. (D) Ocn/B.G.P expression in injectable HCP and HCPAg bionanocomposite treated hUCMSC cells. Asterisks denote significant differences (p<0.05).

Conclusion

Silver NPs were biosynthesized in an aqueous medium of corn silk extract without using toxic chemical reagents. The green synthesis of NPs employing renewable materials and avoiding hazardous compounds and non-environmentally benign solvents makes them more suitable for the clinical and biomedical applications. The new thermosensitive HA-based nanocomposite hydrogels demonstrated good mechanical properties with T_{gel} close to body temperature. The samples revealed desirable antibacterial activity against several gram-positive and gram-negative bacterial strains which can prevent bacterial infection. In addition, from the biological point of view, the nanocomposites revealed appropriate biocompatibility in comparison with the control samples. Moreover, the nanocomposites promoted high bone differentiation of MSC cells that they could be a good candidate as a potential scaffold for bone tissue regeneration.

Acknowledgments

The authors acknowledge for the financial support the project: “Idrogeli nanocompositi innovativi a base di seta di origine vegetale e nanometalli con proprietà battericide ed anticancro” funded by Italian Ministry of Foreign Affairs and International Cooperation in the frame of the Executive Program of Scientific and Technological Cooperation between Italy and Egypt for the years 2016-2018.

References

[1] E. Nazarzadeh Zare, P. Makvandi, B. Ashtari, F. Rossi, A. Motahari, G. Perale, Progresses in conductive polyaniline-based nanocomposites for biomedical applications: A review, Journal of Medecinal Chemistry (2019) In press.

[2] T. Winkler, F. Sass, G. Duda, K. Schmidt-Bleek, A review of biomaterials in bone defect healing, remaining shortcomings and future opportunities for bone tissue engineering: The unsolved challenge, Bone & joint research 7(3) (2018) 232-243.
[3] G. Fernandez de Grado, L. Keller, Y. Idoux-Gillet, Q. Wagner, A.-M. Musset, N. Benkirane-Jessel, F. Bornert, D. Offner, Bone substitutes: a review of their characteristics, clinical use, and perspectives for large bone defects management, Journal of tissue engineering 9 (2018) 2041731418776819.
[4] V. Campana, G. Milano, E. Pagano, M. Barba, C. Cicione, G. Salonna, W. Lattanzi, G. Logroscino, Bone substitutes in orthopaedic surgery: from basic science to clinical practice, J. Mater. Sci. Mater. Med. 25(10) (2014) 2445-2461.
[5] H.J. Haugen, S.P. Lyngstadaas, F. Rossi, G. Perale, Bone grafts: which is the ideal biomaterial?, J. Clin. Periodontol. 46 (2019) 92-102.
[6] J. Baier Leach, K.A. Bivens, C.W. Patrick Jr, C.E. Schmidt, Photocrosslinked hyaluronic acid hydrogels: natural, biodegradable tissue engineering scaffolds, Biotechnol. Bioeng. 82(5) (2003) 578-589.
[7] G. Chen, T. Ushida, T. Tateishi, Scaffold design for tissue engineering, Macromolecular Bioscience 2(2) (2002) 67-77.
[8] M.N. Collins, C. Birkinshaw, Hyaluronic acid based scaffolds for tissue engineering—A review, Carbohydrate polymers 92(2) (2013) 1262-1279.
[9] P.V. Giannoudis, H. Dinopoulos, E. Tsiridis, Bone substitutes: an update, Injury 36(3) (2005) S20-S27.
[10] M. Liu, X. Zeng, C. Ma, H. Yi, Z. Ali, X. Mou, S. Li, Y. Deng, N. He, Injectable hydrogels for cartilage and bone tissue engineering, Bone research 5 (2017) 17014.
[11] J.-M. Bouler, P. Pilet, O. Gauthier, E. Verron, Biphasic calcium phosphate ceramics for bone reconstruction: A review of biological response, Acta biomaterialia 53 (2017) 1-12.
[12] F. Bastami, Z. Paknejad, M. Jafari, M. Salehi, M.R. Rad, A. Khojasteh, Fabrication of a three-dimensional β-tricalcium-phosphate/gelatin containing chitosan-based nanoparticles for sustained release of bone morphogenetic protein-2: Implication for bone tissue engineering, Materials Science and Engineering: C 72 (2017) 481-491.
[13] W.-T. Su, W.-L. Chou, C.-M. Chou, Osteoblastic differentiation of stem cells from human exfoliated deciduous teeth induced by thermosensitive hydrogels with strontium phosphate, Materials Science and Engineering: C 52 (2015) 46-53.
[14] P. Makvandi, C. Esposito Corcione, F. Paladini, A.L. Gallo, F. Montagna, R. Jamaledin, M. Pollini, A. Maffezzoli, Antimicrobial modified hydroxyapatite composite dental bite by stereolithography, Polymers for Advanced Technologies (2017) 1-8.
[15] R. Murugan, S. Ramakrishna, Design strategies of tissue engineering scaffolds with controlled fiber orientation, Tissue Eng. 13(8) (2007) 1845-1866.
[16] F.J. O'brien, Biomaterials & scaffolds for tissue engineering, Mater. Today 14(3) (2011) 88-95.
[17] S.J. Hollister, Porous scaffold design for tissue engineering, Nature materials 4(7) (2005) 518.
[18] R. Jin, L.M. Teixeira, P.J. Dijkstra, M. Karperien, C. Van Blitterswijk, Z. Zhong, J. Feijen, Injectable chitosan-based hydrogels for cartilage tissue engineering, Biomaterials 30(13) (2009) 2544-2551.
[19] A. Sivashanmugam, R.A. Kumar, M.V. Priya, S.V. Nair, R. Jayakumar, An overview of injectable polymeric hydrogels for tissue engineering, Eur. Polym. J. 72 (2015) 543-565.

[20] H. Tan, H. Li, J.P. Rubin, K.G. Marra, Controlled gelation and degradation rates of injectable hyaluronic acid-based hydrogels through a double crosslinking strategy, J. Tissue Eng. Regen. Med. 5(10) (2011) 790-797.
[21] Y. Hong, Y. Gong, C. Gao, J. Shen, Collagen-coated polylactide microcarriers/chitosan hydrogel composite: Injectable scaffold for cartilage regeneration, Journal of Biomedical Materials Research Part A: An Official Journal of The Society for Biomaterials, The Japanese Society for Biomaterials, and The Australian Society for Biomaterials and the Korean Society for Biomaterials 85(3) (2008) 628-637.
[22] S.M. Dorsey, J.R. McGarvey, H. Wang, A. Nikou, L. Arama, K.J. Koomalsingh, N. Kondo, J.H. Gorman III, J.J. Pilla, R.C. Gorman, MRI evaluation of injectable hyaluronic acid-based hydrogel therapy to limit ventricular remodeling after myocardial infarction, Biomaterials 69 (2015) 65-75.
[23] L. Ouyang, C.B. Highley, C.B. Rodell, W. Sun, J.A. Burdick, 3D printing of shear-thinning hyaluronic acid hydrogels with secondary cross-linking, ACS Biomaterials Science & Engineering 2(10) (2016) 1743-1751.
[24] N.R. Raia, B.P. Partlow, M. McGill, E.P. Kimmerling, C.E. Ghezzi, D.L. Kaplan, Enzymatically crosslinked silk-hyaluronic acid hydrogels, Biomaterials 131 (2017) 58-67.
[25] H.J. Sim, T. Thambi, D.S. Lee, Heparin-based temperature-sensitive injectable hydrogels for protein delivery, Journal of Materials Chemistry B 3(45) (2015) 8892-8901.
[26] F. Wang, Z. Li, M. Khan, K. Tamama, P. Kuppusamy, W.R. Wagner, C.K. Sen, J. Guan, Injectable, rapid gelling and highly flexible hydrogel composites as growth factor and cell carriers, Acta biomaterialia 6(6) (2010) 1978-1991.
[27] A. Alexander, J. Khan, S. Saraf, S. Saraf, Poly (ethylene glycol)–poly (lactic-co-glycolic acid) based thermosensitive injectable hydrogels for biomedical applications, J. Control. Release 172(3) (2013) 715-729.
[28] D.A. Ossipov, S. Piskounova, J.n. Hilborn, Poly (vinyl alcohol) cross-linkers for in vivo injectable hydrogels, Macromolecules 41(11) (2008) 3971-3982.
[29] K. Nagahama, A. Takahashi, Y. Ohya, Biodegradable polymers exhibiting temperature-responsive sol–gel transition as injectable biomedical materials, React. Funct. Polym. 73(7) (2013) 979-985.
[30] N. Sood, A. Bhardwaj, S. Mehta, A. Mehta, Stimuli-responsive hydrogels in drug delivery and tissue engineering, Drug Deliv. 23(3) (2016) 748-770.
[31] P. Makvandi, G. W Ali, F. Della Sala, W. I. Abdel-Fattah, A. Borzacchiello, Biosynthesis and characterization of antibacterial thermosensitive hydrogels based on corn silk extract, hyaluronic acid and nanosilver for potential wound healing, Carboyhdrate polymers 223 (2019) 115023-115034.
[32] P. Makvandi, G. W Ali, F. Della Sala, W. I. Abdel-Fattah, A. Borzacchiello, Hyaluronic acid/corn silk extract based injectable nanocomposite: a biomimetic antibacterial scaffold for bone tissue regeneration Materials Science and Engineering: C (2019) (just accepted).
[33] D.-D. Kim, D.-H. Kim, Y.-J. Son, Three-dimensional porous scaffold of hyaluronic acid for cartilage tissue engineering, Active Implants and Scaffolds for Tissue Regeneration, Springer2010, pp. 329-349.
[34] R.A. Muzzarelli, F. Greco, A. Busilacchi, V. Sollazzo, A. Gigante, Chitosan, hyaluronan and chondroitin sulfate in tissue engineering for cartilage regeneration: a review, Carbohydrate polymers 89(3) (2012) 723-739.

[35] L. Astachov, R. Vago, M. Aviv, Z. Nevo, Hyaluronan and mesenchymal stem cells: from germ layer to cartilage and bone, Front. Biosci. 16(1) (2011) 261-276.
[36] F. Yu, X. Cao, Y. Li, L. Zeng, B. Yuan, X. Chen, An injectable hyaluronic acid/PEG hydrogel for cartilage tissue engineering formed by integrating enzymatic crosslinking and Diels–Alder "click chemistry", Polymer Chemistry 5(3) (2013) 1082-1090.
[37] H. Park, B. Choi, J. Hu, M. Lee, Injectable chitosan hyaluronic acid hydrogels for cartilage tissue engineering, Acta biomaterialia 9(1) (2013) 4779-4786.
[38] M.B. Nair, J.D. Kretlow, A.G. Mikos, F.K. Kasper, Infection and tissue engineering in segmental bone defects—a mini review, Current opinion in biotechnology 22(5) (2011) 721-725.
[39] H.J. Mankin, F.J. Hornicek, K.A. Raskin, Infection in massive bone allografts, Clinical Orthopaedics and Related Research® 432 (2005) 210-216.
[40] M.A. Radzig, V.A. Nadtochenko, O.A. Koksharova, J. Kiwi, V.A. Lipasova, I.A. Khmel, Antibacterial effects of silver nanoparticles on gram-negative bacteria: influence on the growth and biofilms formation, mechanisms of action, Colloids Surf. B. Biointerfaces 102 (2013) 300-306.

[41] U. Hess, S. Hill, L. Treccani, P. Streckbein, C. Heiss, K. Rezwan, A mild one-pot process for synthesising hydroxyapatite/biomolecule bone scaffolds for sustained and controlled antibiotic release, Biomedical Materials 10(1) (2015) 015013.
[42] P. Makvandi, M. Ghaemy, A. Ghadiri, M. Mohseni, Photocurable, antimicrobial quaternary ammonium–modified nanosilica, J. Dent. Res. 94(10) (2015) 1401-1407.
[43] P. Makvandi, R. Jamaledin, M. Jabbari, N. Nikfarjam, A. Borzacchiello, Antibacterial quaternary ammonium compounds in dental materials: A systematic review, Dent. Mater. 34(6) (2018) 851-867.
[44] P. Makvandi, M. Ghaemy, M. Mohseni, Synthesis and characterization of photo-curable bis-quaternary ammonium dimethacrylate with antimicrobial activity for dental restoration materials, Eur. Polym. J. 74 (2016) 81-90.
[45] K. Kaviyarasu, N. Geetha, K. Kanimozhi, C.M. Magdalane, S. Sivaranjani, A. Ayeshamariam, J. Kennedy, M. Maaza, In vitro cytotoxicity effect and antibacterial performance of human lung epithelial cells A549 activity of zinc oxide doped TiO2 nanocrystals: investigation of bio-medical application by chemical method, Materials Science and Engineering: C 74 (2017) 325-333.
[46] P. Makvandi, N. Nikfarjam, N. Sanjani, N. Qazvini, Effect of silver nanoparticle on the properties of poly(methyl methacrylate) nanocomposite network made by in situ photoiniferter-mediated photopolymerization, Bull Mater Sci 38(6) (2015) 1625-1631.
[47] R. Lalani, L. Liu, Electrospun zwitterionic poly (sulfobetaine methacrylate) for nonadherent, superabsorbent, and antimicrobial wound dressing applications, Biomacromolecules 13(6) (2012) 1853-1863.
[48] S. Ahmed, M. Ahmad, B.L. Swami, S. Ikram, A review on plants extract mediated synthesis of silver nanoparticles for antimicrobial applications: a green expertise, Journal of advanced research 7(1) (2016) 17-28.
[49] P. Makvandi, E.N. Zare, B. Ashtari, A. Moeini, F.R. Tay, L.-n. Niu, Polymeric and inorganic nanoscopical antimicrobial fillers in dentistry, Acta Biomaterialia (2019) In press.
[50] A. Gour, N.K. Jain, Advances in green synthesis of nanoparticles, Artificial cells, nanomedicine, and biotechnology 47(1) (2019) 844-851.
[51] E.N. Zare, P. Makvandi, F.R. Tay, Recent progress in the industrial and biomedical applications of tragacanth gum: A review, Carbohydrate polymers 212 (2019) 450-467.

[52] S. Mukherjee, C.R. Patra, Biologically synthesized metal nanoparticles: recent advancement and future perspectives in cancer theranostics, Future Science, 2017.
[53] J.K. Patra, K.-H. Baek, Antibacterial activity and synergistic antibacterial potential of biosynthesized silver nanoparticles against foodborne pathogenic bacteria along with its anticandidal and antioxidant effects, Frontiers in microbiology 8 (2017) 167-182.
[54] D.H. Triutomo, A. Miranda, L.J. Tamba, E. Lukitaningsih, Estrogenic Effect Ethanol Extract Corn Silk (Stigma maydis) on Bone Density and Histology Femur Profiles in Ovariectomized Rats Female Sprague Dawley Strain, Indonesian Journal of Cancer Chemoprevention 7(3) (2016) 104-109.
[55] W.I. Abdel-Fattah, N. Atwa, G.W. Ali, Influence of the protocol of fibroin extraction on the antibiotic activities of the constructed composites, Progress in biomaterials 4(2-4) (2015) 77-88.
[56] P. Kumar, V.-K. Lakshmanan, R. Biswas, S.V. Nair, R. Jayakumar, Synthesis and biological evaluation of chitin hydrogel/nano ZnO composite bandage as antibacterial wound dressing, Journal of biomedical nanotechnology 8(6) (2012) 891-900.
[57] G.W. Ali, W. El-Hotaby, B. Hemdan, W.I. Abdel-Fattah, Thermosensitive chitosan/phosphate hydrogel-composites fortified with Ag versus Ag@ Pd for biomedical applications, Life Sci. 194 (2018) 185-195.
[58] W.I. Abdel-Fattah, A.S.M. Sallam, N.A. Atwa, E. Salama, A.M. Maghraby, G.W. Ali, Functionality, antibacterial efficiency and biocompatibility of nanosilver/chitosan/silk/phosphate scaffolds 1. Synthesis and optimization of nanosilver/chitosan matrices through gamma rays irradiation and their antibacterial activity, Materials Research Express 1(3) (2014) 1-16.
[59] T.G.F. Souza, V.S.T. Ciminelli, N.D.S. Mohallem, A comparison of TEM and DLS methods to characterize size distribution of ceramic nanoparticles, IOP Publishing, 2017, p. 012039.
[60] M. Kaasalainen, V. Aseyev, E. von Haartman, D.Ş. Karaman, E. Mäkilä, H. Tenhu, J. Rosenholm, J. Salonen, Size, stability, and porosity of mesoporous nanoparticles characterized with light scattering, Nanoscale research letters 12(1) (2017) 74-83.
[61] J.K. Patra, K.-H. Baek, Biosynthesis of silver nanoparticles using aqueous extract of silky hairs of corn and investigation of its antibacterial and anticandidal synergistic activity and antioxidant potential, IET nanobiotechnology 10(5) (2016) 326-333.
[62] S. Saravanan, S. Nethala, S. Pattnaik, A. Tripathi, A. Moorthi, N. Selvamurugan, Preparation, characterization and antimicrobial activity of a bio-composite scaffold containing chitosan/nano-hydroxyapatite/nano-silver for bone tissue engineering, International journal of biological macromolecules 49(2) (2011) 188-193.
[63] M. Dessi, A. Borzacchiello, T.H. Mohamed, W.I. Abdel-Fattah, L. Ambrosio, Novel biomimetic thermosensitive β-tricalcium phosphate/chitosan-based hydrogels for bone tissue engineering, Journal of Biomedical Materials Research Part A 101(10) (2013) 2984-2993.
[64] J.P. Chen, T.H. Cheng, Thermo-responsive chitosan-graft-poly (N-isopropylacrylamide) injectable hydrogel for cultivation of chondrocytes and meniscus cells, Macromolecular bioscience 6(12) (2006) 1026-1039.
[65] H. Li, Q. Ji, X. Chen, Y. Sun, Q. Xu, P. Deng, F. Hu, J. Yang, Accelerated bony defect healing based on chitosan thermosensitive hydrogel scaffolds embedded with chitosan nanoparticles for the delivery of BMP2 plasmid DNA, Journal of Biomedical Materials Research Part A 105(1) (2017) 265-273.
[66] K.M. Park, S.Y. Lee, Y.K. Joung, J.S. Na, M.C. Lee, K.D. Park, Thermosensitive chitosan–Pluronic hydrogel as an injectable cell delivery carrier for cartilage regeneration, Acta biomaterialia 5(6) (2009) 1956-1965.

[67] Y.s. Jung, W. Park, H. Park, D.-K. Lee, K. Na, Thermo-sensitive injectable hydrogel based on the physical mixing of hyaluronic acid and Pluronic F-127 for sustained NSAID delivery, Carbohydrate polymers 156 (2017) 403-408.
[68] S.-R. Son, S.K. Sarkar, N.-T.B. Linh, A.R. Padalhin, B.R. Kim, H.I. Jung, B.-T. Lee, Platelet-rich plasma encapsulation in hyaluronic acid/gelatin-BCP hydrogel for growth factor delivery in BCP sponge scaffold for bone regeneration, Journal of biomaterials applications 29(7) (2015) 988-1002.
[69] R.A. Muzzarelli, Chitosan composites with inorganics, morphogenetic proteins and stem cells, for bone regeneration, Carbohydrate Polymers 83(4) (2011) 1433-1445.
[70] P. Zhou, Y. Xia, X. Cheng, P. Wang, Y. Xie, S. Xu, Enhanced bone tissue regeneration by antibacterial and osteoinductive silica-HACC-zein composite scaffolds loaded with rhBMP-2, Biomaterials 35(38) (2014) 10033-10045.
[71] E.N. Zare, P. Makvandi, B. Ashtari, F. Rossi, A. Motahari, G. Perale, Progresses in conductive polyaniline-based nanocomposites for biomedical applications: A review, Journal of Medecinal Chemistry (2019) just accepted.
[72] L.C. Yun'an Qing, R. Li, G. Liu, Y. Zhang, X. Tang, J. Wang, H. Liu, Y. Qin, Potential antibacterial mechanism of silver nanoparticles and the optimization of orthopedic implants by advanced modification technologies, International journal of nanomedicine 13 (2018) 3311.
[73] I.M. Aboushady, Z.A. Salem, D. Sabry, A. Mohamed, Comparative study of the osteogenic potential of mesenchymal stem cells derived from different sources, Journal of clinical and experimental dentistry 10(1) (2018) e7.
[74] J.E. Aubin, Regulation of osteoblast formation and function, Reviews in Endocrine and Metabolic Disorders 2(1) (2001) 81-94.
[75] R. Zhang, P. Lee, V.C. Lui, Y. Chen, X. Liu, C.N. Lok, M. To, K.W. Yeung, K.K. Wong, Silver nanoparticles promote osteogenesis of mesenchymal stem cells and improve bone fracture healing in osteogenesis mechanism mouse model, Nanomedicine: Nanotechnology, Biology and Medicine 11(8) (2015) 1949-1959.
[76] H. Qin, C. Zhu, Z. An, Y. Jiang, Y. Zhao, J. Wang, X. Liu, B. Hui, X. Zhang, Y. Wang, Silver nanoparticles promote osteogenic differentiation of human urine-derived stem cells at noncytotoxic concentrations, International journal of nanomedicine 9 (2014) 2469-2473.

Chapter 4

Hyaluronic acid-based devices for delivery of drugs and viscosupplementation applications

Abstract

Osteoarthritis (OA), a destructive joint disease, causes extracellular matrix (ECM) degradation, deterioration of cartilage and alters the subchondral bone and synovium. Here, we aim to exploit the advantages of local drug delivery by developing a platform with improved efficacy. The hyaluronic acid-based device containing diclofenac sodium-encapsulated (2-Hydroxypropyl)-β-cyclodextrin (CD) possessed high drug loading along with prolonged release. The platform showed high mechanical properties along with low friction indications high lubricity of the platform. L929 cell morphology and viability assay showed a over the 100 % (approximately 110%) for the injectable device.

Keywords: Osteoarthritis, non-steroidal anti-inflammatory drugs (NSAIDs), viscosupplementation.

4.1. Introduction

4.1.1. Osteoarthritis

Osteoarthritis (OA), a destructive joint disease, causes extracellular matrix (ECM) degradation, deterioration of cartilage and alters the subchondral bone and synovium [1]. Patients are suffered from bone damage and morphological changes following by inflammation [2]. Knee osteoarthritis is responsible for a large burden of care and cost within health care. Osteoarthritis results from an imbalance between the breakdown and repair of articular cartilage in any joint and occurs as a result of multiple risk factors including mechanical overload (obesity, heavy lifting), trauma, overuse (repetitive knee bending), and genetic predisposition [3]. The incidence of new knee osteoarthritis in the U.S. is estimated at 240 persons per 100,000 per year [4]. The prevalence of the condition increases with age, especially in women. In adults over fifty years of age, it is estimated that the incidence of knee osteoarthritis in women is 45% higher than in men [5]. The prevalence of symptomatic knee osteoarthritis in patients at least forty-five years of age has been estimated to be 5.9% to 13.5% in men and 7.2% to 18.7% in women. Physician visits for knee pain in patients over the age of sixty-one years in the U.S. increased from 4.48 million in 2002 to 6.11 million in 2006 [3]. The economic impact of the treatment of osteoarthritis in the U.S. was estimated to be $185.5 billion in a 2009 study, with a large portion of those dollars being spent for knee osteoarthritis [6].

The pathogenesis of osteoarthritis is perhaps best understood as excessive mechanical stress applied in the context of systemic susceptibility. Susceptibility may be increased in part by genetic factors (a family history increases risk), older age, ethnic background (e.g., hip osteoarthritis is more common among white Americans than among Chinese people), nutritional factors (vitamin D or K deficiency), and female sex [7, 8]. In persons vulnerable to the development of knee osteoarthritis, local mechanical factors such as abnormal joint

congruity, joint malalignment, muscle weakness, or alterations in the structural integrity of the joint environment, such as meniscal damage or ligament rupture, can increase susceptibility to and progression of osteoarthritis. Loading can also be affected by obesity or joint injury (either acute, as in a sporting injury, or after repetitive overuse, such as in occupational exposure). The pathogenesis of osteoarthritis is characterized by progressive cartilage loss, subchondral bone remodeling, osteophyte formation, and synovial inflammation (**Fig. 1**) [9].

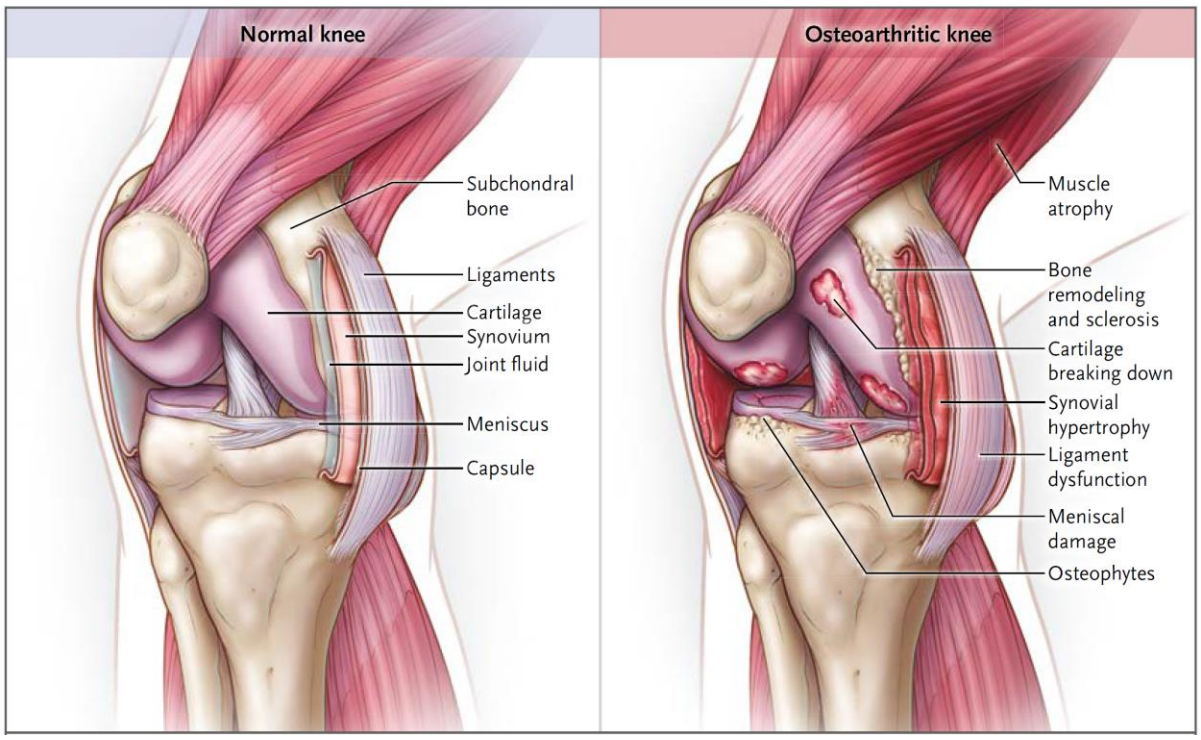

Fig. 1 Schematic of the Knee Joint, Showing the Synovial Joint Tissues Affected in Osteoarthritis**.** This schematic shows the way in which each structural part of the knee is affected by osteoarthritis, an observation that is consistent with the theory that osteoarthritis is a disease of the entire synovial joint [9].

4.1.2. Hyaluronic acid-based viscosupplementation materials

Hyaluronate is a naturally occurring component of the cartilage and the synovial fluid. It is a polysaccharide composed of continuously repeating molecular sequences of β-D-glucuronic acid and β-D-*N*-acetylglucosamine, with a molecular mass in normal synovial fluid ranging

from 6500 to 10,900 kDa. It can be either synthesized by means of bacterial fermentation or extracted from animal tissues (e.g., rooster comb). [9].

About one half of the overall HA content of the adult human body is located within the skin. The synovial fluid is also rich in HA. With advancing age, the HA content largely decreases in the epidermis and synovial fluid. The decline is more pronounced in the latter when osteoarthritic alterations emerge as well. Late in life, the human body contains about one half to two thirds less HA [10].

Within the normal adult knee, there is approximately 2 ml of synovial fluid, with a hyaluronate concentration of 2.5 to 4.0 mg per milliliter [11]. Hyaluronate is responsible for the rheologic properties of synovial fluid, enabling it to act as a lubricant or shock absorber, depending on the forces exerted on it [12]. In osteoarthritis, synovial hyaluronate is depolymerized (molecular mass, 2700 to 4500 kDa) and cleared at higher rates than normal [13]. In a normal joint, the average intrasynovial half-life of hyaluronate is approximately 20 hours [11]. In an inflamed joint, this half-life is decreased to 11 to 12 hours. These changes reduce the viscoelasticity of the synovial fluid.

The current therapeutic approaches for OA consists of intra-articular injection of hyaluronic acid (HA) and its derivatives to joints offering viscoelastic properties to the synovial fluid (**Fig. 2)** [14]. HA is a naturally occurring carbohydrate polymer which is the major component of the extracellular matrix (ECM) in mammalian connective tissues. HA also controls viscoelastic properties, cell growth, proliferation, and tissue remodeling where to fulfill both physiochemical and biological functions [15].

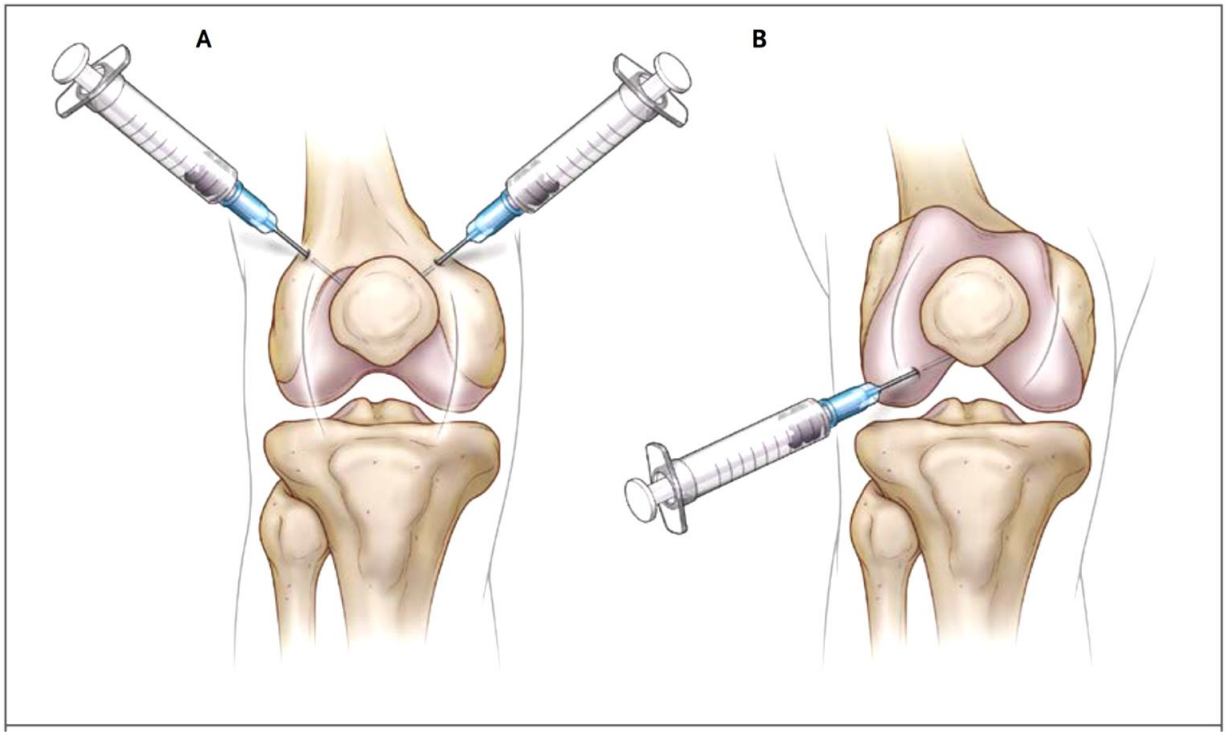

Fig. 2 Injection Sites. Panel A shows the superomedial and superolateral injection sites. These injections are performed with the knee extended. Panel B shows the lateral joint line injection site, with the right knee flexed 90 degrees.

The injected polymers range in size from 100 to 10,000 kDa. The therapeutic goal of administration of intraarticular hyaluronate is to provide and maintain intraarticular lubrication, which increases the viscoelastic properties of synovial fluid [16]; this form of therapy is therefore sometimes termed “viscosupplementation”. It is also claimed that hyaluronate exerts anti-inflammatory, analgesic, and possibly chondroprotective effects on the articular cartilage and joint synovium [11]. The clinical benefits of treatment with intraarticular hyaluronate, which may persist well beyond the intraarticular residence time of the product, have been suggested to be caused by the reestablishment of joint homeostasis as a result of an increase in the endogenous production of hyaluronate that persists long after the exogenous injected material has left the joint [13].

4.1.3. Delivery of anti-inflammatory drugs

In addition, non-steroidal anti-inflammatory drugs (NSAIDs), e.g. diclofenac sodium, are employed for reducing the pain and inflammation [17]. Local administration of diclofenac sodium can minimize the amount of orally administrated drug along with maximizing the concentration of diclofenac sodium at the joint. Nevertheless, diclofenac sodium possesses a half-life of approximately 5 h and is eliminated from the synovial fluid. Accordingly, frequent intra-articular injections are not welcome by patients [18, 19]. Moreover, conventional dosage forms do not provide a prolonged release of the drug, hence, leading to the necessity of frequent injections which can cause inflammations and raise patient suffering. However, since the current devices for intra-articular injection are targeted to be used in human body, they are mainly water-based systems and, hence, the loading of diclofenac sodium (as a lipophilic drug) in these systems is low [20]. In order to conquer the problem and improve drug loading, (2-Hydroxypropyl)-β-cyclodextrin (CD) has been employed for aqueous-based carriers [21, 22]. CD is chemically and physically stable in physiochemical condition which is water-soluble, biocompatible in nature with hydrophilic outer surface and lipophilic inner cavity [22].

Therefore, the aim of this study is to design a delivery system able to prolong the release of an anti-inflammatory drug into the joint cavity and, at the same time, able to restore the viscoelastic features of pathologic synovial fluid. Hence, we formulated a hyaluronic acid-based device for delivery of non-steroidal anti-inflammatory drugs. Vitamin E is used for two purposes including enhancing the loading of diclofenac sodium and improving the thermal stability of the formulations due to its antioxidant activity. The physical properties, e.g. rheological and tribological behaviors, and drug release study as well as *in vitro* and *in vivo* biological activity, such as cytotoxicity, cell morphology, intra-articular injection on mice, were evaluated.

4.2. Materials and methods

4.2.1. Materials

Hyaluronic acid (HA) with a weight-average molecular weight (Mw) of 1490 kDa and diclofenac sodium were kindly provided by Altergon Italia. (2-Hydroxypropyl)-β-cyclodextrin (CD), and vitamin E acetate (Tocopherol acetate) were purchase from Sigma-Aldrich.

4.2.2. Formulation and preparation

CD and VE and HA were mixed and PBS solution was added to the mixture with maintaining stirring for at least 8 hours at room temperature. Many formulations were prepared and investigated by means of rheological properties and thermal stability and, finally, the optimized formulations are reported in table 1.

Table 1. Formulations of the prepared samples. The values of G' and G" at 1 Hz for formulations of at 37 °C. Friction data for sliding velocity of 1 mm/s at 37 °C.

Entry	HA	CD	VE	G'	G''	Friction
	w/w %			Pa		μ
HA	2	0	0	72	68	0.165
HC	2	2	0	62	56	0.085
HV	2	0	2	57	50	0.126
HCV	2	2	2	172	121	0.050

4.3.Rheological properties

Small amplitude oscillatory shear tests were performed to evaluate the time-dependent response of the thermosensitive hydrogels and their linear viscoelastic properties. The frequency was in the range from 0.01 to 15 Hz. The measurements were carried out through a strain controlled rotational rheometer (Mars III, HAAKE Rheometer, Waltham, MA, USA),

using a parallel plate geometry. The tests were carried out at the controlled temperatures of 20 and 37 °C using a thermostatic bath. In order to identify the linear viscoelastic response range of the materials, preliminary strain sweep tests were performed on the samples, at the oscillation frequency of 1 Hz. The tests were repeated at least three times on each sample.

4.4.Rotational tribometry

The tribology measurements were performed using a Physica molecular compact rheometer (MCR 302, Anton Paar, Graz, Austria) equipped with a tribology measuring ball (BC12.7) and sample pin (polydimethylsiloxane, PDMS 155994). The test procedure was described in detail elsewhere [23]. In brief, a glass sphere with a diameter of 1.27 cm (0.5 inch) was lowered on to three osteochondral cylinders (three PDMS pins) fixed inside a sample holder, and the samples were fully submersed by adding 1 ml of the lubricant. During the measurements, a normal force of 6N was applied resulting in a contact pressure of approximately 0.1 MPa. Each sample was subjected to three friction tests at rotational velocities from 0.1 to 1000 mm/s.

4.5.Drug solubility

Different amounts of DF including 2.5, 5.7, and 20 mg/ml were added to the formulation of HCV, the formulations were stirred until being completely homogenized. Once prepared they were kept for 24 h and after centrifuged (6000 rpm for 15 min). Finally, the supernatant was analyzed by means of UV spectrophotometer. The tests were performed in triplicate and the wavelengths used for the detection of diclofenac sodium was 276 nm. Moreover, a calibration curve was constructed by plotting absorbance against predetermined concentration of DF in PBS. Then, linear regression was used to determine the regression equation representing the calibration curve. Solubilized fraction (SF) expressed by:

$$SF\% = \frac{solubilized\ DF}{Total\ DF} \times 100 \qquad (1)$$

4.6.Drug release

To perform the release test, 1 gr of the formulation containing DF at 1% w/w was inserted in a dialysis membrane (cut off 500 to 1000 Da) and then it was immersed in PBS medium (18 ml) at the temperature of 37 ˚C. At predetermined time intervals, 50 μL aliquots of the medium was withdrawn and the same volume of fresh medium was replaced. The drug concentration released into the PBS buffer was detected by UV spectrophotometer as a function of time.

4.7.Release kinetic

Data obtained from the release studies were fitted to the following kinetic equations, which adapted from methods reported in literature and describing drug release from HA-based systems as the result of a dissolutive and a Fickian diffusional mechanisms [24, 25]. The dissolutive contribution is given by the following equation:

$$F_{diss} = F_{diss,\infty} k_{diss} t^{0.5} \quad (2)$$

here F_{diss} and $F_{diss,\infty}$ are the drug fractions released by dissolution at time t and after an infinite time, respectively, k_{diss} is the kinetic dissolution parameter. The diffusional contribution to drug release is expresse by:

$$F_{diff} = (1 - F_{diff,\infty})(1 - \exp[-k_{diff} t]) \quad (3)$$

where F_{diff} is the drug fraction released due to diffusion at time t and k_{diff} is the kinetic diffusional parameter. Therefore, the overall released fraction (F_{tot}) is obtained by the sum of diffusion and dissolution contributions, as given by the following equation:

$$F_{tot} = F_{diss} + F_{diff} = F_{diss,\infty} k_{diss} t^{0.5} + (1 - F_{diff,\infty})(1 - \exp[-k_{diff} t]) \quad (4)$$

The drug released data were fitted also to Korsmeyer–Peppas equation (eq. 5)

$$Q_t/Q_\infty = k_k t^n \quad (5)$$

Where Q_t and Q_∞ are the amounts of drug released at the time (t) and at equilibrium, respectively. k_k is the release rate constant that considers the geometric and structural features of the carrier, and n is the release or diffusional exponent which demonstrate the drug release mechanism [26, 27].

4.8.Cell culture

In order to evaluate the biological response to our injectable hydrogels, L929 cells deriving from Mouse C34/An connective tissues were obtained from the European Collection of cell cultures (Sigma-Aldrich, USA), were used. L929 cells were grown in T-75 cell culture flask (Falcon, Italy), in cell culture medium Dulbecco's Modified Eagle's Medium (DMEM, Hyclone, USA) supplemented with 10% fetal bovine serum (FBS) and antibiotics (penicillin G sodium 100 U/mL, streptomycin 100 □g/mL) at 37°C and 5% CO2. The medium was changed every 3-4 days.

4.9. Cell viability and morphology assay

In order to understand the cells viability, L929 cells were seeded at a density of 8×10^4 cells/ml on 96-wells (World Precision Instruments, Inc). The hydrogels were sterilized by steam autoclaving at 121 °C for 20 min. The cells were incubated with 5µl of the formulations HA, HCV for each well in triplicate up to 72 h and then Alamar blue assay (AB) was performed by adding AB reagent to the samples (at 10% v/v with respect to the medium) and incubated at 37°C for 4 hours. The absorbance of the samples was measured using a spectrophotometer plate reader (Multilabel Counter, 1420 Victor, Perkin Elmer) at 570 nm and 600 nm. AB is an indicator dye that incorporates an oxidation-reduction indicator that changes color in response to the chemical reduction in the growth medium, resulting from cell viability. L929 seeded wells were used as a control. Data are expressed as the percentage difference between treated

and control to evaluate the percentage of reduction (Reduction %), which is calculated with the following formula:

$$Reduction\ (\%) = \frac{(O_2 \times A_1) - (O_1 \times A_2)}{(O_2 \times P_1) - (O_1 \times P_2)} \times 100 \quad (6)$$

where $O1$ is the molar extinction coefficient (E) of oxidized AB at 570 nm; $O2$ is the E of oxidized AB at 600 nm; $A1$ is the absorbance of test wells at 570 nm; $A2$ is the absorbance of test wells at 600 nm; $P1$ is the absorbance of control well at 570 nm; and $P2$ is the absorbance of control well at 600 nm. The percentage of reduction for each sample was normalized to the percentage of reduction for the control to obtain the cell viability percentage [28].

For cell morphology assay, cells were seeded at a density of 1×10^4 cells/ml on fluorodish-35 mm (World Precision Instruments, Inc) and 5µl of the formulations HC, HCV were incubated for 24 h. Then, the samples were washed two times with PBS and fixed with 10% formaldehyde for 1 hour at 4 °C. The fixed cells were permeabilized with Triton X-100 0.1% in Phosphate-buffered saline (PBS) for 3-5 min. The actin filaments were stained with TRITC phalloidin (Cayman Chemical Company) in PBS for 30 minutes at room temperature. Finally, after two washes with PBS in order to remove unbound phalloidin conjugate, cell nuclei were stained with 4',6-diamidino-2-phenylindole, DAPI, (SIGMA-ALDRICH). The samples were observed by confocal microscope system (Leica TCS SP8) with a 63X oil immersion objective. Images were acquired with a resolution of 1024×1024 pixel.

5. Results

3.1. Rheological and tribological properties

Fig. 3A and **B** show the mechanical spectra of samples at 37 °C. As can be seen, HCV formulation has better mechanical properties (both G' and G'') in comparison with other samples including HA, HC, and HV. Accordingly, as the viscoelastic parameters at f = 1 Hz

are reported in Table 2, HCV has higher elastic and viscos moduli. These results indicate that the addition of CD and VE to a solution of HA has an important role in creating a network that stabilizes the solution and lead to an improvement of the viscoelastic parameter.

The results of tribology test are shown in **Fig. 3C**. Pure HA sample has the highest friction following by HV and HC ones and, finally, the lowest friction was achieved for HCV platform. In detail, HCV had friction factor 0.5 μ whereas the other systems showed higher values of friction factor. In fact, for the all range of sliding velocity, the HCV sample showed the highest lubricity.

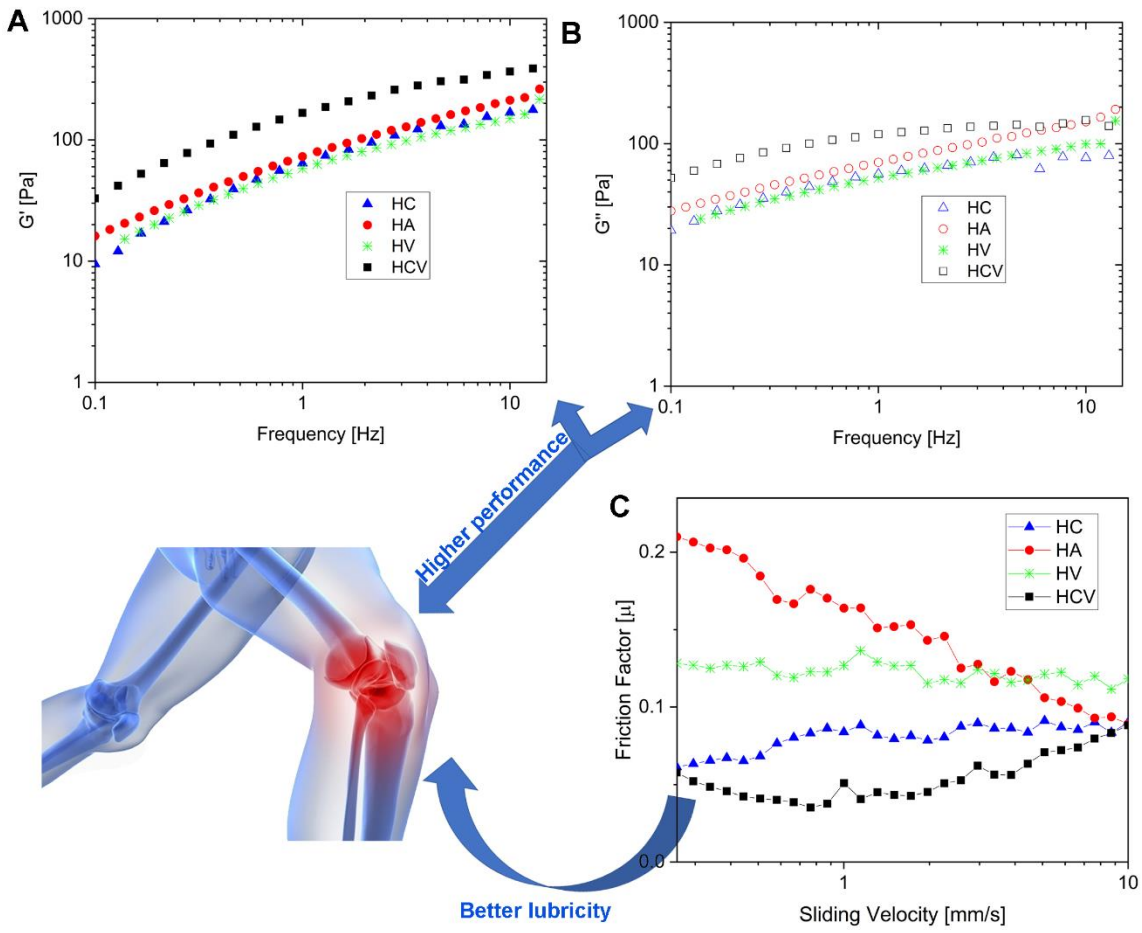

Fig. 3 Mechanical spectra (A and B) and friction factor (C) of HC, HA, HV, and HCV formulations. Elastic (G') and viscus (G'') modulus of the formulations at 37 ˚C. (C) Tribology test (at 37 ˚C) to

define the lubricity of the formulations. Higher mechanical properties along with better lubricity were achieved for HCV samples.

The rheological synergy can be quantified by the interaction parameter that is, the difference between the dynamic modulus values of the mixture evaluated by rheological test and the theoretical one given by adding the dynamic modulus values of the primary components.

The results of the calculation of synergistic parameters for HCV are reported in Table 3. In all conditions, including with and without AC treatment as well as different temperatures, the system shows synergistic effect.

T**able 2.** Effect of VE on the viscoelastic parameters. The values of G' and G" at 1 Hz for formulations of HC and HCV before and after autoclaving (AC) at 20 and 37 °C.

Entry	Before AC at 20		After AC at 20		Before AC at 37		After AC at 37	
	G' [Pa]	G" [Pa]	G'[Pa]	G" [Pa]	G'[Pa]	G" [Pa]	G'[Pa]	G" [Pa]
HC	66	57	17	24	53	49	15	20
HCV	166	119	78	98	126	98	43	67

Table 3. Synergistic effect of formulation viscoelastic parameters at 1 Hz.

Condition	G'_{HCV} [Pa]	G'_{HA+VE} [Pa]	G'_{CD} [Pa]	$\Delta G'_{Synergistic}$ [Pa]
20 °C	166	78	0.013	88
20 °C After AC	78	13	0.011	65
37 °C	130	53	0.013	77
37 °C After AC	48	8	0.013	40

3.2. Drug solubility and release kinetic

The results of the dissolution tests are reported in **Fig. 4A** as calculated the ratio of DF which was found into the supernatant of the solution and total dissolved DF. The solubilized fraction of DF declined by increasing the DF concentration.

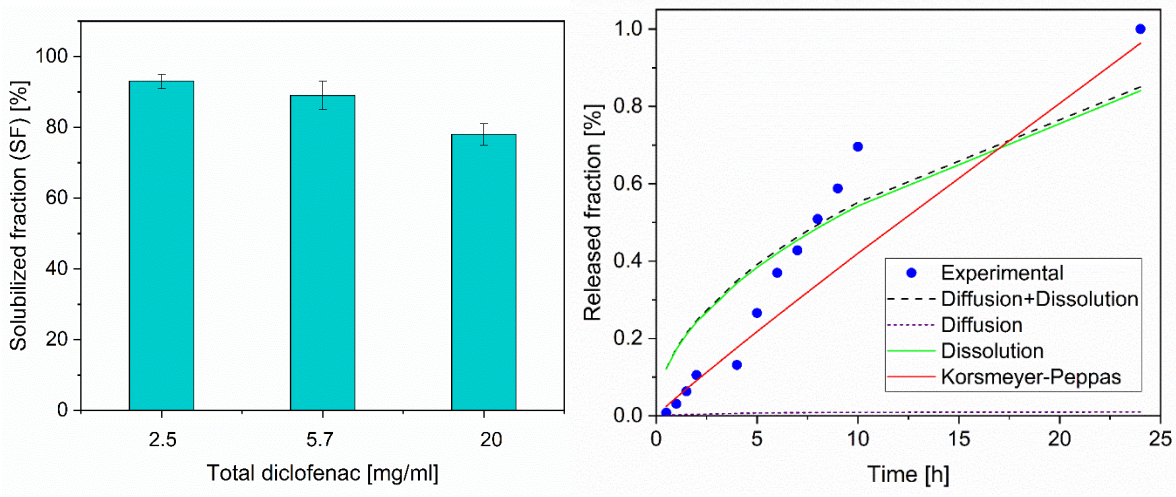

Fig. 4 Diclofenac sodium solubility (A) and its release (B) from the HCV. Drug release kinetic were fitted the kinetic equations. It can be seen that after 10 hours only 48% of the drug was released in the medium and after 24 h there is the complete release of the drug which shows the controlled release of the composition.

Experimental and simulated *in vitro* fractional release profiles of DF in phosphate buffer are shown in **Fig. 4B**. It can be seen that after 10 h only 48% of the drug was released in the medium and after 24 h there is the complete release of the drug which shows the controlled release of the composition. There was very good reproducibility between the triplicates. Prominently, no significant differences between samples was observed which indicate a homogenous diffusion in the prepared composition. The analysis of release profiles shows that, in all cases, dissolution is faster in comparison with diffusion; for example, at least initial release is governed by diffusion. However, the results displayed that the Korsmeyer–Peppas equation gave better fit with high correlation coefficient (R^2=0.96) for the composition. The value of n=0.5 demonstrates Fickian diffusion (Higuchi matrix), 0.5<n<1.0 indicates

anomalous (non-Fickian) diffusion, n=1.0 indicates case II transport (zero-order release) and n>1.0 indicates super case II transport [26, 27].

3.3.Cell viability and morphology

In order to assess the biocompatibility of the injectable hydrogels, L929 cells viability was evaluated by Alamar Blue assay. It is clear from the results in **Fig. 5A** that the hydrogels (HA, HCV) showed good safety after 24 and 72 h of incubation in L929 cells, compared to the untreated controls. In particular, after 24 h of incubation with both formulations, L929 cells viability is around 80%, noting, that, at 72 h, the viability increases around 100% and in particular over the 100 % (about 110%) for the sample with HCV. The results collectively indicated that the prepared formulations exhibit good *in vitro* biocompatibility. This biocompatibility data was also confirmed by cells morphology. Actin filaments, a constituent of the cytoskeleton, were stained with TRIC phalloidin after 24 h of incubation with HA and HCV hydrogels. L929 cells, indeed, exhibited a noncytotoxic and typical mouse fibroblast-like cellular morphology after the incubation with the two formulations (**Fig. 5B**). Their morphology was alike to the characteristic *in vitro* L929 cells morphology that is spread or spindle-shaped, often characterized by several extending processes, which consists of cells protrusion adhering at the flat surface. These results indicate that these devices have a good biocompatibility and the most important confirmation appears to be that the HCV, containing both HA, CD and VE, maintain a good biocompatibility, which is increased after 72 h of incubation, suggesting that the combination of these three materials could be positively affect the viability of cells.

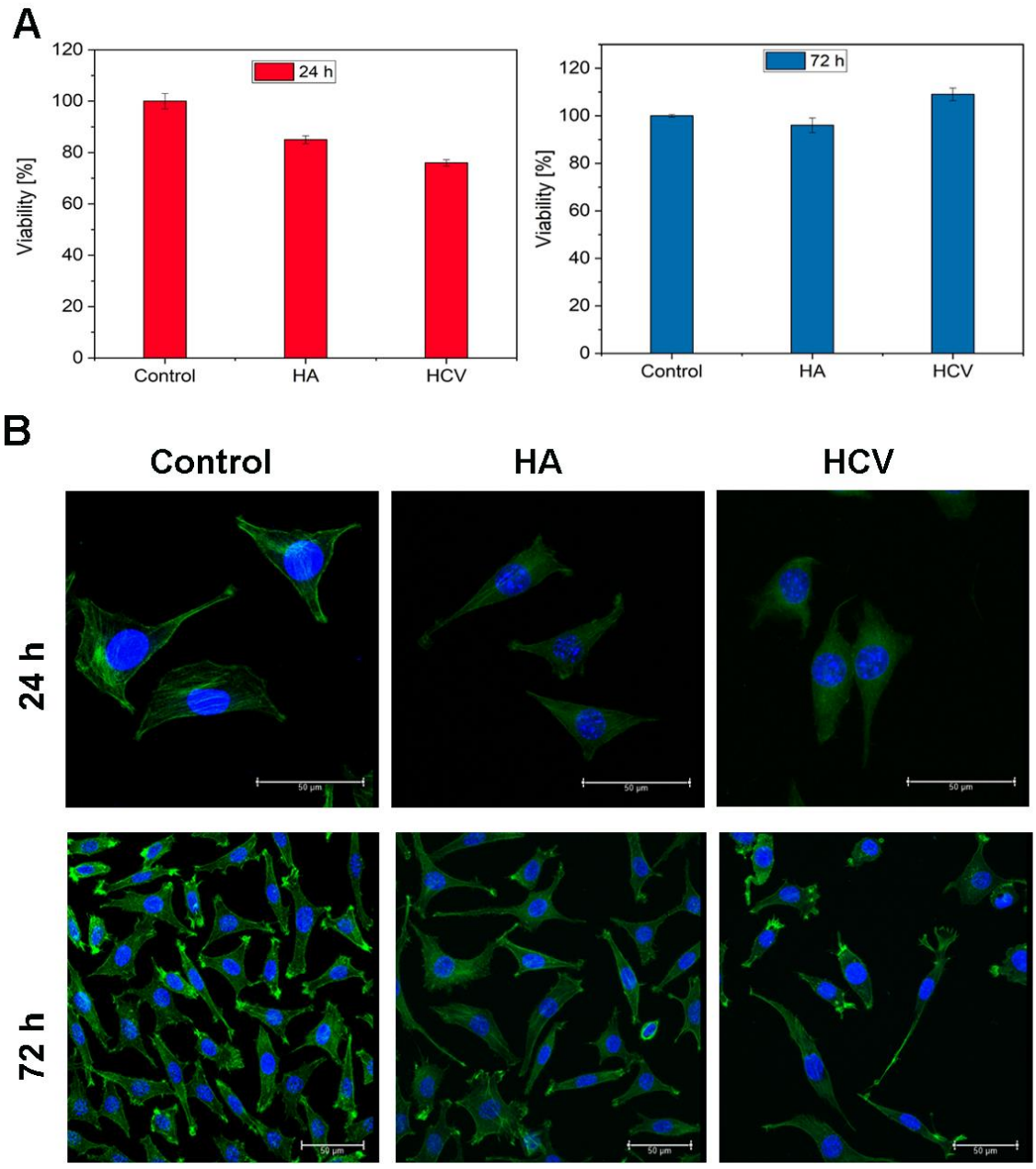

Fig. 5 (A) Cytotoxicity of samples at 24 and 72 h. p-value<0.05 for the same symbol as compared to SP. All results are presented as mean ± standard deviation. The data are representatives of three repeated. (B) Cell morphology for the control and thermosensitive hydrogels after 24 h. In Green Actin filaments stained by phalloidin-TRIC and in Blue DAPI stained nuclei cells. The typical cellular morphology of L929 cell lines was used. All bars represent 50 µm).

4. Discussion

OA is one of the main sources of disability of the adult population. HA-based viscosupplementation platforms not only offers in the pain relief but also improves the structure of the diseased joint declining the progression rate of OA specially in the early stages [29, 30]. As OA progresses, the concentration, distribution and molecular weight of HA within the joint diminish which cause the declining of viscoelastic features of the endogenous synovial fluid [31]. The primary goals for clinical management of OA of the knee are to minimize pain, maintain or improve joint mobility, and to minimize functional impairment [32].

Both CD and VE interact with HA through secondary bonds cooperating in the formation of complexes among the molecules that stabilize the network. These cooperating complexes are further stabilized when the formulations are thermally processed by heating at a temperature 120°C for a processing time between 10 and 30 min and then cooled at 20/37°C. After the thermal treatment (autoclaving), there is an increase of the elastic modulus that up to 4 times due to the presence of CD/VE in the formulations.

The synovial joint is a perfect tribological system with low friction and high wear resistance [33]. The use of tribology test is a simplified model of the joint movement in mammalian. The decrease of friction coefficient of aluminum with the increase of sliding speed may be due to the change in the shear rate which can influence the mechanical properties of the mating materials [34].

Topical administration to the site of action is preferred to the available oral drugs for pharmacologic therapy which has shortcomings, such as first-pass metabolism of oral drugs [20]. In addition, parenteral administration of diclofenac sodium does not offer sustained release, thus leading to the necessity of frequent injections which may suffer patients. On contrary, locally injected devices containing DF possess more favorable tolerability profile and sustained release [17, 35]. In this work, diclofenac sodium was encapsulated into β-CD to improve the drug loading and enhanced release time. Regarding the other sorts of CD, the

cavity size of α-CD is small for a number of drugs/biomolecules and γ-CD is expensive. β-CD has been broadly used in pharmaceutical sector due to its availability and cavity size is appropriate for the extensive range of drugs/biomolecules [21].

The practical applications of intra-articular injectable devices require significant tribological properties. Friction can be defined as the resistance to motion which exists when one solid body slides over another. The friction force is a tangential force which acts in a direction directly opposite to the direction of motion [36]. The lowest friction of HCV device is equal to higher lubricity which is an important factor for viscosupplementation devices aimed to be injected to human joint.

References

[1] P. Chen, C. Xia, S. Mei, J. Wang, Z. Shan, X. Lin, S. Fan, Intra-articular delivery of sinomenium encapsulated by chitosan microspheres and photo-crosslinked GelMA hydrogel ameliorates osteoarthritis by effectively regulating autophagy, Biomaterials 81 (2016) 1-13.
[2] B. von Lospichl, S. Hemmati-Sadeghi, P. Dey, T. Dehne, R. Haag, M. Sittinger, J. Ringe, M. Gradzielski, Injectable hydrogels for treatment of osteoarthritis–A rheological study, Colloids Surf. B. Biointerfaces 159 (2017) 477-483.
[3] D. Jevsevar, P. Donnelly, G.A. Brown, D.S. Cummins, Viscosupplementation for osteoarthritis of the knee: a systematic review of the evidence, JBJS 97(24) (2015) 2047-2060.
[4] S.A. Oliveria, D.T. Felson, J.I. Reed, P.A. Cirillo, A.M. Walker, Incidence of symptomatic hand, hip, and knee osteoarthritis among patients in a health maintenance organization, Arthritis & Rheumatism: Official Journal of the American College of Rheumatology 38(8) (1995) 1134-1141.
[5] V.K. Srikanth, J.L. Fryer, G. Zhai, T.M. Winzenberg, D. Hosmer, G. Jones, A meta-analysis of sex differences prevalence, incidence and severity of osteoarthritis, Osteoarthritis Cartilage 13(9) (2005) 769-781.
[6] H. Kotlarz, C.L. Gunnarsson, H. Fang, J.A. Rizzo, Insurer and out-of-pocket costs of osteoarthritis in the US: Evidence from national survey data, Arthritis & Rheumatism: Official Journal of the American College of Rheumatology 60(12) (2009) 3546-3553.
[7] D.J. Hunter, Lower extremity osteoarthritis management needs a paradigm shift, Br. J. Sports Med. 45(4) (2011) 283-288.

[8] K.D. Allen, Y.M. Golightly, Epidemiology of osteoarthritis: state of the evidence, Curr. Opin. Rheumatol. 27(3) (2015) 276.
[9] D.J. Hunter, Viscosupplementation for osteoarthritis of the knee, N. Engl. J. Med. 372(11) (2015) 1040-1047.
[10] S. Reitinger, G. Lepperdinger, Hyaluronan, a ready choice to fuel regeneration: a mini-review, Gerontology 59(1) (2013) 71-76.
[11] E.J. Strauss, J.A. Hart, M.D. Miller, R.D. Altman, J.E. Rosen, Hyaluronic acid viscosupplementation and osteoarthritis: current uses and future directions, The American journal of sports medicine 37(8) (2009) 1636-1644.
[12] T. Conrozier, X. Chevalier, Long-term experience with hylan GF-20 in the treatment of knee osteoarthritis, Expert Opin. Pharmacother. 9(10) (2008) 1797-1804.
[13] E.A. Balazs, J.L. Denlinger, Viscosupplementation: a new concept in the treatment of osteoarthritis, The Journal of rheumatology. Supplement 39 (1993) 3-9.
[14] T.M. Duymus, S. Mutlu, B. Dernek, B. Komur, S. Aydogmus, F.N. Kesiktas, Choice of intra-articular injection in treatment of knee osteoarthritis: platelet-rich plasma, hyaluronic acid or ozone options, Knee Surg. Sports Traumatol. Arthrosc. 25(2) (2017) 485-492.
[15] P. Makvandi, G. W Ali, F. Della Sala, W. I. Abdel-Fattah, A. Borzacchiello, Biosynthesis and characterization of antibacterial thermosensitive hydrogels based on corn silk extract, hyaluronic acid and nanosilver for potential wound healing, Carboyhdrate polymers 223 (2019) 115023-115034.
[16] P. Ghosh, D. Guidolin, Potential mechanism of action of intra-articular hyaluronan therapy in osteoarthritis: are the effects molecular weight dependent?, Semin. Arthritis Rheum., Elsevier, 2002, pp. 10-37.
[17] A. Sulistio, F.M. Mansfeld, F. Reyes Ortega, A.M. D'Souza, S.M. Ng, S. Birkett, A. Blencowe, G.G. Qiao, C.B. Little, C.C. Shu, Intra-articular treatment of osteoarthritis with diclofenac-conjugated polymer reduces inflammation and pain, ACS Applied Bio Materials (2019).
[18] M.L. Kang, G.-I. Im, Drug delivery systems for intra-articular treatment of osteoarthritis, Expert opinion on drug delivery 11(2) (2014) 269-282.
[19] Z. Unlu, K. Ay, C. Tuzun, Comparison of intra-articular tenoxicam and oral tenoxicam for pain and physical functioning in osteoarthritis of the knee, Clin. Rheumatol. 25(1) (2006) 54-61.
[20] N. Gerwin, C. Hops, A. Lucke, Intraarticular drug delivery in osteoarthritis, Adv. Drug Del. Rev. 58(2) (2006) 226-242.
[21] R. Challa, A. Ahuja, J. Ali, R. Khar, Cyclodextrins in drug delivery: an updated review, AAPS PharmSciTech 6(2) (2005) E329-E357.
[22] B. Gidwani, A. Vyas, A comprehensive review on cyclodextrin-based carriers for delivery of chemotherapeutic cytotoxic anticancer drugs, BioMed research international 2015 (2015).
[23] K. Boettcher, B. Winkeljann, T.A. Schmidt, O. Lieleg, Quantification of cartilage wear morphologies in unidirectional sliding experiments: Influence of different macromolecular lubricants, Biotribology 12 (2017) 43-51.
[24] C. Nastruzzi, E. Esposito, R. Cortesi, R. Gambari, E. Menegatti, Kinetics of bromocriptine release from microspheres: comparative analysis between different in vitro models, J. Microencapsul. 11(5) (1994) 565-574.
[25] N.A. Peppas, P.A. Buri, Surface, interfacial and molecular aspects of polymer bioadhesion on soft tissues, J. Control. Release 2(0) (1985) 257-275.
[26] R.W. Korsmeyer, R. Gurny, E. Doelker, P. Buri, N.A. Peppas, Mechanisms of solute release from porous hydrophilic polymers, Int. J. Pharm. 15(1) (1983) 25-35.
[27] J. Monjezi, R. Jamaledin, M. Ghaemy, A. Moeini, P. Makvandi, A Performance Comparison of Graft Copolymer Hydrogels Based on Functionalized-Tragacanth

Gum/Polyacrylic Acid and Polyacrylamide as Antibacterial and Antifungal Drug Release Vehicles, American Journal of Nanotechnology & Nanomedicine (2018).
[28] P. Makvandi, G. W Ali, F. Della Sala, W. I. Abdel-Fattah, A. Borzacchiello, Hyaluronic acid/corn silk extract based injectable nanocomposite: a biomimetic antibacterial scaffold for bone tissue regeneration Materials Science and Engineering: C (2019) In press.
[29] M. Wobig, G. Bach, P. Beks, A. Dickhut, J. Runzheimer, G. Schwieger, G. Vetter, E. Balazs, The role of elastoviscosity in the efficacy of viscosupplementation for osteoarthritis of the knee: a comparison of hylan GF 20 and a lower-molecular-weight hyaluronan, Clin. Ther. 21(9) (1999) 1549-1562.
[30] M. Abate, P. Pelotti, D. De Amicis, A. Di Iorio, S. Galletti, V. Salini, Viscosupplementation with hyaluronic acid in hip osteoarthritis (a review), Ups. J. Med. Sci. 113(3) (2008) 261-278.
[31] R.D. Altman, A. Manjoo, A. Fierlinger, F. Niazi, M. Nicholls, The mechanism of action for hyaluronic acid treatment in the osteoarthritic knee: a systematic review, BMC Musculoskelet. Disord. 16(1) (2015) 321.
[32] J.G. Divine, B.T. Zazulak, T.E. Hewett, Viscosupplementation for knee osteoarthritis: a systematic review, Clinical Orthopaedics and Related Research® 455 (2007) 113-122.
[33] P. Bhuanantanondh, Rheology of synovial fluid with and without viscosupplements in patients with osteoarthritis: a pilot study, (2009).
[34] M.A. Chowdhury, M.K. Khalil, D.M. Nuruzzaman, M.L. Rahaman, The effect of sliding speed and normal load on friction and wear property of aluminum, Int. J. Mech. Mechatron. Eng 11(01) (2011) 53-57.
[35] P. Hartmann, E. Butt, Á. Fehér, Á.L. Szilágyi, K.D. Jász, B. Balázs, M. Bakonyi, S. Berkó, G. Erős, M. Boros, Electroporation-enhanced transdermal diclofenac sodium delivery into the knee joint in a rat model of acute arthritis, Drug Des. Devel. Ther. 12 (2018) 1917.
[36] R.D. Arnell, P. Davies, J. Halling, T. Whomes, Tribology: Principles and Design Applications: Principles and Design Applications, Macmillan International Higher Education1991.

General Conclusion

We have prepared different antibacterial platforms containing hyaluronic acid and silver nanoparticles. Silver nanoparticles (Ag NPs) were biosynthesized by a microwave-assisted green technique using corn silk extract in an organic solvent-free medium. The thermosensitive and injectable hydrogels were prepared and their potential use as wound care materials and bone regeneration were investigated. Rheological analysis demonstrated that the nanocomposites have good mechanical properties with gelation temperature close to the body temperature; hence, they can be easily administrated locally on wounded skins and bone defect. The samples exhibited antibacterial activity toward gram-positive and gram-negative bacteria. Cytotoxicity assay showed that the hydrogels have good biocompatibility. Interestingly, an *in-vitro* model of wound healing revealed that the nanocomposites allow faster wound closure and repair, compared to the control. Regarding the bone tissue engineering applications, mesenchymal stem cells seeded in the nanocomposite exhibited high bone differentiation which indicate that they could be a good candidate as a potential scaffold for bone tissue regeneration.

In another study, we exploited the advantages of local drug delivery by developing a platform with improved efficacy. Having this in mind, we prepared hyaluronic acid-based device containing diclofenac sodium-encapsulated (2-Hydroxypropyl)-β-cyclodextrin (CD) that possess high drug loading along with prolonged release. The platform showed high mechanical properties along with low friction indications high lubricity of the platform. L929 cell morphology and viability assay showed a over the 100 % (approximately 110%) for the injectable device.